

LONG-TIME ASYMPTOTICS AND THE RADIATION CONDITION FOR LINEAR EVOLUTION EQUATIONS ON THE HALF-LINE WITH TIME-PERIODIC BOUNDARY CONDITIONS

YIFENG MAO*, DIONYSSIOS MANTZAVINOS†, AND MARK A. HOEFER*

*Department of Applied Mathematics, University of Colorado, Boulder, CO, 80309, USA

†Department of Mathematics, University of Kansas, Lawrence, KS, 66045, USA

ABSTRACT. The large time t asymptotics for scalar, constant coefficient, linear, third order, dispersive equations are obtained for asymptotically time-periodic Dirichlet boundary data and zero initial data on the half-line modeling a wavemaker acting upon an initially quiescent medium. The asymptotic Dirichlet-to-Neumann (D-N) map is constructed by expanding upon the recently developed Q -equation method. The D-N map is proven to be unique if and only if the radiation condition that selects the unique wavenumber branch of the dispersion relation for a sinusoidal, time-dependent boundary condition holds: (i) for frequencies in a finite interval, the wavenumber is real and corresponds to positive group velocity, (ii) for frequencies outside the interval, the wavenumber is complex with positive imaginary part. For fixed spatial location x , the corresponding asymptotic solution is (i) a traveling wave or (ii) a spatially decaying, time-periodic wave. Uniform-in- x asymptotic solutions for the physical cases of the linearized Korteweg-de Vries and Benjamin-Bona-Mahony (BBM) equations are obtained via integral asymptotics. The linearized BBM asymptotics are found to quantitatively agree with viscous core-annular fluid experiments.

1. INTRODUCTION

The forced generation of waves from a boundary is a fundamental problem in applied mathematics with broad applications in fluid dynamics [7], material science [44], seismology [3], and astronomy [1] just to name a few. The fundamental mathematical problem can be posed as follows. Consider a linear evolutionary equation subject to time-harmonic forcing at a localized source or boundary $\propto e^{-i\omega_0 t}$ and decay at infinity. We would expect the solution to exhibit spatial dependence via the wavevector \mathbf{k}_0 consistent with the system's dispersion relation such that $u(\mathbf{x}, t) \propto e^{i(\mathbf{k}_0 \cdot \mathbf{x} - \omega_0 t)}$ near the source or boundary. However, for any evolutionary equation whose spatial order is higher than one, the wavevector \mathbf{k}_0 is not unique. In the context of the time-independent Helmholtz equation $(\nabla^2 + k_0^2)u = -f(\mathbf{x})$, Sommerfeld's eponymous *radiation condition* in three-dimensional space, $\lim_{r \rightarrow \infty} r(\frac{\partial u}{\partial r} - ik_0 u) = 0$, was formulated to select the unique wave that propagates away from a source or boundary to ensure well-posedness on an infinite domain [36]. Another, closely related approach to this problem is called the

E-mail address: mantzavinos@ku.edu.

Date: July 27, 2023.

2020 *Mathematics Subject Classification.* 35G16, 76B15, 35Q53, 35C20.

Key words and phrases. local and nonlocal linear evolution equations, wavemaker problem, time-periodic boundary conditions on the half-line, Dirichlet-to-Neumann map, Sommerfeld radiation condition, long-time asymptotics, linear KdV and linear BBM equations, Fokas method, unified transform.

Acknowledgements. The authors would like to thank the Isaac Newton Institute for Mathematical Sciences, Cambridge, U.K. for support and hospitality during the program "Dispersive Hydrodynamics", when work on this paper was undertaken (EPSRC Grant Number EP/R014604/1). D.M. gratefully acknowledges support from the U.S. National Science Foundation (NSF-DMS 2206270). Y.M. and M.A.H. acknowledge support from NSF-DMS 1816934.

limiting absorption principle for the resolvent $R(k_0) = (\Delta + k_0^2)^{-1}$ [39]. The unique solution is selected by taking a limit of the resolvent whose spectrum is perturbed off the real, essential spectrum into the appropriate half of the complex plane. Ultimately, this boils down to selecting the appropriate branch of the square root.

Both the radiation condition and the limiting absorption principle are mathematical workarounds to the fundamental problem that the Helmholtz equation exhibits two linearly independent, decaying solutions (in two or more dimensions). A physically-inspired approach to the problem is to consider a wavemaker in which a boundary or source time-harmonically forces an initially quiescent ($u(\mathbf{x}, 0) = 0$) medium. In the context of the forced wave equation $u_{tt} - \Delta u = -e^{-i\omega_0 t} f(\mathbf{x})$, solving this initial-boundary value problem and taking $t \rightarrow \infty$ is known as the limiting amplitude principle, which selects the same outgoing wave as the Sommerfeld radiation condition and corresponds to the causal solution by perturbing the essential spectrum of the Helmholtz resolvent into the upper half of the complex plane [40, 33].

A simple, physically inspired calculation [7] demonstrates the limiting amplitude principle. Consider a linear, first order in time evolutionary equation for $u(x, t)$ on the half-line $x > 0$ with real-valued dispersion relation $\omega = \omega(k)$, the asymptotic Dirichlet boundary condition $u(0, t) \sim e^{-i\omega_0 t}$, $t \rightarrow \infty$ with $\omega_0 \in \mathbb{R}$, and decay $\lim_{x \rightarrow \infty} u(x, t) = 0$ for each $t \in \mathbb{R}$. Anticipating the wave

$$u(x, t) \sim e^{i(k_0 x - \omega_0 t)}, \quad t \rightarrow \infty, \quad x = \mathcal{O}(1), \quad (1.1)$$

we seek the correct wavenumber branch $k_0 = k(\omega_0)$ selected from the multivalued inverse $k(\omega_0) = \omega^{-1}(\omega_0)$. The limiting amplitude principle states that, initially, the solution is zero, $u(x, 0) = 0$ for each $x > 0$. Consequently, the *causal* solution can be modeled by perturbing the frequency into the upper half of the complex plane $\omega_0 \rightarrow \omega_0 + i\epsilon$, $0 < \epsilon \ll |\omega_0|$ so that the boundary condition becomes $u(0, t) = e^{-i\omega_0 t} e^{\epsilon t}$ with initially slow amplitude growth to eventually attain the asymptotically periodic boundary condition. Assuming that $k(\omega)$ is analytic in a neighborhood of ω_0 , we expand

$$k(\omega_0 + i\epsilon) = k(\omega_0) + i\epsilon \frac{dk}{d\omega}(\omega_0) + \dots = k_0 + i \frac{\epsilon}{c_g(\omega_0)} + \dots, \quad (1.2)$$

where $c_g \equiv d\omega/dk$ is the group velocity. Then, the anticipated solution takes the form

$$u(x, t) \sim e^{\epsilon t} e^{i(k(\omega_0)x - \omega_0 t)} = e^{\epsilon[t - x/c_g(\omega_0)] + \dots} e^{i(k_0 x - \omega_0 t)}. \quad (1.3)$$

Since $u(x, t) \sim e^{i(k_0 - \epsilon/c_g)x - (i\omega_0 - \epsilon)t}$, in order to ensure $\lim_{x \rightarrow \infty} u(x, t) = 0$ in (1.3) as $\epsilon \rightarrow 0^+$, we require

$$k_0 \in \mathbb{R} \text{ and } c_g(\omega_0) > 0, \quad \text{or} \quad \text{Im } k_0 > 0.$$

These inequalities are the radiation condition for the wavemaker problem. The positive group velocity for real wavenumbers corresponds to waves being emitted from the boundary into the domain. For complex k , the positive imaginary part implies spatial decay. The boundary case $c_g(\omega_0) = 0$ is not included in this argument because $k(\omega)$ has a branch point at ω_0 ; therefore it is not analytic. Zero group velocity corresponds to a critical value of the frequency that represents a transition between propagating and spatially decaying waves. We will prove the general radiation condition

$$k_0 \in \mathbb{R} \text{ and } c_g(\omega_0) \geq 0, \quad \text{or} \quad \text{Im } k_0 > 0. \quad (1.4)$$

Although we have given a physically inspired, plausible argument for the radiation condition (1.4), its proof is more involved.

In this paper, we prove that the radiation condition (1.4) uniquely determines the asymptotic form of the solution (1.1) by constructing the Dirichlet-to-Neumann (D-N) map for the wavemaker initial-boundary value problem

$$(1 - A_{-2} \partial_x^2) u_t = iA_0 u + A_1 u_x + iA_2 u_{xx} + A_3 u_{xxx}, \quad x, t > 0, \quad (1.5a)$$

$$u(x, 0) = 0, \quad x > 0, \quad (1.5b)$$

$$u(0, t) = g_0(t), \quad t > 0, \quad (1.5c)$$

where $A_{-2} \geq 0$ to ensure well-posedness, $A_0, A_1, A_2 \in \mathbb{R}$, and $A_3 \leq 0$ so that only one boundary condition is required at $x = 0$. By scaling t and x , we can restrict $A_3 \in \{-1, 0\}$ and $A_{-2} \in \{0, 1\}$ without loss of generality. For real wavenumbers, these restrictions guarantee the real-valued dispersion relation

$$\omega(k) = \frac{-A_0 - A_1 k + A_2 k^2 + A_3 k^3}{1 + A_{-2} k^2}. \quad (1.6)$$

The choice of parameters $\{A_{-2} = A_0 = A_2 = 0, A_1 = A_3 = -1\}$ corresponds to the linear Korteweg-de Vries (KdV) equation, also known as the first Stokes equation, while for the parameters $\{A_{-2} = 1, A_1 = -1, A_0 = A_2 = A_3 = 0\}$, equation (1.5a) becomes the linear Benjamin-Bona-Mahoney (BBM) equation.

In 1997, Fokas introduced a new approach for the analytical solution of initial-boundary value problems [19]. The main motivation for Fokas's method, otherwise known as the unified transform, was twofold:

- (i) to provide an analogue of the inverse scattering transform method, which is used for solving the initial value problem of completely integrable systems like the KdV and NLS equations, when such systems are considered in domains that involve a boundary, e.g. the half-line or the finite interval, thereby giving rise to nonlinear initial-boundary value problems;
- (ii) to provide a natural analogue of the Fourier transform, which yields the solution to linear evolution equations in the initial value problem setting, when these linear equations are instead formulated in the setting of initial-boundary value problems.

While the difficulty associated with task (i) can be easily appreciated due to the presence of nonlinearity, task (ii) comes with significant challenges as well, despite the fact that it concerns linear equations. This becomes evident through the realization that, for general nonzero boundary conditions, no classical spatial transform is available for solving initial-boundary value problems that involve linear evolution equations of spatial order higher than two. Moreover, even for second-order linear equations, classical techniques fail when the boundary data are non-separable.

The Fokas method effectively addresses both of the above objectives as a unified way of treating initial-boundary value problems for a plethora of linear and nonlinear equations, formulated in various domains and supplemented with different kinds of boundary conditions. Since its inception, the method has been further developed within the completely integrable systems and applied analysis communities in various directions such as the analytical solution of nonlinear equations via the Riemann-Hilbert/dbar problem approach, the solution of linear evolution and elliptic equations, asymptotics, and numerical studies; see the books [20, 18] as well as the review articles [15, 10] for a detailed list of references on the above topics and beyond.

It should be emphasized that the solution formulae obtained via the unified transform have significant advantages even when the relevant problems can be solved via classical approaches. Importantly, they involve integrals with exponentially decaying integrands, due to the fact that integration takes place along complex contours in the spectral plane. As a result, they are uniformly convergent up to the boundary of the domain — a feature that turns out particularly helpful for our purposes here.

In this work, we employ the Fokas method to prove the existence and uniqueness of the Dirichlet-to-Neumann (D-N) map for the wavemaker problem (1.5) and use it to construct a series representation of the solution for fixed $x > 0$ as $t \rightarrow \infty$, thereby providing a constructive proof of the radiation condition (1.4). We also obtain the large t asymptotics along rays $x/t = \text{constant}$ of the wavemaker problem for

the physically important linear KdV and linear BBM equations. Finally, we report experiments on a two-fluid system that agree quantitatively with solutions of the linear BBM wavemaker problem.

We are now ready to precisely state the above results. We begin with the former result, which is actually valid for generic, nonzero initial data provided these have sufficient smoothness and decay (e.g. of Schwartz type).

Theorem 1.1 (Dirichlet-to-Neumann map). *Consider the evolution equation (1.5a) formulated on the half-line $\{x > 0\}$ with a sufficiently smooth and decaying initial datum and the Dirichlet boundary datum (1.5c) that is infinitely smooth and asymptotically periodic in time, i.e. $g_0 \in C^\infty(0, \infty)$ and*

$$g_0(t) \sim \sum_{n \in \mathbb{Z}} a_n e^{in\omega_0 t}, \quad t \rightarrow \infty, \quad \omega_0 \geq 0, \quad a_n \in \mathbb{C}$$

with the infinite sum being absolutely convergent. Assume further that the initial datum and the boundary datum $g_0(t)$ satisfy the necessary compatibility conditions at the origin. Suppose that either $\{A_{-2} = 0, A_3 < 0\}$ (local, third-order) or $\{A_{-2} > 0, A_3 = 0\}$ (nonlocal, second-order) with $A_2/(\omega_0 A_{-2}) \notin \mathbb{Z}$ in the latter case. Then, under the assumption that the solution $u(x, t)$ and its boundary values $\partial_x^j u(0, t)$, $j \in \mathbb{N}$, are asymptotically time-periodic, the associated generalized D-N map satisfies to leading order the asymptotic formula

$$\partial_x^j u(0, t) \sim i^j \sum_{n \in \mathbb{Z}} [k_0(n)]^j a_n e^{in\omega_0 t}, \quad t \rightarrow \infty, \quad j \in \mathbb{N} \cup \{0\}, \quad (1.7)$$

where $k_0(n)$ is the unique solution of the equation $A_3 k^3 + (A_2 + n\omega_0 A_{-2})k^2 - A_1 k - A_0 + n\omega_0 = 0$ that lies along the positively oriented boundary ∂D^+ of the region $D^+ = \{k \in \mathbb{C} : \text{Im}(k) > 0 \text{ and } \text{Re}(\frac{i(A_3 k^3 + A_2 k^2 - A_1 k - A_0)}{1 + A_{-2} k^2}) < 0\}$.

Theorem 1.1 is established in Section 2, where the overall framework for the general, five-parameter equation (1.5a) is first laid out and the analysis specific to the cases $\{A_{-2} = 0, A_3 < 0\}$ (local, third-order) and $\{A_{-2} > 0, A_3 = 0\}$ (nonlocal, second-order) addressed by Theorem 1.1 is then carried out in detail.

Corollary 1.1 (Radiation condition). *Under the assumptions of Theorem 1.1, $k_0(n)$ is the unique branch of the dispersion relation (1.6) satisfying $n\omega_0 = -\omega(k_0(n))$ if and only if the radiation condition (1.4) holds. Furthermore, the asymptotic solution of the wavemaker problem (1.5) takes the form*

$$u(x, t) \sim \sum_{n \in \mathbb{Z}} a_n e^{i(k_0(n)x + n\omega_0 t)}, \quad t \rightarrow \infty, \quad x = \mathcal{O}(1). \quad (1.8)$$

Finally, there exist real numbers ω_{cr}^\pm such that $\text{Im } k_0(1) = 0$ if and only if $\omega_{cr}^- \leq \omega_0 \leq \omega_{cr}^+$.

A few remarks are in order.

1. In the nonlocal, second-order case $\{A_{-2} > 0, A_3 = 0\}$, the scenario $A_2/(\omega_0 A_{-2}) \in \mathbb{Z}$, which is not covered by Theorem 1.1, is discussed separately at the end of Subsection 2.3.
2. The assumption $g_0 \in C^\infty(0, \infty)$ implies that the Fourier series coefficients a_n decay faster than any power of $n \in \mathbb{Z}$, thus the infinite sum in (1.7) is absolutely convergent. To see this, note that $k_0(n)$ grows like $n^{\frac{1}{3}}$ and $n^{\frac{1}{2}}$ in the third-order and second-order cases, respectively.
3. The uniqueness of the D-N map (1.7) follows from the requirement that $k_0(n)$ is the unique root of the cubic $A_3 k^3 + (A_2 + n\omega_0 A_{-2})k^2 - A_1 k - A_0 + n\omega_0$ that lies along the boundary of the domain D^+ . As explained in Section 2, this requirement is easy to justify for $n\omega_0$ outside of the interval $[\omega_{cr}^-, \omega_{cr}^+]$ (supercritical regime). However, within the interval (subcritical regime), things become more subtle and uniqueness follows by studying the large t limit of the Fokas solution formulae for fixed $x > 0$. This is done in Section 2 for the linear KdV and linear BBM equations, where,

by taking advantage of the analyticity and exponential decay properties of the integrands involved in the solution formulae, we perform suitable contour deformations that allow us to quickly derive the leading-order, long-time asymptotics of the corresponding solutions for each fixed $x > 0$. We emphasize that this approach is not valid when $t \rightarrow \infty$ along rays $x/t = \text{constant}$, which is addressed in Theorems 1.2 and 1.3. Importantly, these calculations show that the choice of $k_0(n)$ as the unique root of the aforementioned cubic that lies on ∂D^+ is directly related to the fact that D^+ corresponds to the region in the upper half of the complex k -plane where the imaginary part of the dispersion relation $k(\omega)$ of equation (1.5a) is positive, as in the radiation condition (1.4). Moreover, in the general case covered by Theorem 1.1 that goes beyond the linear KdV and BBM equations, the same analysis can be carried out to reach the same criterion for $k_0(n)$. This analysis addresses a relevant uniqueness issue that was identified in [17].

4. In the case of real roots of the aforementioned cubic, the root $k_0(n)$ is the only one that corresponds to a non-negative group velocity. Indeed, the group velocity associated with equation (1.5a) is

$$\frac{d}{dk} \left(\frac{A_3 k^3 + A_2 k^2 - A_1 k - A_0}{1 + A_{-2} k^2} \right) = \frac{A_{-2} A_3 k^4 + (3A_3 + A_{-2} A_1) k^2 + 2(A_2 + A_{-2} A_0) k - A_1}{(1 + A_{-2} k^2)^2}.$$

Thus, for $k \in \mathbb{R}$, the condition that $k \in \partial D^+$ is equivalent to the group velocity being non-negative at that solution as in the radiation condition (1.4). In the case of complex roots, the root $k_0(n)$ is the unique root with $\text{Im } k_0(n) > 0$ that leads to a spatially decaying solution.

5. The calculations performed in Section 2 are under the assumption of smooth data that lead to a smooth solution with sufficient decay as $x \rightarrow \infty$. Nevertheless, depending on the precise choice of coefficients in 1.5a, these conditions can be relaxed significantly — see, for example, the works [21, 25] where the Fokas method is combined with harmonic analysis techniques for the study of well-posedness of the KdV equation on the half-line and the finite interval with data in appropriate Sobolev spaces. Such an investigation of optimal regularity properties is not our task here.
6. A major assumption in the hypothesis of Theorem 1.1 is that, for zero initial data and asymptotically periodic Dirichlet data, the solutions of the models corresponding to (1.5a) with the choices $\{A_{-2} = 0, A_3 < 0\}$ and $\{A_{-2} > 0, A_3 = 0\}$, as well as the various boundary values of these solutions, are asymptotically periodic in time. The explicit formulae obtained via the Fokas method for the wavemaker problem of the linear KdV and the linear BBM equations allow us to verify this fact and hence remove the time-periodicity assumption from the hypothesis of Theorem 1.1 in the case of these two physical models. More specifically, in Section 2 it is shown that by taking the asymptotic limit x fixed and $t \rightarrow \infty$ in the solution formulae, we obtain the asymptotically time-periodic solution (1.8) and therefore verify the periodicity assumption in Theorem 1.1. Then, in Sections 3 and 4, we combine the solution formulae with the steepest descent method to derive the leading-order asymptotics of these solutions as $t \rightarrow \infty$ and $x/t = \mathcal{O}(1)$, i.e. the behavior of these solutions along rays in the x - t plane. This type of limit provides detailed information about the propagation of waves away from the origin in the wavemaker problem. We also obtain a uniform asymptotic approximation by demonstrating that the asymptotic results from each region $x = \mathcal{O}(1)$ and $x = \mathcal{O}(t)$ match as $t \rightarrow \infty$. The precise asymptotic solution statements to the wavemaker problems are as follows.

Theorem 1.2 (Linear KdV wavemaker problem). *Consider the linear KdV wavemaker problem with input frequency ω_0 ,*

$$\begin{aligned} u_t + u_x + u_{xxx} &= 0, & 0 < x < \infty, & \quad t > 0, \\ u(x, 0) &= 0, & 0 \leq x < \infty, & \end{aligned}$$

$$u(0, t) = \sin(-\omega_0 t), \quad t \geq 0.$$

There exists a critical frequency $\omega_{cr} := 2/(3\sqrt{3})$. Assuming that the solution is sufficiently smooth, its leading-order asymptotic behavior as $t \rightarrow \infty$ and $\xi := x/t = \mathcal{O}(1)$ is:

- (I) A time-periodic sinusoidal function, when $0 < \omega_0 < \omega_{cr}$ and $0 < \xi < c_g := 1 - 3k_0^2 < 1$ with $k_0 = k_3(\omega_0)$ given by (3.1), namely

$$u(\xi t, t) \sim \sin[(k_0 \xi - \omega_0)t]. \quad (1.9)$$

Moreover, this is a uniform asymptotic approximation that is also valid for $\xi t = \mathcal{O}(1)$, $t \rightarrow \infty$.

- (II) A sinusoidal function in t with an algebraically decaying amplitude of $\mathcal{O}(t^{-1/2})$, when $0 < \omega_0 < \omega_{cr}$ and $c_g < \xi < 1$, or when $\omega_0 > \omega_{cr}$ and $0 < \xi < 1$ with the condition $l_1(\xi, \omega_0) < 0$ where l_1 is defined in (3.13), i.e.

$$u(\xi t, t) \sim \frac{27\xi\omega_0 \cos\left(\frac{2}{9}t\sqrt{3(1-\xi)}(1-\xi)\right)}{-(\xi+3)\xi^2 - 27\omega_0^2 + 4} \sqrt{\frac{1}{2\pi t\sqrt{3(1-\xi)}}}. \quad (1.10)$$

- (III) A sinusoidal function in t with an algebraically decaying amplitude of $\mathcal{O}(t^{-1/2})$ associated with an exponentially decaying sinusoidal function when $\omega_0 > \omega_{cr}$ and $0 < \xi < 1$ with the condition $l_1(\xi, \omega_0) > 0$ where l_1 is defined in (3.13), that is

$$u(\xi t, t) \sim e^{-\text{Im}(k_0)\xi t} \sin[(\text{Re}(k_0)\xi - \omega_0)t] + \frac{27\xi\omega_0 \cos\left(\frac{2}{9}t\sqrt{3(1-\xi)}(1-\xi)\right)}{-(\xi+3)\xi^2 - 27\omega_0^2 + 4} \sqrt{\frac{1}{2\pi t\sqrt{3(1-\xi)}}}, \quad (1.11)$$

with $k_0 = k_3(\omega_0)$ now given by (3.2). While the first term is beyond all orders in t when $\xi = \mathcal{O}(1)$, this is a uniform asymptotic approximation that is also valid for $\xi t = \mathcal{O}(1)$, $t \rightarrow \infty$, where the first term is the dominant contribution.

- (IV) An exponential, decaying in time function when $\xi > 1$, i.e.

$$u(\xi t, t) \sim \frac{27\xi\omega_0 e^{-\frac{2}{9}\sqrt{3\xi-3}(\xi-1)t}}{-2(\xi+3)\xi^2 - 54\omega_0^2 + 8} \sqrt{\frac{1}{t\pi\sqrt{3(\xi-1)}}}. \quad (1.12)$$

Theorem 1.3 (Linear BBM wavemaker problem). Consider the linear BBM wavemaker problem with input frequency ω_0 ,

$$\begin{aligned} u_t + u_x - u_{xxt} &= 0, & 0 < x < \infty, & \quad t > 0, \\ u(x, 0) &= 0, & 0 \leq x < \infty, & \\ u(0, t) &= \sin(-\omega_0 t), & t \geq 0. & \end{aligned}$$

There exists a critical frequency $\omega_{cr} := 1/2$. Assuming that the solution is sufficiently smooth, its leading-order asymptotic behavior as $t \rightarrow \infty$ and $\xi := x/t = \mathcal{O}(1)$ is described by:

- (I) A time-periodic sinusoidal function, when $0 < \omega_0 < \omega_{cr}$ and $0 < \xi < c_g := \frac{1-4\omega_0^2 + \sqrt{1-4\omega_0^2}}{2} < 1$, namely

$$u(\xi t, t) \sim \sin\left[\left(\frac{1 - \sqrt{1 - 4\omega_0^2}}{2\omega_0}\xi - \omega_0\right)t\right]. \quad (1.13)$$

Moreover, this is a uniform asymptotic approximation that is also valid for $\xi t = \mathcal{O}(1)$, $t \rightarrow \infty$.

(II) A sinusoidal function in t with an algebraically decaying amplitude of $\mathcal{O}(t^{-1/2})$, when $0 < \omega_0 < \omega_{cr}$ and $c_g < \xi < 1$, or when $\omega_0 > \omega_{cr}$ and $0 < \xi < 1$ with the condition $l_3(\xi, \omega_0) < 0$ where l_3 is defined in (4.12), i.e.

$$u(\xi t, t) := u_{s1}(\xi t, t)$$

$$\sim \frac{\omega_0 (-4\xi + \sqrt{8\xi + 1} - 1) \left(\frac{\xi^{1/2} (\sqrt{8\xi + 1} - 1)^3}{t(8\xi + 1 - \sqrt{8\xi + 1})\sqrt{-2\xi - 1 + \sqrt{8\xi + 1}}} \right)^{1/2} \cos \left[\frac{2\sqrt{2\xi}}{(\sqrt{8\xi + 1} - 1)^2} (-2\xi + \sqrt{8\xi + 1} - 1)^{3/2} t \right]}{2^{5/4} \sqrt{\pi} ((4\xi - \sqrt{8\xi + 1} + 1)\omega_0^2 + \xi(2\xi - \sqrt{8\xi + 1} + 1))}. \quad (1.14)$$

(III) A sinusoidal function in t with an algebraically decaying amplitude of $\mathcal{O}(t^{-1/2})$ associated with an exponentially decaying sinusoidal function when $\omega_0 > \omega_{cr}$ and $0 < \xi < 1$ with the condition $l_3(\xi, \omega_0) > 0$ where l_3 is defined in (4.12), that is

$$u(\xi t, t) \sim \exp \left[-\frac{t\xi \sqrt{4\omega_0^2 - 1}}{2\omega_0} \right] \sin \left[\left(\frac{\xi}{2\omega_0} - \omega_0 \right) t \right] + u_{s1}(\xi t, t). \quad (1.15)$$

While the first term is beyond all orders in t when $\xi = \mathcal{O}(1)$, this is a uniform asymptotic approximation that is also valid for $\xi t = \mathcal{O}(1)$, $t \rightarrow \infty$, where the first term is the dominant contribution.

(IV) An exponentially decaying in time function when $\xi > 1$, i.e.

$$u(\xi t, t) \sim -\frac{\omega_0 \left(\frac{\xi^{1/2} (\sqrt{8\xi + 1} - 1)^3}{t\sqrt{2\xi - \sqrt{8\xi + 1} + 1}(8\xi - \sqrt{8\xi + 1} + 1)} \right)^{1/2} (4\xi + \sqrt{8\xi + 1} + 8\omega_0^2 - 1) \exp \left(-\frac{\sqrt{2\xi^2 - \xi\sqrt{8\xi + 1} + \xi(\sqrt{8\xi + 1} - 3)}}{\sqrt{2}(\sqrt{8\xi + 1} - 1)} t \right)}{4 \cdot 2^{3/4} \sqrt{\pi} ((4\xi - 1)\omega_0^2 + (\xi - 1)\xi + 4\omega_0^4)}. \quad (1.16)$$

The positive group velocity c_g in Theorems 1.2 and 1.3 is defined to be $c_g := \omega'(k_0)$, where k_0 is the unique root of the dispersion relation $\omega(k)$ that lies on ∂D^+ defined in Theorem 1.1. The ray $x/t = c_g$ for large time $t \rightarrow \infty$ represents the leading edge of the wave's transition from temporally periodic to temporally damped. Theorems 1.2 and 1.3 are established in Sections 3 and 4, respectively. Moreover, in Section 5, the analytical results of Section 4 are found to be in excellent agreement with experimental observations of a viscous fluid conduit modeled by the linear BBM equation in the long wavelength and small amplitude regime. A lighter, less viscous fluid is injected into a tall reservoir of fluid to establish a vertical fluid conduit rising buoyantly. The spontaneous introduction of a sinusoidal injection rate amounts to the wavemaker problem. As in previous experiments [32], we observe a critical frequency below which waves propagate and above which waves spatially decay. New measurements include spatiotemporal wave patterns along rays $x/t = \text{constant}$ that agree quantitatively with our large t predictions. These measurements include non-decaying waves, algebraically decaying waves, and exponentially decaying waves. The transition between non-decaying and algebraically decaying waves in the subcritical regime is observed to occur when x/t coincides with the group velocity, in agreement with asymptotic predictions.

The universal nature of the Fokas method allows us to formulate a conjecture about the D-N map of the general nonlocal, third-order model (1.5a) in the case of asymptotically periodic Dirichlet data on the half-line. Although we do not prove this conjecture in the case of general coefficients $A_{-2}, A_0, A_1, A_2, A_3$, we anticipate that one should be able to establish it for any specific choice of these coefficients by suitably adapting the arguments leading to the proofs of Theorems 1.1-1.3.

Conjecture Consider the general initial-boundary value problem (1.5) with an asymptotically periodic Dirichlet boundary condition $u(0, t) = g_0(t) \sim \sum_{n \in \mathbb{Z}} a_n e^{in\omega_0 t}$, $t \rightarrow \infty$, where $\omega_0 \geq 0$, $a_n \in \mathbb{C}$. Then, under the assumption that the solution $u(x, t)$ along with its boundary values $\partial_x^j u(0, t)$, $j \in \mathbb{N}$, are asymptotically time-periodic, the associated generalized D-N map satisfies the asymptotic formula of

Theorem 1.1. Furthermore, the uniqueness of the D-N map is equivalent to the radiation condition (1.4).

The paper is organized as follows. Theorem 1.1 is proven, under various assumptions, in Sec. 2. In Sec. 2.1, we construct the asymptotic D-N map (1.7) for the general model (1.5a), which is used to obtain the series representation (1.8) of the asymptotic solution. The asymptotic D-N map involves the root $k_0(n)$ of the cubic polynomial $\omega(k_0(n)) = n\omega_0$ that is proved to be the unique root lying on ∂D^+ obtained in the restricted settings when $A_{-2} = 0$ (Sec. 2.2) or $A_3 = 0$ (Sec. 2.3), provided the frequency $n\omega_0$ lies outside an interval. The proof for all real frequencies $n\omega_0$ is obtained for the linear KdV (Sec. 2.2) and linear BBM (Sec. 2.3) equations where we also prove the asymptotic periodicity of the solution. Consequently, the radiation condition (1.4) is proven for the important physical cases of the linear KdV and linear BBM equations. Theorems 1.2 and 1.3 are proven in Secs. 3 and 4, respectively. Viscous core-annular fluid experiments that quantitatively realize Theorems 1.1 and 1.3 are presented in Sec. 5. We conclude with a discussion of the implications of this work in Sec. 6.

2. THE D-N MAP VIA THE FOKAS METHOD

As noted in the introduction, beyond its main purpose as a universal approach for the solution of linear evolution equations in the initial-boundary value problems setting, the Fokas method provides an effective and efficient way of determining the (generalized) D-N map associated with such problems when the boundary conditions are asymptotically periodic in time. This aspect of the method has been the subject of the recent articles by Fokas and van der Weele [17] and Fokas, Pelloni and Smith [14] for problems on the half-line and the finite interval, respectively.

Here, we consider the Dirichlet problem on the half-line for the general third-order model (1.5a), which includes the linear KdV equation discussed in [17] but additionally involves a mixed spatiotemporal derivative like the one present in the linear BBM equation. Through our analysis, we demonstrate that the Fokas method for the characterization of the D-N map in the case of asymptotically time-periodic boundary conditions remains effective for this general third-order model. We note that the analysis of this section is valid for generic initial data and not just for the zero initial condition stated in the wavemaker problem (1.5).

Importantly, we address a uniqueness issue that arises for temporal frequencies below a certain threshold (the *subcritical regime*) and manifests itself through the presence of solely real singularities among which only one specific choice gives rise to the correct D-N map, despite the fact that, at first sight, all of them qualify as removable. In particular, by deriving the leading-order long-time asymptotics directly from the explicit solution formulae obtained via the Fokas method, we rigorously justify the empirical “rule of thumb” used previously in the literature, according to which, in the subcritical regime, the singularities that must be made removable are the ones along the boundary of the region D^- defined by (2.10) below.

2.1. General framework. Define the half-line Fourier transform of u with respect to x by

$$\widehat{u}(k, t) := \int_{x=0}^{\infty} e^{-ikx} u(x, t) dx, \quad \text{Im}(k) \leq 0. \quad (2.1)$$

We emphasize that, unlike the traditional whole-line Fourier transform, the half-line transform (2.1) is valid not only for $k \in \mathbb{R}$ but also for $\text{Im}(k) < 0$, due to the fact that $x \geq 0$. Upon taking the transform (2.1) and integrating by parts, equation (1.5a) yields

$$\begin{aligned} & (1 + A_{-2} k^2) \widehat{u}_t(k, t) + i(A_3 k^3 + A_2 k^2 - A_1 k - A_0) \widehat{u}(k, t) \\ &= -A_3 g_2(t) - A_{-2} g_1'(t) - i(A_3 k + A_2) g_1(t) - iA_{-2} k g_0'(t) + (A_3 k^2 + A_2 k - A_1) g_0(t), \end{aligned} \quad (2.2)$$

where we have introduced the following notation for the various (known or unknown) boundary values of u at $x = 0$:

$$\partial_x^j u(0, t) =: g_j(t), \quad j = 0, 1, 2. \quad (2.3)$$

Consider now the case of an asymptotically periodic Dirichlet boundary datum, i.e. suppose that g_0 is given and satisfies

$$g_0(t) \sim \sum_{n \in \mathbb{Z}} a_n e^{in\omega_0 t}, \quad t \rightarrow \infty. \quad (2.4)$$

Furthermore, suppose that the remaining (unknown) boundary values g_1 and g_2 , as well as the solution u , are also asymptotically time-periodic with the same periodicity as g_0 ¹, i.e.

$$g_1(t) \sim \sum_{n \in \mathbb{Z}} b_n e^{in\omega_0 t}, \quad g_2(t) \sim \sum_{n \in \mathbb{Z}} c_n e^{in\omega_0 t}, \quad u(x, t) \sim \sum_{n \in \mathbb{Z}} U_n(x) e^{in\omega_0 t}, \quad t \rightarrow \infty. \quad (2.5)$$

Under these assumptions, the characterization of the D-N map for equation (1.5a) on the half-line amounts to expressing the unknown coefficients b_n and c_n in terms of the coefficients a_n , which are known since they correspond to the prescribed boundary datum.

Under the assumption that the half-line Fourier transform in x can be interchanged with the infinite series over n to infer asymptotic time periodicity for \widehat{u} , namely

$$\widehat{u}(k, t) \sim \sum_{n \in \mathbb{Z}} \widehat{U}_n(k) e^{in\omega_0 t}, \quad t \rightarrow \infty, \quad (2.6)$$

and also that the various infinite series can be differentiated term by term, equation (2.2) yields

$$\begin{aligned} & \sum_{n \in \mathbb{Z}} i [\Omega + n\omega_0(1 + A_{-2} k^2)] \widehat{U}_n(k) e^{in\omega_0 t} \\ & \sim \sum_{n \in \mathbb{Z}} \{-A_3 c_n - i(A_3 k + A_2 + n\omega_0 A_{-2}) b_n + [A_3 k^2 + (A_2 + n\omega_0 A_{-2}) k - A_1] a_n\} e^{in\omega_0 t}, \quad t \rightarrow \infty, \end{aligned} \quad (2.7)$$

where we have introduced the notation

$$\Omega = \Omega(k) := A_3 k^3 + A_2 k^2 - A_1 k - A_0. \quad (2.8)$$

Consequently, $\omega(k) = \Omega(k)/(1 + A_{-2} k^2)$ is the dispersion relation (1.6). We deduce from (2.7)

$$\widehat{U}_n(k) = \frac{-A_3 c_n - i(A_3 k + A_2 + n\omega_0 A_{-2}) b_n + [A_3 k^2 + (A_2 + n\omega_0 A_{-2}) k - A_1] a_n}{i [\Omega + n\omega_0(1 + A_{-2} k^2)]}. \quad (2.9)$$

Zeros of the denominator correspond to roots of $\omega(k) = -n\omega_0$. Note that the negative sign is due to the fact that the dispersion relation (1.6) was defined for waves in the form (1.1), i.e., opposite that of the frequency defined in (2.6).

As mentioned above, $\widehat{u}(k, t)$ is analytic for $\text{Im}(k) < 0$ and well-defined in the L^2 -sense for $\text{Im}(k) \leq 0$ (e.g. see Theorem 7.2.4 in [37]). Hence, it would be reasonable to expect that the expression (2.9) for $\widehat{U}_n(k)$ is well-defined for $\text{Im}(k) \leq 0$. In turn, this would imply that any zeros of the quantity $\Omega + n\omega_0(1 + A_{-2} k^2)$ that arise in $\{\text{Im}(k) \leq 0\}$ are actually removable singularities of (2.9). We shall see later, however, that this is true only for the zeros of $\Omega + n\omega_0(1 + A_{-2} k^2)$ that lie on the *boundary* ∂D^- of the domain D^- , where

$$D^\pm = \left\{ k \in \mathbb{C} : \text{Im}(k) \gtrless 0 \text{ and } \text{Re} \left(\frac{i\Omega}{1 + A_{-2} k^2} \right) < 0 \right\}. \quad (2.10)$$

¹This assumption can be justified by computing the long-time asymptotics of the solution obtained from integral asymptotics of the Fokas method solution — see Sections 2.2 and 2.3 for linear KdV and linear BBM respectively.

Observe that, since $n\omega_0 \in \mathbb{R}$, the zeros of $\Omega + n\omega_0(1 + A_{-2}k^2)$ always satisfy the equation $\operatorname{Re}\left(\frac{i\Omega}{1 + A_{-2}k^2}\right) = 0$ and hence lie on $\partial D^+ \cup \partial D^-$, as $\mathbb{R} \subset (\partial D^+ \cup \partial D^-)$. To see this, note that

$$\operatorname{Re}\left(\frac{i\Omega}{1 + A_{-2}k^2}\right) = \frac{\operatorname{Im}(k)}{|1 + A_{-2}k^2|^2} \left[A_1 - 2(A_2 + A_0 A_{-2}) \operatorname{Re}(k) - (3A_3 + A_1 A_{-2}) \operatorname{Re}(k)^2 - A_{-2} A_3 \operatorname{Re}(k)^4 \right. \\ \left. - (A_1 A_{-2} - A_3 + 2A_{-2} A_3 \operatorname{Re}(k)^2) \operatorname{Im}(k)^2 - A_{-2} A_3 \operatorname{Im}(k)^4 \right] \quad (2.11)$$

and so $\operatorname{Re}\left(\frac{i\Omega}{1 + A_{-2}k^2}\right)$ vanishes for $k \in \mathbb{R}$ and is odd with respect to $\operatorname{Im}(k)$. Thus, $\mathbb{R} \subset (\partial D^+ \cup \partial D^-)$ since $(\partial D^+ \cup \partial D^-) \cap \mathbb{R} \neq \emptyset$ and the conjugate of any point in D^+ belongs to $\{\operatorname{Im}(k) < 0\} \setminus D^-$ and the conjugate of any point in D^- belongs to $\{\operatorname{Im}(k) > 0\} \setminus D^+$.

Remark 2.1. The departure from the original intuition that the expression (2.9) for $\widehat{U}_n(k)$ should make sense for all $\operatorname{Im}(k) \leq 0$ is due to the fact that, although related to each other, the quantities $\widehat{U}_n(k)$ and $\widehat{u}(k, t)$ are not quite the same; it seems that the manipulations between infinite series and integrals required in order to derive (2.9) do not fully preserve analyticity in k from $\widehat{u}(k, t)$ to $\widehat{U}_n(k)$.

Explicitly, $\Omega + n\omega_0(1 + A_{-2}k^2) = 0$ corresponds to the cubic equation

$$A_3 k^3 + (A_2 + n\omega_0 A_{-2}) k^2 - A_1 k - A_0 + n\omega_0 = 0. \quad (2.12)$$

The requirement that the zeros of (2.12) along ∂D^- are removable singularities of the right-hand side of (2.9) implies that these zeros must also satisfy the equation

$$-A_3 c_n - i(A_3 k + A_2 + n\omega_0 A_{-2}) b_n + [A_3 k^2 + (A_2 + n\omega_0 A_{-2}) k - A_1] a_n = 0. \quad (2.13)$$

Then, for $A_3 \neq 0$, assuming that precisely two roots $k_1^- = k_1^-(n)$ and $k_2^- = k_2^-(n)$ of the cubic equation (2.12) lie on ∂D^- while the third root $k_0 = k_0(n)$ lies on ∂D^+ , we have the following system for the coefficients b_n and c_n :

$$\begin{aligned} -A_3 c_n - i(A_3 k_1^- + A_2 + n\omega_0 A_{-2}) b_n + [A_3 (k_1^-)^2 + (A_2 + n\omega_0 A_{-2}) k_1^- - A_1] a_n &= 0, \\ -A_3 c_n - i(A_3 k_2^- + A_2 + n\omega_0 A_{-2}) b_n + [A_3 (k_2^-)^2 + (A_2 + n\omega_0 A_{-2}) k_2^- - A_1] a_n &= 0. \end{aligned} \quad (2.14)$$

Solving this system while noting that, by Vieta's formulae, $k_1^- + k_2^- + k_0 = -(A_2 + n\omega_0 A_{-2})/A_3$ and $k_1^- k_2^- + k_2^- k_0 + k_0 k_1^- = -A_1/A_3$, we obtain the D-N map for the third-order model (1.5a) as

$$b_n = i k_0(n) a_n, \quad c_n = -[k_0(n)]^2 a_n, \quad n \in \mathbb{Z}. \quad (2.15)$$

Similarly, for $A_3 = 0$, which corresponds to the special case where (1.5a) reduces to a second-order model, assuming that precisely one root $k_1^- = k_1^-(n)$ of the now quadratic equation (2.12) lies on ∂D^- while the second root $k_0 = k_0(n)$ lies on ∂D^+ , we obtain the first of the relations (2.15), which amounts to the D-N map for this second-order reduction.

Remark 2.2. (Series representation of the leading-order asymptotics via the D-N map).

Under the assumption of sufficient smoothness, the leading-order long-time asymptotics of the solution of the general model (1.5a) on the half-line can be directly constructed via the D-N map (2.15) by means of the Maclaurin series $u(x, t) = \sum_{j=0}^{\infty} \frac{\partial_x^j u(0, t)}{j!} x^j$. Indeed, for $A_3 \neq 0$ (2.15) yields

$$u_x(0, t) \sim i \sum_{n \in \mathbb{Z}} k_0(n) a_n e^{in\omega_0 t}, \quad u_{xx}(0, t) \sim - \sum_{n \in \mathbb{Z}} [k_0(n)]^2 a_n e^{in\omega_0 t},$$

which can be combined with (1.5a) evaluated at the boundary $x = 0$ and the fact that $k_0(n)$ satisfies (2.12) to obtain

$$u_{xxx}(0, t) \sim -i \sum_{n \in \mathbb{Z}} [k_0(n)]^3 a_n e^{in\omega_0 t}.$$

Moreover, along the same lines and using induction while assuming that the x -derivatives of the solution are asymptotically time-periodic at $x = 0$, we have the general formula

$$\partial_x^j u(0, t) \sim i^j \sum_{n \in \mathbb{Z}} [k_0(n)]^j a_n e^{in\omega_0 t}, \quad j \in \mathbb{N} \cup \{0\}. \quad (2.16)$$

Similarly, for $A_3 = 0$ we can use the first of the relations (2.15) to establish (2.16) via induction. Therefore, in view of the Maclaurin series of u with respect to x , and assuming that we can interchange the order of summation, we deduce

$$u(x, t) \sim \sum_{j=0}^{\infty} \frac{i^j x^j}{j!} \sum_{n \in \mathbb{Z}} [k_0(n)]^j a_n e^{in\omega_0 t} = \sum_{n \in \mathbb{Z}} a_n e^{ik_0(n)x + in\omega_0 t}, \quad t \rightarrow \infty, \quad (2.17)$$

which shows that, for asymptotically periodic boundary data that are otherwise arbitrary, the leading-order asymptotics of the solution of (1.5a) is a superposition of waves that either propagate (if $k_0(n) \in \mathbb{R}$) or spatially decay (if $\text{Im } k_0(n) > 0$).

In order to rigorously justify the D-N map (2.15), one must study the location of the roots of the cubic equation (2.12) with respect to the curves ∂D^- and ∂D^+ . For general parameters A_j , this task involves the study of the quartic polynomial in $\text{Re}(k)$ and $\text{Im}(k)$ that appears in the expression (2.11) for $\text{Re}\left(\frac{i\Omega}{1+A_{-2}k^2}\right)$. Hence, below we focus on two particular sets of parameters, namely $\{A_{-2} = 0, A_3 < 0\}$ and $\{A_3 = 0, A_{-2} > 0\}$, which still correspond to generalizations of the linear KdV and the linear BBM equations, respectively, that are more tractable due to the fact that the aforementioned quartic reduces to a quadratic.

2.2. A general local third-order model: $A_{-2} = 0$ and $A_3 < 0$. For $A_{-2} = 0$ and $A_3 < 0$, equation (1.5a) no longer involves a mixed spatiotemporal derivative as it takes the form

$$u_t = iA_0 u + A_1 u_x + iA_2 u_{xx} + A_3 u_{xxx} \quad (2.18)$$

and the denominator in (2.9) reduces to $i(\Omega + n\omega_0)$ with equation (2.12) simplifying to

$$A_3 k^3 + A_2 k^2 - A_1 k - A_0 + n\omega_0 = 0. \quad (2.19)$$

Before discussing the roots of (2.19), it is useful to give the precise characterization of the domains D^- and D^+ . Starting from (2.8), we compute

$$\text{Re}\left(\frac{i\Omega}{1+A_{-2}k^2}\right) = \text{Re}(i\Omega) = \text{Im}(k) [A_1 - 2A_2 \text{Re}(k) - 3A_3 \text{Re}(k)^2 + A_3 \text{Im}(k)^2] \quad (2.20)$$

so that, according to the definition (2.10),

$$D^- = \{k \in \mathbb{C} : \text{Im}(k) < 0 \text{ and } A_1 - 2A_2 \text{Re}(k) - 3A_3 \text{Re}(k)^2 + A_3 \text{Im}(k)^2 > 0\}. \quad (2.21)$$

Thus, for real solutions of (2.19) that lie along the boundary ∂D^- we must have

$$3A_3 k^2 + 2A_2 k - A_1 \leq 0. \quad (2.22)$$

Similarly, the region D^+ is described by

$$D^+ = \{k \in \mathbb{C} : \text{Im}(k) > 0 \text{ and } A_1 - 2A_2 \text{Re}(k) - 3A_3 \text{Re}(k)^2 + A_3 \text{Im}(k)^2 < 0\} \quad (2.23)$$

and, therefore, any real solution of (2.19) that lies along the boundary ∂D^+ must satisfy

$$3A_3 k^2 + 2A_2 k - A_1 \geq 0. \quad (2.24)$$

We now turn our attention to the solution of equation (2.19). The roots of this cubic are given by

$$k_j = \nu_j - \frac{A_2}{3A_3}, \quad j = 1, 2, 3, \quad (2.25)$$

where ν_j are the solutions of the depressed cubic

$$\nu^3 + p\nu + q = 0 \quad \text{with} \quad p = -\frac{3A_1A_3 + A_2^2}{3A_3^2}, \quad q = \frac{2A_2^3 + 9A_1A_2A_3 - 27A_3^2(A_0 - n\omega_0)}{27A_3^3}. \quad (2.26)$$

The discriminant of this depressed cubic is $\Delta = -4p^3 - 27q^2$. According to the classical result by del Ferro and Tartaglia, also known as Cardano's formula, there are three cases:

Case 1: $\Delta < 0$. This is equivalent to $\frac{q^2}{4} + \frac{p^3}{27} > 0$. Note that this inequality is satisfied for all $n \in \mathbb{Z}$ if $p > 0$. On the other hand, if $p \leq 0$ then taking square roots and defining

$$\omega_{cr}^\pm := \bar{\omega} \mp 2A_3 \sqrt{\left(-\frac{p}{3}\right)^3} \quad \text{where} \quad \bar{\omega} := \frac{-2A_2^3 - 9A_1A_2A_3 + 27A_3^2A_0}{27A_3^2} \quad (2.27)$$

we must have either $n\omega_0 > \omega_{cr}^+$ or $n\omega_0 < \omega_{cr}^-$ (note that $\omega_{cr}^- \leq \bar{\omega} \leq \omega_{cr}^+$ since $A_3 < 0$ and $p \leq 0$). That is, $\Delta < 0$ if either $p > 0$, or $p \leq 0$ and $n\omega_0 > \omega_{cr}^+$ or $n\omega_0 < \omega_{cr}^-$. Then, the depressed cubic (2.26) has the real solution $\nu_1 = \left(-\frac{q}{2} + \sqrt{\frac{q^2}{4} + \frac{p^3}{27}}\right)^{\frac{1}{3}} + \left(-\frac{q}{2} - \sqrt{\frac{q^2}{4} + \frac{p^3}{27}}\right)^{\frac{1}{3}}$ and the complex conjugate solutions $\nu_2 = \left(-\frac{q}{2} + \sqrt{\frac{q^2}{4} + \frac{p^3}{27}}\right)^{\frac{1}{3}} e^{i\frac{2\pi}{3}} + \left(-\frac{q}{2} - \sqrt{\frac{q^2}{4} + \frac{p^3}{27}}\right)^{\frac{1}{3}} e^{-i\frac{2\pi}{3}}$ and $\nu_3 = \left(-\frac{q}{2} + \sqrt{\frac{q^2}{4} + \frac{p^3}{27}}\right)^{\frac{1}{3}} e^{-i\frac{2\pi}{3}} + \left(-\frac{q}{2} - \sqrt{\frac{q^2}{4} + \frac{p^3}{27}}\right)^{\frac{1}{3}} e^{i\frac{2\pi}{3}}$. In turn, the cubic (2.19) has one real root and two complex conjugate roots, namely

$$\begin{aligned} k_1 &= \left(-\frac{q}{2} + \sqrt{\frac{q^2}{4} + \frac{p^3}{27}}\right)^{\frac{1}{3}} + \left(-\frac{q}{2} - \sqrt{\frac{q^2}{4} + \frac{p^3}{27}}\right)^{\frac{1}{3}} - \frac{A_2}{3A_3}, \\ k_2 &= \left(-\frac{q}{2} + \sqrt{\frac{q^2}{4} + \frac{p^3}{27}}\right)^{\frac{1}{3}} e^{i\frac{2\pi}{3}} + \left(-\frac{q}{2} - \sqrt{\frac{q^2}{4} + \frac{p^3}{27}}\right)^{\frac{1}{3}} e^{-i\frac{2\pi}{3}} - \frac{A_2}{3A_3}, \\ k_3 &= \left(-\frac{q}{2} + \sqrt{\frac{q^2}{4} + \frac{p^3}{27}}\right)^{\frac{1}{3}} e^{-i\frac{2\pi}{3}} + \left(-\frac{q}{2} - \sqrt{\frac{q^2}{4} + \frac{p^3}{27}}\right)^{\frac{1}{3}} e^{i\frac{2\pi}{3}} - \frac{A_2}{3A_3}. \end{aligned} \quad (2.28)$$

Recalling that $\text{Re}(i\Omega) = 0$ at the roots k_j , it follows that precisely one of the complex conjugate roots k_2 and k_3 lies on ∂D^- . Moreover, we claim that $k_1 \in \partial D^-$. Indeed, we begin by observing that $\nu_1^2 \geq -\frac{p}{3}$. This is clearly true if $p \geq 0$. In addition, if $p < 0$ then, noting that for $q \geq 0$ we have $\frac{q}{2} - \sqrt{\frac{q^2}{4} + \frac{p^3}{27}} \geq 0$ while for $q < 0$ we have $-\frac{q}{2} - \sqrt{\frac{q^2}{4} + \frac{p^3}{27}} \geq 0$, we infer that $-\nu_1 \geq \left(\frac{q}{2}\right)^{1/3}$ for $q \geq 0$ while $\nu_1 \geq \left(-\frac{q}{2}\right)^{1/3}$ for $q < 0$. Hence, if $p < 0$ then $|\nu_1| \geq \left(\frac{|q|}{2}\right)^{1/3}$ which in view of the fact that $\Delta < 0$ implies $\nu_1^2 \geq -\frac{p}{3}$ as desired. In turn, using (2.25) and substituting for p while recalling that $A_3 < 0$, we obtain precisely the condition (2.22) for k_1 and thus prove that $k_1 \in \partial D^-$ as claimed.

Case 2: $\Delta > 0$. This amounts to $\frac{q^2}{4} + \frac{p^3}{27} < 0$, which yields $\omega_{cr}^- < n\omega_0 < \omega_{cr}^+$ with σ_\pm given by (2.27) (note that $\omega_{cr}^+ > \omega_{cr}^-$ because $A_3 < 0$ and for $\Delta > 0$ we must have $p < 0$). Then, the depressed cubic (2.26) has three distinct real roots, $\nu_1 = \left(-\frac{q}{2} + i\sqrt{-\frac{q^2}{4} - \frac{p^3}{27}}\right)^{\frac{1}{3}} - \frac{p}{3} \left(-\frac{q}{2} + i\sqrt{-\frac{q^2}{4} - \frac{p^3}{27}}\right)^{-\frac{1}{3}}$, $\nu_2 = \left(-\frac{q}{2} + i\sqrt{-\frac{q^2}{4} - \frac{p^3}{27}}\right)^{\frac{1}{3}} e^{i\frac{2\pi}{3}} - \frac{p}{3} \left(-\frac{q}{2} + i\sqrt{-\frac{q^2}{4} - \frac{p^3}{27}}\right)^{-\frac{1}{3}} e^{-i\frac{2\pi}{3}}$ and $\nu_3 = \left(-\frac{q}{2} + i\sqrt{-\frac{q^2}{4} - \frac{p^3}{27}}\right)^{\frac{1}{3}} e^{-i\frac{2\pi}{3}} - \frac{p}{3} \left(-\frac{q}{2} + i\sqrt{-\frac{q^2}{4} - \frac{p^3}{27}}\right)^{-\frac{1}{3}} e^{i\frac{2\pi}{3}}$.

$\frac{p}{3} \left(-\frac{q}{2} + i\sqrt{-\frac{q^2}{4} - \frac{p^3}{27}} \right)^{-\frac{1}{3}} e^{i\frac{2\pi}{3}}$, which correspond to the following distinct real roots for the cubic (2.19):

$$\begin{aligned} k_1 &= \left(-\frac{q}{2} + i\sqrt{-\frac{q^2}{4} - \frac{p^3}{27}} \right)^{\frac{1}{3}} - \frac{p}{3} \left(-\frac{q}{2} + i\sqrt{-\frac{q^2}{4} - \frac{p^3}{27}} \right)^{-\frac{1}{3}} - \frac{A_2}{3A_3}, \\ k_2 &= \left(-\frac{q}{2} + i\sqrt{-\frac{q^2}{4} - \frac{p^3}{27}} \right)^{\frac{1}{3}} e^{i\frac{2\pi}{3}} - \frac{p}{3} \left(-\frac{q}{2} + i\sqrt{-\frac{q^2}{4} - \frac{p^3}{27}} \right)^{-\frac{1}{3}} e^{-i\frac{2\pi}{3}} - \frac{A_2}{3A_3}, \\ k_3 &= \left(-\frac{q}{2} + i\sqrt{-\frac{q^2}{4} - \frac{p^3}{27}} \right)^{\frac{1}{3}} e^{-i\frac{2\pi}{3}} - \frac{p}{3} \left(-\frac{q}{2} + i\sqrt{-\frac{q^2}{4} - \frac{p^3}{27}} \right)^{-\frac{1}{3}} e^{i\frac{2\pi}{3}} - \frac{A_2}{3A_3}. \end{aligned} \quad (2.29)$$

We will now show that $k_1, k_2 \in \partial D^-$ while $k_3 \in \partial D^+$. Writing $-\frac{q}{2} + i\sqrt{-\frac{q^2}{4} - \frac{p^3}{27}} = re^{i\theta}$ with $r = \sqrt{-\frac{p^3}{27}}$ and $\tan \theta = \sqrt{-\frac{q^2}{4} - \frac{p^3}{27}} / (-\frac{q}{2})$, we have

$$\begin{aligned} k_1 &= r^{\frac{1}{3}} e^{i\frac{\theta}{3}} - \frac{p}{3} r^{-\frac{1}{3}} e^{-i\frac{\theta}{3}} - \frac{A_2}{3A_3} = 2\sqrt{-\frac{p}{3}} \cos\left(\frac{\theta}{3}\right) - \frac{A_2}{3A_3}, \\ k_2 &= r^{\frac{1}{3}} e^{i\frac{\theta}{3}} e^{i\frac{2\pi}{3}} - \frac{p}{3} r^{-\frac{1}{3}} e^{-i\frac{\theta}{3}} e^{-i\frac{2\pi}{3}} - \frac{A_2}{3A_3} = 2\sqrt{-\frac{p}{3}} \cos\left(\frac{\theta + 2\pi}{3}\right) - \frac{A_2}{3A_3}, \\ k_3 &= r^{\frac{1}{3}} e^{i\frac{\theta}{3}} e^{-i\frac{2\pi}{3}} - \frac{p}{3} r^{-\frac{1}{3}} e^{-i\frac{\theta}{3}} e^{i\frac{2\pi}{3}} - \frac{A_2}{3A_3} = 2\sqrt{-\frac{p}{3}} \cos\left(\frac{\theta - 2\pi}{3}\right) - \frac{A_2}{3A_3}. \end{aligned} \quad (2.30)$$

Since $\omega_{cr}^- < \bar{\omega} < \omega_{cr}^+$ for $p < 0$ and, in addition, $\bar{\omega} = -A_3q + n\omega_0$ and $A_3 < 0$, we have two subcases:

(i) If $\bar{\omega} \leq n\omega_0 < \omega_{cr}^+$, then $q \leq 0$ and so $\theta \in (0, \frac{\pi}{2}]$. Hence, $\frac{\sqrt{3}}{2} \leq \cos \frac{\theta}{3} < 1$, $-\frac{\sqrt{3}}{2} \leq \cos \frac{\theta+2\pi}{3} < -\frac{1}{2}$ and $-\frac{1}{2} < \cos \frac{\theta-2\pi}{3} \leq 0$, which imply $\sqrt{-p} - \frac{A_2}{3A_3} \leq k_1 < 2\sqrt{-\frac{p}{3}} - \frac{A_2}{3A_3}$, $-\sqrt{-p} - \frac{A_2}{3A_3} \leq k_2 < -\sqrt{-\frac{p}{3}} - \frac{A_2}{3A_3}$ and $-\sqrt{-\frac{p}{3}} - \frac{A_2}{3A_3} < k_3 \leq -\frac{A_2}{3A_3}$. Thus, since by (2.22) the portion of ∂D^- along \mathbb{R} is given by $(-\infty, -\sqrt{-\frac{p}{3}} - \frac{A_2}{3A_3}] \cup [\sqrt{-\frac{p}{3}} - \frac{A_2}{3A_3}, \infty)$, we deduce that $k_1, k_2 \in \partial D^-$ and $k_3 \in \partial D^+$. In particular, inequalities (2.22) and (2.24) hold strictly at k_1, k_2 and at k_3 , respectively.

(ii) If $\omega_{cr}^- < n\omega_0 \leq \bar{\omega}$, then $q \geq 0$ and so $\theta \in [\frac{\pi}{2}, \pi)$. Hence, $\frac{1}{2} < \cos \frac{\theta}{3} \leq \frac{\sqrt{3}}{2}$, $-1 < \cos \frac{\theta+2\pi}{3} \leq -\frac{\sqrt{3}}{2}$ and $0 \leq \cos \frac{\theta-2\pi}{3} < \frac{1}{2}$, which imply $\sqrt{-\frac{p}{3}} - \frac{A_2}{3A_3} < k_1 \leq \sqrt{-p} - \frac{A_2}{3A_3}$, $-2\sqrt{-\frac{p}{3}} - \frac{A_2}{3A_3} < k_2 \leq -\sqrt{-p} - \frac{A_2}{3A_3}$ and $-\frac{A_2}{3A_3} \leq k_3 < \sqrt{-\frac{p}{3}} - \frac{A_2}{3A_3}$. Thus, as in the previous subcase, we have $k_1, k_2 \in \partial D^-$ and $k_3 \in \partial D^+$ with inequalities (2.22) and (2.24) holding strictly at k_1, k_2 and at k_3 , respectively.

Case 3: $\Delta = 0$. This is equivalent to $4p^3 + 27q^2 = 0$, thus either $n\omega_0 = \omega_{cr}^+$ or $n\omega_0 = \omega_{cr}^-$. In the former case, the cubic (2.19) admits the real solutions

$$n\omega_0 = \omega_{cr}^+ \quad \Rightarrow \quad k_1 = -2\sqrt{-\frac{p}{3}} - \frac{A_2}{3A_3}, \quad k_2 = k_3 = \sqrt{-\frac{p}{3}} - \frac{A_2}{3A_3}. \quad (2.31)$$

When $n\omega_0 = \omega_{cr}^-$, the cubic (2.19) admits the real solutions

$$n\omega_0 = \omega_{cr}^- \quad \Rightarrow \quad k_1 = 2\sqrt{-\frac{p}{3}} - \frac{A_2}{3A_3}, \quad k_2 = k_3 = -\sqrt{-\frac{p}{3}} - \frac{A_2}{3A_3}. \quad (2.32)$$

Hence, in view of the fact that $\partial D^- \cap \mathbb{R} = (-\infty, -\sqrt{-\frac{p}{3}} - \frac{A_2}{3A_3}] \cup [\sqrt{-\frac{p}{3}} - \frac{A_2}{3A_3}, \infty)$, we deduce that if $p < 0$ then $k_1 \in \partial D^-$ with strict inequality in (2.22) and $k_2 = k_3 \in \partial D^- \cap \partial D^+$ with equality in (2.24), while if $p = 0$ then $k_1 = k_2 = k_3 \in \partial D^- \cap \partial D^+$ with equality in (2.22) and (2.24).

Overall, our analysis leads to the following conclusions:

- If $3A_1A_3 + A_2^2 < 0$, then the solutions of (2.19) are given by (2.28) for all $n \in \mathbb{Z}$.
- If $3A_1A_3 + A_2^2 > 0$, then the solutions of (2.19) are given by (2.28) for $n\omega_0 > \omega_{cr}^+$ or $n\omega_0 < \omega_{cr}^-$, by (2.29) for $\omega_{cr}^- < n\omega_0 < \omega_{cr}^+$, and by (2.31) for $n\omega_0 = \omega_{cr}^+$ or (2.32) for $n\omega_0 = \omega_{cr}^-$, where ω_{cr}^\pm are defined by (2.27).
- If $3A_1A_3 + A_2^2 = 0$, then $\omega_{cr}^+ = \omega_{cr}^- = \bar{\omega}$ defined by (2.27) and the solutions of (2.19) are given by (2.28) for $n\omega_0 \neq \bar{\omega}$ and by (2.31) for $n\omega_0 = \bar{\omega}$.

Importantly, in all three of the above cases, the contour ∂D^- contains precisely two solutions of (2.19) whereas the contour ∂D^+ contains only one, which we label k_0 . That is, we have shown that for $A_{-2} = 0$ and $A_3 < 0$ is satisfied, and hence the D-N map for the general third-order model (2.18) is indeed given by (2.15).

This proves Theorem 1.1 when $A_{-2} = 0$.

Remark 2.3. (connection to the radiation condition (1.4)) The group velocity associated with the third-order equation (2.18) is $c_g = \Omega'(k) = 3A_3k^2 + 2A_2k - A_1$. Thus, for a real solution of the cubic (2.19), the condition that this solution lies on ∂D^+ (equation (2.24)) is equivalent to the group velocity being non-negative at that solution. In particular, recall that the scenario $k_0 \in \partial D^+ \cap \mathbb{R}$ is possible if either $3A_1A_3 + A_2^2 > 0$ and $\omega_{cr}^- < n\omega_0 < \omega_{cr}^+$, or $3A_1A_3 + A_2^2 > 0$ and either $n\omega_0 = \omega_{cr}^+$ or $n\omega_0 = \omega_{cr}^-$, or $3A_1A_3 + A_2^2 = 0$ and $n\omega_0 = \bar{\omega}$. Hence, we have a strictly positive group velocity in the first scenario (see ‘‘Case 2’’ above) and zero group velocity in the other three scenarios (see ‘‘Case 3’’ above), which deals with the boundary case $c_g = 0$. Furthermore, if $k_0 \in \partial D^+ \setminus \mathbb{R}$ then it follows from the definition (2.23) of D^+ that $\text{Im}(k) > 0$.

This proves Corollary 1.1 when $A_{-2} = 0$.

The linear KdV equation on the half-line. The analysis of the roots of the cubic $\Omega + n\omega_0$ (i.e. of equation (2.19)) for the general third-order model (2.18) provided a complete justification of the assumption used in the derivation of the D-N map (2.15) that precisely two of those three roots lie on the contour ∂D^- . However, there is one more assumption that was needed for deducing (2.15) and is yet to be justified, namely that the right-hand side of (2.9) should have removable singularities only at those roots of $\Omega + n\omega_0$ that occur along ∂D^- . Above a certain threshold of values for $|n\omega_0|$, it is easy to see why this latter assumption must be imposed; below that threshold, however, the situation becomes more delicate.

More precisely, for those values of $n\omega_0$ for which the roots of $\Omega + n\omega_0$ involve a complex conjugate pair (i.e. in Case 1: $\Delta < 0$ above, $n\omega_0 \in [\omega_{cr}^-, \omega_{cr}^+]^C$), one of the complex roots lies in the upper half of the k -plane where $\hat{u}(k, t)$ (and hence $\hat{U}_n(k)$) is not well-defined (recall discussion below (2.1)). Thus, this root cannot be a removable singularity of (2.9). On the other hand, the remaining two roots do lie in the domain of definition $\{\text{Im}(k) \leq 0\}$ of $\hat{u}(k, t)$ and so they must be removable singularities of (2.9), thereby leading to the system (2.14) and hence to the D-N map (2.15). The same is true in the degenerate case of one distinct and two repeated real roots (i.e. in Case 3: $\Delta = 0$ above, $n\omega_0 \in \{\omega_{cr}^-, \omega_{cr}^+\}$) since, counting without multiplicities, there are exactly two roots that belong to $\{\text{Im}(k) \leq 0\}$ and hence must be removable singularities of (2.9).

Nevertheless, in the case of three distinct real roots (i.e. Case 2: $\Delta > 0$ above, $n\omega_0 \in (\omega_{cr}^-, \omega_{cr}^+)$), we encounter the following issue: while all three roots, namely the two lying on ∂D^- and the one lying on ∂D^+ , belong to $\{\text{Im}(k) \leq 0\}$ and hence, according to our previous reasoning, should be removable

singularities of (2.9), requiring that all three of them are removable results via (2.13) in three equations for the two unknowns b_n and c_n , i.e. an overdetermined system. Therefore, the question is: *which two of the three distinct real roots of $\Omega + n\omega_0$ are actually removable singularities of (2.13)?* Note that each of the three possible choices leads to a different D-N map since, via Vieta's formulae, the root which is not a removable singularity is the one that eventually appears in the D-N relations (2.15). From this point of view, the challenge we are facing is directly related to the uniqueness of the D-N map.

Our conjecture is that, even in the case of three distinct real roots, our earlier assumption that led to (2.15) is correct, namely the roots of $\Omega + n\omega_0$ that must be removable singularities of (2.9) are precisely the two roots that lie along ∂D^- (and not the one along ∂D^+ — see remark below (2.10) for a possible explanation of this fact in connection with the domains of definition of $\widehat{u}(k, t)$ and $\widehat{U}_n(k)$). In what follows, we prove this conjecture for the special case of the linear KdV equation by exploiting the explicit solution formula produced by the Fokas method.

The linear KdV equation

$$u_t + u_x + u_{xxx} = 0 \quad (2.33)$$

is included in the four-parameter family of third-order models (2.18) (it corresponds to $A_0 = A_2 = 0$ and $A_1 = A_3 = -1$), thus the general framework developed earlier can readily be employed. In particular, the dispersion relation is $\Omega(k) = k - k^3$, the regions D^+ and D^- are given by

$$D^+ = \{k \in \mathbb{C} : \text{Im}(k) > 0, 3\text{Re}(k)^2 - \text{Im}(k)^2 < 1\}, \quad D^- = D_1^- \cup D_2^-, \quad (2.34)$$

where (see Figure 2.1)

$$\begin{aligned} D_1^- &= \{k \in \mathbb{C} : \text{Im}(k) < 0, 3\text{Re}(k)^2 - \text{Im}(k)^2 > 1, \text{Re}(k) < 0\}, \\ D_2^- &= \{k \in \mathbb{C} : \text{Im}(k) < 0, 3\text{Re}(k)^2 - \text{Im}(k)^2 > 1, \text{Re}(k) > 0\}, \end{aligned} \quad (2.35)$$

and the discriminant of the cubic $\Omega + n\omega_0$ is $\Delta = 4 - 27(n\omega_0)^2$, which defines symmetric critical interval endpoints $\omega_{cr}^\pm = \pm\omega_{cr} = \pm 2/(3\sqrt{3})$. Moreover, in all three scenarios $\Delta < 0$, $\Delta > 0$ and $\Delta = 0$, each of the contours ∂D^+ , ∂D_1^- and ∂D_2^- contains precisely one of the three roots k_0 , k_1^- and k_2^- of the cubic $\Omega + n\omega_0$ respectively.

As explained above, the challenge is how to justify that, among the three distinct real roots that arise in the case $\Delta > 0$, i.e. $|n\omega_0| < 2/(3\sqrt{3})$, the two roots $k_1^- \in \partial D_1^-$ and $k_2^- \in \partial D_2^-$ that lie on $\partial D^- = \partial D_1^- \cup \partial D_2^-$ should be removable singularities of (2.9) while the remaining root $k_0 \in \partial D^+$ should not, despite the fact that it belongs to the domain of definition $\{\text{Im}(k) \leq 0\}$ of $\widehat{u}(k, t)$ (see remark below (2.10) for a possible explanation of this fact). Therefore, we consider equation (2.33) in the context of the wavemaker problem associated with the data

$$u(x, 0) = 0, \quad u(0, t) = \sin(-\omega_0 t) \quad (2.36)$$

and restrict our attention to the scenario $|\omega_0| < 2/(3\sqrt{3})$ which, in the case of the data (2.36), corresponds to $\Omega + n\omega_0$ having three distinct real roots since $u(0, t) = -\sum_{n=\pm 1} \frac{\text{sgn}(n)}{2i} e^{in\omega_0 t}$ and, regardless of which two roots end up satisfying (2.13), the resulting D-N relations will imply that the Fourier series coefficients b_n, c_n of the boundary values $u_x(0, t), u_{xx}(0, t)$ vanish whenever the coefficient a_n of $u(0, t)$ does.

In what follows, we will show that choosing k_1^- and k_2^- as the two removable singularities of (2.9) does indeed produce the correct D-N map, namely the first relation given in (2.15). We will do so by independently deriving that D-N relation directly from the solution formula obtained for the linear KdV wavemaker problem (2.33)-(2.36) via the Fokas method, which is given by (see [20], Example 1.12)

$$u(x, t) = \frac{1}{2i\pi} \sum_{n=\pm 1} a_n \int_{\partial D^+} e^{ikx} \Omega' \frac{e^{in\omega_0 t} - e^{-i\Omega t}}{\Omega + n\omega_0} dk, \quad a_{\pm 1} = \mp \frac{1}{2i}. \quad (2.37)$$

Note that the three roots k_0, k_1^-, k_2^- of $\Omega + n\omega_0$ are removable singularities of the above integrand, which is therefore analytic in k . Hence, in the particular case that k_0, k_1^-, k_2^- are real and distinct, we invoke Cauchy's theorem to deform the contour of integration ∂D^+ in (2.37) to the modified contour $\partial \tilde{D}^+$ that bypasses the removable singularity $k_0 \in \partial D^+$ from below as shown in Figure 2.1 and thus obtain

$$u(x, t) = \frac{1}{2i\pi} \sum_{n=\pm 1} a_n \int_{\partial \tilde{D}^+} e^{ikx} \Omega' \frac{e^{in\omega_0 t} - e^{-i\Omega t}}{\Omega + n\omega_0} dk. \quad (2.38)$$

Since k_0 no longer lies on the contour of integration, we can split the fraction in the integrand to write

$$u(x, t) = \frac{1}{2i\pi} \sum_{n=\pm 1} a_n \left(e^{in\omega_0 t} \int_{\partial \tilde{D}^+} e^{ikx} \frac{\Omega'}{\Omega + n\omega_0} dk - \int_{\partial \tilde{D}^+} e^{ikx} \frac{\Omega' e^{-i\Omega t}}{\Omega + n\omega_0} dk \right). \quad (2.39)$$

Furthermore, for $k \in \{\text{Im}(k) \geq 0 : k \notin D^+\}$ we have $|e^{-i\Omega t}| \leq 1$ so if, in addition, k is large in modulus and stays away from k_1^- and k_2^- , then $\left| \frac{\Omega' e^{-i\Omega t}}{\Omega + n\omega_0} \right| \lesssim \frac{1}{|k|}$. This decay bound combined with analyticity allows us to employ Cauchy's theorem and Jordan's lemma in the second integral of (2.39) in order to deform $\partial \tilde{D}^+$ to the union $\mathcal{L}_1 \cup \mathcal{L}_2$ of the half-lines (with orientation as shown in Figure 2.1)

$$\mathcal{L}_1 = \{k \in \mathbb{C} : k = -i + re^{i\frac{2\pi}{3}}, r \geq 0\}, \quad \mathcal{L}_2 = \{k \in \mathbb{C} : k = -i + re^{i\frac{\pi}{3}}, r \geq 0\}, \quad (2.40)$$

and hence express (2.39) in the form

$$u(x, t) = \frac{1}{2i\pi} \sum_{n=\pm 1} a_n \left(e^{in\omega_0 t} \int_{\partial \tilde{D}^+} e^{ikx} \frac{\Omega'}{\Omega + n\omega_0} dk - \int_{\mathcal{L}_1 \cup \mathcal{L}_2} e^{ikx} \frac{\Omega' e^{-i\Omega t}}{\Omega + n\omega_0} dk \right). \quad (2.41)$$

We emphasize the significance of the bound $\left| \frac{\Omega' e^{-i\Omega t}}{\Omega + n\omega_0} \right| \lesssim \frac{1}{|k|}$, which provides uniform decay in k along the circular arcs connecting $\partial \tilde{D}^+$ with \mathcal{L}_1 and \mathcal{L}_2 and thus allows us to argue that the relevant integrals vanish by invoking Jordan's lemma (or, alternatively, by a direct estimation of those integrals along the lines of the integral I_R below).

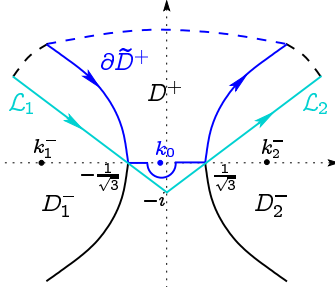


FIGURE 2.1. The domains D^+, D_1^-, D_2^- for the linear KdV equation as given by (2.34)-(2.35). Inside these domains $\text{Re}(i\Omega) < 0$, while outside of them $\text{Re}(i\Omega) > 0$. In the case of the wavemaker data (2.36), if $|\omega_0| < 2/(3\sqrt{3})$ then the three roots of $\Omega + n\omega_0$ are real and distinct with $k_1^- \in \partial D_1^-, k_2^- \in \partial D_2^-, k_0 \in \partial D^+$ as shown, and the contour of integration in the Fokas method solution (2.37) is deformed from the boundary ∂D^+ of D^+ to the contour $\partial \tilde{D}^+$ that bypasses the real root $k_0 \in \partial D^+$ from below. The resulting formula (2.38) is used for deriving the D-N map of the wavemaker problem by computing the long-time asymptotics via Cauchy's residue theorem, exponential decay and, when necessary, the deformation of $\partial \tilde{D}^+$ to the half-lines $\mathcal{L}_1, \mathcal{L}_2$ given by (2.40), along which $\text{Re}(i\Omega) > 0$ (except for $k = \pm \frac{1}{\sqrt{3}}$ where $\text{Re}(i\Omega) = 0$).

We will now use the modified solution formula (2.41) in order to compute the leading-order long-time asymptotics of $u_x(x, t)$ for any finite $x > 0$. Differentiating with respect to x yields

$$u_x(x, t) = \frac{1}{2\pi} \sum_{n=\pm 1} a_n \left(e^{in\omega_0 t} \int_{\partial\tilde{D}^+} e^{ikx} \frac{k\Omega'}{\Omega + n\omega_0} dk - \int_{\mathcal{L}_1 \cup \mathcal{L}_2} e^{ikx} \frac{k\Omega' e^{-i\Omega t}}{\Omega + n\omega_0} dk \right). \quad (2.42)$$

Let $\partial\tilde{D}_R^+$ denote the finite portion of the contour $\partial\tilde{D}^+$ that lies below the circular arc $C_R = \{Re^{i\theta} : \frac{\pi}{3} \leq \theta \leq \frac{2\pi}{3}, R > 1\}$. With this notation, the first integral on the right-hand side of (2.42) can be regarded as the limit

$$\int_{\partial\tilde{D}^+} e^{ikx} \frac{k\Omega'}{\Omega + n\omega_0} dk = \lim_{R \rightarrow \infty} \int_{\partial\tilde{D}_R^+} e^{ikx} \frac{k\Omega'}{\Omega + n\omega_0} dk.$$

Therefore, by Cauchy's residue theorem,

$$\int_{\partial\tilde{D}^+} e^{ikx} \frac{k\Omega'}{\Omega + n\omega_0} dk = 2i\pi \operatorname{Res} \left[e^{ikx} \frac{k\Omega'}{\Omega + n\omega_0} \right]_{k=k_0} - \lim_{R \rightarrow \infty} I_R(x, t) \quad (2.43)$$

where $I_R(x, t) := \int_{C_R} e^{ikx} \frac{k\Omega'}{\Omega + n\omega_0} dk$. We claim that $\lim_{R \rightarrow \infty} I_R(x, t) = 0$ for any $x > 0, t > 0$ and hence, calculating the residue in (2.43),

$$\int_{\partial\tilde{D}^+} e^{ikx} \frac{k\Omega'}{\Omega + n\omega_0} dk = 2i\pi k_0 e^{ik_0 x}. \quad (2.44)$$

Indeed, for $k \in C_R$ we have $|e^{ikx}| = e^{-xR\sin\theta}$, $|\Omega'| \leq 1 + 3R^2$ and, for $R^2 \geq 2[1 + 2/(3\sqrt{3})]$ (recall that $n = \pm 1$ and $|n\omega_0| = |\omega_0| < 2/(3\sqrt{3})$), $|\Omega + n\omega_0| = |Re^{i\theta} - R^3 e^{3i\theta} + n\omega_0| \geq |Re^{i\theta} - R^3 e^{3i\theta}| - |n\omega_0| \geq R^3 - R - |n\omega_0| \geq \frac{1}{2}R^3$. Thus,

$$|I_R(x, t)| \leq \frac{2R^2(1 + 3R^2)}{R^3} \int_{\frac{\pi}{3}}^{\frac{2\pi}{3}} e^{-xR\sin\theta} d\theta$$

and, using the symmetry of $\sin\theta$ about $\frac{\pi}{2}$ as well as the well-known inequality $\sin\theta \geq \frac{2\theta}{\pi}$, $0 \leq \theta \leq \frac{\pi}{2}$, we find

$$|I_R(x, t)| \leq \frac{2R^2(1 + 3R^2)}{R^3} \cdot \frac{\pi}{2xR} \left(e^{-\frac{2xR}{3}} - e^{-xR} \right),$$

which implies the claim for any $x > 0, t > 0$. In turn, combining (2.42) with (2.44) we obtain

$$u_x(x, t) - \sum_{n=\pm 1} ik_0 a_n e^{ik_0 x + in\omega_0 t} = -\frac{1}{2\pi} \sum_{n=\pm 1} a_n \int_{\mathcal{L}_1 \cup \mathcal{L}_2} e^{ikx} \frac{k\Omega' e^{-i\Omega t}}{\Omega + n\omega_0} dk. \quad (2.45)$$

Remark 2.4. We could have chosen the contour $\partial\tilde{D}^+$ to bypass k_0 from above. This would have made the first integral of (2.42) equal to zero and would have moved the residue contribution over to the second integral.

Next, we will prove that, for any $x > 0$, the integral on the right-hand side of (2.45) vanishes as $t \rightarrow \infty$. We emphasize that the deformation from $\partial\tilde{D}^+$ to $\mathcal{L}_1 \cup \mathcal{L}_2$ in (2.41) was possible because $\operatorname{Re}(i\Omega) \geq 0$ in the upper half-plane and outside D^+ . In fact, $\operatorname{Re}(i\Omega) \geq 0$ also in the lower half-plane and outside D_1^- and D_2^- and, more precisely, $\operatorname{Re}(i\Omega) > 0$ for $k \in \mathcal{L}_1 \cup \mathcal{L}_2 \setminus \{\pm 1/\sqrt{3}\}$ so that the exponential $e^{-i\Omega t}$ is strictly decaying there. This fact will allow us to show that the integral on the right-hand side of (2.45) decays like $O(1/\sqrt{t})$ as $t \rightarrow \infty$. We remark that our argument will not work without the presence of the exponential $e^{-i\Omega t}$, which decays as $|k| \rightarrow \infty$ along $\mathcal{L}_1 \cup \mathcal{L}_2$. Thus, the deformation from $\partial\tilde{D}^+$ to $\mathcal{L}_1 \cup \mathcal{L}_2$ is only possible and helpful for the second integral in (2.39) and not for the first one, which does not involve $e^{-i\Omega t}$.

Since the estimation along the half-lines \mathcal{L}_1 and \mathcal{L}_2 is entirely analogous, we provide the details only for \mathcal{L}_2 . Then, $k = -i + re^{i\frac{\pi}{3}} = \frac{r}{2} + i(\frac{\sqrt{3}r}{2} - 1)$ and so $\text{Re}(i\Omega) = \frac{3}{2}(r - \frac{2}{\sqrt{3}})^2$. Importantly, observe that due to the definition of \mathcal{L}_2 the expression for $\text{Re}(i\Omega)$ is quadratic (as opposed to cubic) in r . Also, similar to the proof of (2.45), for r sufficiently large, say $r \geq 10$, we have $|\Omega + n\omega_0| \gtrsim r^3$. Furthermore, $|\Omega + n\omega_0|$ is strictly positive by the definition of \mathcal{L}_2 and the fact that $|n\omega_0| = |\omega_0| < 2/(3\sqrt{3})$, i.e. $|\Omega + n\omega_0| \geq C(n\omega_0) > 0$ for some positive constant depending on $n\omega_0$. Hence,

$$\begin{aligned} & \left| \int_{\mathcal{L}_2} e^{ikx} \frac{k\Omega' e^{-i\Omega t}}{\Omega + n\omega_0} dk \right| \leq \int_0^{10} e^{-(\frac{\sqrt{3}}{2}r-1)x} \frac{|k\Omega'| e^{-\text{Re}(i\Omega)t}}{|\Omega + n\omega_0|} dr + \int_{10}^{\infty} e^{-(\frac{\sqrt{3}}{2}r-1)x} \frac{|k\Omega'| e^{-\text{Re}(i\Omega)t}}{|\Omega + n\omega_0|} dr \\ & \lesssim \int_0^{10} e^x \frac{10 \cdot (1 + 3 \cdot 10^2) \cdot e^{-\frac{3}{2}(r-\frac{2}{\sqrt{3}})^2 t}}{C(n\omega_0)} dr + \int_{10}^{\infty} e^{-(\frac{\sqrt{3}}{2}r-1)x} \frac{r \cdot r^2 \cdot e^{-\frac{3}{2}(r-\frac{2}{\sqrt{3}})^2 t}}{r^3} dr \\ & \lesssim e^x \int_0^{\infty} \left(\frac{1}{C(n\omega_0)} + 1 \right) e^{-\frac{3}{2}(r-\frac{2}{\sqrt{3}})^2 t} dr \leq e^x \int_{-\infty}^{\infty} \left(\frac{1}{C(n\omega_0)} + 1 \right) e^{-\frac{3}{2}tr^2} dr \simeq e^x \frac{\frac{1}{C(n\omega_0)} + 1}{\sqrt{t}}. \end{aligned} \quad (2.46)$$

A similar result holds for the integral along \mathcal{L}_1 and hence for (2.45).

Overall, we have shown that, in the scenario $|\omega_0| < 2/(3\sqrt{3})$ of three distinct real roots of $\Omega + n\omega_0$, for any $x, t > 0$ the spatial derivative of the solution to the linear KdV wavemaker problem (2.33)-(2.36) satisfies

$$\left| u_x(x, t) - \sum_{n=\pm 1} ik_0 a_n e^{ik_0 x + in\omega_0 t} \right| \lesssim \frac{1}{2\pi} \sum_{n=\pm 1} |a_n| \left(\frac{1}{C(n\omega_0)} + 1 \right) \frac{e^x}{\sqrt{t}}. \quad (2.47)$$

In other words, for each $x \in [0, L]$, some $L > 0$,

$$u_x(x, t) \sim \sum_{n=\pm 1} ik_0 a_n e^{ik_0 x + in\omega_0 t}, \quad t \rightarrow \infty. \quad (2.48)$$

As we will see in Sec. 3, the bound (2.47) is not tight and can be refined to $O(t^{-3/2})$. Taking the limit, we find $\lim_{x \rightarrow 0^+} u_x(x, t) \sim \sum_{n=\pm 1} ik_0 a_n e^{in\omega_0 t}$ as $t \rightarrow \infty$, in agreement with the first of the D-N relations (2.15). A similar analysis of the solution representation (2.41) can be used to prove that the second spatial derivative u_{xx} satisfies the second of the D-N relations (2.15).

We have shown that the D-N relations are obtained from the solution formula (2.41). In fact, essentially the same analysis implies the asymptotic form of the solution

$$u(x, t) \sim \sum_{n=\pm 1} a_n e^{ik_0 x + in\omega_0 t}, \quad t \rightarrow \infty, \quad x = \mathcal{O}(1). \quad (2.49)$$

By linearity, this result extends to the more general boundary data $g_0(t) \sim \sum_{n \in \mathbb{Z}} a_n e^{in\omega_0 t}$. In particular, we have also proven that the solution is asymptotically time periodic for each fixed $x \geq 0$. Thus, for the linear KdV wavemaker problem, we have proven Theorem 1.1 and the radiation condition (1.4) (Corollary 1.1) for any frequency $\omega_0 \in \mathbb{R}$ without the assumption of asymptotic time periodicity of the solution.

The asymptotic solution (2.49) is only valid for fixed x as $t \rightarrow \infty$. In Sec. 3, we extend the analysis of the linear KdV wavemaker problem to obtain an asymptotic expansion of the solution for large t that is uniform in $x \geq 0$.

Remark 2.5. The above arguments and, in particular, estimate (2.46), crucially rely on the fact that $\text{Re}(i\Omega) \geq 0$ along \mathcal{L}_1 and \mathcal{L}_2 . Attempting to deform the contour ∂D^+ differently in order to also enclose one or both of the roots k_1, k_2 would force us to include contours in regions where $\text{Re}(i\Omega) < 0$ (see Figure 2.1) and hence would result in exponentially growing terms, thus an estimate like (2.46) would no longer hold. This is why the only root contributing to the D-N map (through the residue calculation (2.43)) is the pole along ∂D^+ , namely k_0 .

2.3. A general nonlocal second-order model: $A_{-2} > 0$ and $A_3 = 0$. For $A_{-2} > 0$ and $A_3 = 0$, the third-order equation (1.5a) becomes of second order but still involves the mixed spatiotemporal derivative term, namely

$$(1 - A_{-2}\partial_x^2)u_t = iA_0u + A_1u_x + iA_2u_{xx}. \quad (2.50)$$

Moreover, the equation $\Omega + n\omega_0(1 + A_{-2}k^2) = 0$, which in general corresponds to the cubic (2.12), now reduces to the quadratic

$$(A_2 + n\omega_0A_{-2})k^2 - A_1k - A_0 + n\omega_0 = 0. \quad (2.51)$$

In addition, according to definition (2.10),

$$D^- = \{k \in \mathbb{C} : \text{Im}(k) < 0 \text{ and } A_1 - 2(A_2 + A_0A_{-2})\text{Re}(k) - A_1A_{-2}\text{Re}(k)^2 - A_1A_{-2}\text{Im}(k)^2 > 0\}. \quad (2.52)$$

Thus, for real solutions of (2.51) that lie along the boundary ∂D^- , we must have

$$A_1A_{-2}k^2 + 2(A_2 + A_0A_{-2})k - A_1 \leq 0. \quad (2.53)$$

Likewise, the region D^+ is given by

$$D^+ = \{k \in \mathbb{C} : \text{Im}(k) > 0 \text{ and } A_1 - 2(A_2 + A_0A_{-2})\text{Re}(k) - A_1A_{-2}\text{Re}(k)^2 - A_1A_{-2}\text{Im}(k)^2 < 0\} \quad (2.54)$$

and, therefore, any real solution of (2.51) that lies along the boundary ∂D^+ must satisfy

$$A_1A_{-2}k^2 + 2(A_2 + A_0A_{-2})k - A_1 \geq 0. \quad (2.55)$$

Next, we focus on the solution of equation (2.51). We begin with the scenario in which the parameters A_{-2} , A_2 , ω_0 are such that $A_2 + n\omega_0A_{-2} \neq 0$ for all $n \in \mathbb{Z}$. Then, (2.51) is a quadratic equation with solutions

$$k_{\pm} = k_{\pm}(n) := \frac{A_1 \pm \sqrt{\Delta}}{2(A_2 + n\omega_0A_{-2})}, \quad (2.56)$$

where the discriminant Δ is given by

$$\Delta = A_1^2 + 4(A_0 - n\omega_0)(A_2 + n\omega_0A_{-2}).$$

Observe that Δ is itself a quadratic in the quantity $n\omega_0$ with corresponding discriminant

$$\tilde{\Delta} = 16 \left[(A_0A_{-2} + A_2)^2 + A_{-2}A_1^2 \right].$$

Note that $\tilde{\Delta} \geq 0$ since $A_{-2} > 0$.

Case 1: $\tilde{\Delta} > 0$. This case amounts to either $A_1 \neq 0$ or $A_2 + A_0A_{-2} \neq 0$. Then, Δ has two distinct real roots

$$\omega_{cr}^{\pm} = \frac{A_0A_{-2} - A_2 \pm \sqrt{(A_2 + A_0A_{-2})^2 + A_1^2A_{-2}}}{2A_{-2}}, \quad (2.57)$$

that determine a bifurcation in solution behavior. If $n\omega_0 > \omega_{cr}^+$ or $n\omega_0 < \omega_{cr}^-$ then $\Delta < 0$ and the solutions k_+ , k_- of equation (2.51) given by (2.56) form a complex conjugate pair; if $\omega_{cr}^- < n\omega_0 < \omega_{cr}^+$ then $\Delta > 0$ and k_+ , k_- are real and distinct; and if $n\omega_0 = \omega_{cr}^+$ or $n\omega_0 = \omega_{cr}^-$ then k_+ , k_- reduce to a double real solution.

Importantly, for each $n \in \mathbb{Z}$ there is precisely one solution of (2.51) that lies on ∂D^- . This is straightforward to see if $n\omega_0 > \omega_{cr}^+$ or $n\omega_0 < \omega_{cr}^-$ since, by the definition of the regions D^+ and D^- , any non-real solution of (2.51) must lie either on ∂D^+ or on ∂D^- . On the other hand, if $k_{\pm} \in \mathbb{R}$ then more details are needed:

(i) If $A_1 = 0$ and $A_2 + A_0A_{-2} > 0$, then (2.53) requires $k \leq 0$. However, by Vieta's formulae, $k_+ + k_- = 0$. Thus precisely one (possibly double, if equal to zero) solution of (2.51) lies on ∂D^- and, since $\mathbb{R} \subset (\partial D^+ \cap \partial D^-)$, the remaining solution lies on ∂D^+ .

(ii) If $A_1 = 0$ and $A_2 + A_0A_{-2} < 0$, then (2.53) requires $k \geq 0$ and, as in (i), precisely one (possibly double, if equal to zero) solution of (2.51) lies on ∂D^- and the remaining solution lies on ∂D^+ .

(iii) If $A_1 > 0$ then, since $A_{-2} > 0$, (2.53) requires that $\beta_- \leq k \leq \beta_+$, where

$$\beta_{\pm} = \frac{-(A_2 + A_0A_{-2}) \pm \sqrt{(A_2 + A_0A_{-2})^2 + A_1^2A_{-2}}}{A_1A_{-2}}. \quad (2.58)$$

First, we claim that $\beta_- \leq k_- \leq \beta_+$ (and hence, via (2.53), that $k_- \in \partial D^-$). Indeed, note that $\omega_{cr}^{\pm} = \frac{A_1\beta_{\pm}}{2} + A_0$ and, since $k_{\pm} \in \mathbb{R}$ amounts to having $\omega_{cr}^- \leq n\omega_0 \leq \omega_{cr}^+$, it follows that $A_1\beta_- \leq 2(n\omega_0 - A_0) \leq A_1\beta_+$. Hence, observing that $k_- = \frac{2(n\omega_0 - A_0)}{A_1 + \sqrt{\Delta}}$ and $A_1 + \sqrt{\Delta} > 0$, we infer that $\frac{A_1\beta_-}{A_1 + \sqrt{\Delta}} \leq k_- \leq \frac{A_1\beta_+}{A_1 + \sqrt{\Delta}}$ which, in view of the inequalities $0 < \frac{A_1}{A_1 + \sqrt{\Delta}} \leq 1$, $\beta_+ > 0$, $\beta_- < 0$, allows us to conclude that $\beta_- \leq k_- \leq \beta_+$ as claimed. Note that the equalities are attained only when $\Delta = 0$, i.e. only when $n\omega_0 = \omega_{cr}^+$ or $n\omega_0 = \omega_{cr}^-$, in which case $k_-(\omega_{cr}^+) = k_+(\omega_{cr}^+) = \beta_+$ or $k_-(\omega_{cr}^-) = k_+(\omega_{cr}^-) = \beta_-$, respectively.

In addition, we claim that $k_+ \geq \beta_+$ or $k_+ \leq \beta_-$, with equalities attained only when $\Delta = 0$ (and hence that $k_+ \notin \partial D^-$ except when $k_+ = k_-$). Indeed, in view of (2.56), (2.58) and the fact that $A_1A_{-2} > 0$, if $A_2 + n\omega_0A_{-2} > 0$ then the inequality $A_1^2A_{-2} \geq 2(A_2 + n\omega_0A_{-2}) \left[\sqrt{(A_2 + A_0A_{-2})^2 + A_1^2A_{-2}} - (A_2 + A_0A_{-2}) \right]$, which is valid since $n\omega_0 \leq \omega_{cr}^+$ implies $2(A_2 + n\omega_0A_{-2}) \leq A_0A_{-2} + A_2 + \sqrt{(A_2 + A_0A_{-2})^2 + A_1^2A_{-2}}$, yields $k_+ \geq \beta_+$. Similarly, if $A_2 + n\omega_0A_{-2} < 0$ then, noting that $n\omega_0 \geq \omega_{cr}^-$ implies $-2(A_2 + n\omega_0A_{-2}) \leq \sqrt{(A_2 + A_0A_{-2})^2 + A_1^2A_{-2}} - (A_0A_{-2} + A_2)$, it follows that $A_1^2A_{-2} \geq -2(A_2 + n\omega_0A_{-2}) \left[\sqrt{(A_2 + A_0A_{-2})^2 + A_1^2A_{-2}} + (A_2 + A_0A_{-2}) \right]$, and, in turn, $k_+ \leq \beta_-$, establishing the claim.

(iv) Finally, if $A_1 < 0$ then, since $A_{-2} > 0$, we have $\beta_+ < 0$ and $\beta_- > 0$, and (2.53) requires either $k \geq \beta_-$ or $k \leq \beta_+$. Via entirely analogous steps as in (iii), using the fact that $\omega_{cr}^- \leq n\omega_0 \leq \omega_{cr}^+$ we obtain $\beta_+ \leq k_+ \leq \beta_-$ and $k_- \geq \beta_-$ (for $A_2 + n\omega_0A_{-2} < 0$) or $k_- \leq \beta_+$ (for $A_2 + n\omega_0A_{-2} > 0$), with equalities possible only when $\Delta = 0$, i.e. only when $n\omega_0 = \omega_{cr}^+$ or $n\omega_0 = \omega_{cr}^-$, in which case $k_-(\omega_{cr}^+) = k_+(\omega_{cr}^+) = \beta_+$ or $k_-(\omega_{cr}^-) = k_+(\omega_{cr}^-) = \beta_-$, respectively. Thus, once again we see that there exists precisely one (possibly double) root along ∂D^- , namely k_- , while the other root, i.e. k_+ , lies on ∂D^+ .

Therefore, in the case $\tilde{\Delta} > 0$ we have shown that for each $n \in \mathbb{Z}$ there is precisely one (possibly double) solution of (2.51) that lies on ∂D^- , with the remaining solution lying on ∂D^+ .

Case 2: $\tilde{\Delta} = 0$. This case is much simpler because it requires $A_1 = A_2 + A_0A_{-2} = 0$ and so it reduces our second-order model (2.50) to the equation

$$(1 - A_{-2}\partial_x^2)(u_t - iA_0u) = 0, \quad (2.59)$$

which can be solved by elementary techniques. Indeed, the ODE in x along with the boundary conditions $u(0, t) = g_0(t)$ and $\lim_{x \rightarrow \infty} u(x, t) = 0$ can be integrated to yield an expression for the quantity $u_t - iA_0u$, which can be integrated in t to imply, upon imposing the initial condition $u(x, 0) = u_0(x)$,

$$u(x, t) = e^{iA_0t}u_0(x) + [g_0(t) - e^{iA_0t}g_0(0)]e^{-\frac{x}{\sqrt{A_{-2}}}}. \quad (2.60)$$

The analysis of the scenario $A_2 + n\omega_0A_{-2} \neq 0$ for all $n \in \mathbb{Z}$ is complete and leads to the following conclusions:

- If either $A_1 \neq 0$ or $A_2 + A_0A_{-2} \neq 0$, then one of the solutions k_+ , k_- of the quadratic (2.51) given

by (2.56) lies on the contour ∂D^- while the other solution does not lie on ∂D^- (with the exception of the special case $k_+ = k_-$). Denote the solution along ∂D^- by k_1^- and the solution off ∂D^- (which, as explained above, lies on ∂D^+) by k_0 . Then, setting $k = k_1^-$ into the D-N map condition (2.13), which for the second-order model (2.50) reads

$$i(A_2 + n\omega_0 A_{-2})b_n = [(A_2 + n\omega_0 A_{-2})k - A_1]a_n, \quad (2.61)$$

and using the Vieta formula $k_0 + k_1^- = \frac{A_1}{A_2 + n\omega_0 A_{-2}}$ for equation (2.51), we obtain the D-N relation $b_n = ik_0 a_n$ which was conjectured in (2.15).

• If $A_1 = A_2 + A_0 A_{-2} = 0$, then the solution to the Dirichlet problem of equation (2.50) on the half-line is given by the simple formula (2.60) and the D-N map can be computed by directly differentiating this formula.

Finally, we consider the scenario of $A_2 + n_*\omega_0 A_{-2} = 0$ for some $n_* \in \mathbb{Z}$, i.e. the possibility that the parameters A_{-2} , A_2 , ω_0 are such that $n_* := -A_2/(\omega_0 A_{-2}) \in \mathbb{Z}$. Then, equation (2.13) does not yield information about b_{n_*} , as either it becomes an identity (if $A_1 = 0$) or it forces $a_{n_*} = 0$ (if $A_1 \neq 0$).

If $A_1 = 0$, then equation (2.51) evaluated at n_* implies $A_0 A_{-2} + A_2 = 0$ so we recover the simple model (2.59) with the explicit solution formula (2.60).

If $A_1 \neq 0$, then we note that under the transformation $u \mapsto u + a_{n_*} e^{in_*\omega_0 t}$, which in view of (2.4) eliminates the term corresponding to n_* from the series expansion of $u(0, t)$, equation (2.50) becomes

$$(1 - A_{-2}\partial_x^2)(u_t + in_*\omega_0 a_{n_*} e^{in_*\omega_0 t}) = iA_0(u + a_{n_*} e^{in_*\omega_0 t}) + A_1 u_x + iA_2 u_{xx}. \quad (2.62)$$

If $A_0 A_{-2} + A_2 = 0$ then $n_*\omega_0 = A_0$ and equation (2.62) is identical to equation (2.50), so without loss of generality we can take $a_{n_*} = 0$. In particular, this is the case for the linear BBM equation considered below. On the other hand, if $A_0 A_{-2} + A_2 \neq 0$ then $n_*\omega_0 \neq A_0$ and (2.62) is different from (2.50), so the case $n_* = -A_2/(\omega_0 A_{-2}) \in \mathbb{Z}$ and $A_1(A_0 A_{-2} + A_2) \neq 0$ is not covered by our analysis unless the associated Dirichlet datum actually satisfies $a_{n_*} = 0$.

Concerning the value of b_{n_*} , if the Dirichlet datum is actually periodic (and not just asymptotically periodic) then using the compatibility between the initial and boundary values at $x = t = 0$ and assuming that $u(x, t)$ is continuously differentiable up to the boundary, we find $b_{n_*} = u'_0(0) - \sum_{n \in \mathbb{Z}, n \neq n_*} b_n$, with the coefficients b_n for $n \neq n_*$ given by the first of the D-N relations (2.15). Furthermore, if $A_2 = 0$ and hence $n_* = 0$, then $b_{n_*} = b_0$ can be determined even if the solution is only asymptotically periodic. In particular, evaluating equation (2.50) at $x = 0$ and then integrating over $[t, t + \frac{2\pi}{\omega_0}]$ with t arbitrary, we exploit the periodicity of the relevant exponentials to deduce, by taking the limit $t \rightarrow \infty$,

$$b_0 = -i \frac{A_0}{A_1} a_0. \quad (2.63)$$

Note that, in the particular case of the linear BBM equation, the above expression yields $b_0 = 0$.

This proves Theorem 1.1 when $A_3 = 0$.

Remark 2.6. (connection to the radiation condition (1.4)) The group velocity associated with the second-order equation (2.50) is $c_g = \omega'(k) = \frac{A_1 A_{-2} k^2 + 2(A_2 + A_0 A_{-2})k - A_1}{(1 + A_{-2} k^2)^2}$. Thus, for a real solution of the quadratic (2.51), the condition that this solution lies on ∂D^+ (equation (2.55)) amounts precisely to the group velocity being non-negative at that solution. In particular, in the non-trivial scenario of either $A_1 \neq 0$ or $A_2 + A_0 A_{-2} \neq 0$, recall that $k_0 \in \partial D^+ \cap \mathbb{R}$ is possible if either $\omega_{cr}^- < n\omega_0 < \omega_{cr}^+$ or $n\omega_0 = \omega_{cr}^\pm$. In the first case we have a strictly positive group velocity, while in the second case the group velocity is zero. Furthermore, if $k_0 \in \partial D^+ \setminus \mathbb{R}$ then $\text{Im } k_0 > 0$.

This proves Corollary 1.1 when $A_3 = 0$.

The linear BBM on the half-line. Recall that the main idea behind deriving the D-N map (2.15) is that each root of $\Omega + n\omega_0(1 + A_{-2}k^2)$ that occurs along ∂D^- should be a removable singularity of the right-hand side of (2.9) and hence a solution of (2.61). In this connection, the analysis provided above for the quadratic (2.51) associated with the second-order model (2.50) justifies the assumption made in the derivation of (2.15) that precisely one of the two roots of $\Omega + n\omega_0(1 + A_{-2}k^2)$ lies on the contour ∂D^- . Nevertheless, the additional assumption that *only* this root must satisfy (2.61) has not yet been justified and, although this is an easy task for $n\omega_0$ outside the interval $[\omega_{cr}^-, \omega_{cr}^+]$ — since then the root off ∂D^- is in the upper half-plane where (2.1) is generally not defined — it becomes more subtle for values within the interval. In what follows, we address this outstanding uniqueness issue in the case of the wavemaker problem (2.36) for the linear BBM equation, which reads

$$u_t + u_x - u_{xxt} = 0 \quad (2.64)$$

and corresponds to the choice of parameters $A_0 = A_2 = 0$, $A_{-2} = 1$, $A_1 = -1$ in the general model (2.50). We remark that, despite the absence of the second spatial derivative term, the mixed derivative term — an essential element of the model (2.50) when compared to the model (2.18) — is still present in equation (2.64) and makes the analysis quite different from that of the linear KdV equation.

In the case of the linear BBM equation (2.64), the regions D^- and D^+ of (2.52) and (2.54) are given by

$$D^- = \{k \in \mathbb{C} : \text{Im}(k) < 0, \text{Re}(k)^2 + \text{Im}(k)^2 > 1\}, \quad D^+ = \{k \in \mathbb{C} : \text{Im}(k) > 0, \text{Re}(k)^2 + \text{Im}(k)^2 < 1\}, \quad (2.65)$$

i.e. D^+ is the interior of the upper half of the unit disk centered at the origin and D^- is the exterior of that disk in the lower half of the complex plane, as shown in Figure 2.2. The critical interval endpoints are symmetric $\omega_{cr}^\pm = \pm\omega_{cr} = \pm 1/2$. Furthermore,

$$\Omega + n\omega_0(1 + A_{-2}k^2) = k + n\omega_0(1 + k^2) = 0 \quad (2.66)$$

when (cf. eqs. (2.51) and (2.56))

$$k = k_\pm(n) = \begin{cases} \frac{-1 \pm \sqrt{1 - (2n\omega_0)^2}}{2n\omega_0}, & n \neq 0, \\ 0, & n = 0. \end{cases} \quad (2.67)$$

If $|2n\omega_0| > 1$ then (2.67) form a pair of complex conjugate roots that lie on the unit circle. Thus, due to the domain of (2.1), only the root lying in the lower half of the complex plane — and hence on ∂D^- — must satisfy (2.61). The same is true if $|2n\omega_0| = 1$, since then the roots (2.67) reduce to a single double root equal to $\mp 1 \in \partial D^-$. On the other hand, if $0 < |2n\omega_0| < 1$ then the roots (2.67) are real and distinct, with one of them, denoted by k_0 , lying inside $(-1, 1) \subset \partial D^+$ and the other one, denoted by k_1^- , lying in $[-1, 1]^c \subset \partial D^-$ (see Figure 2.2). In this case, as noted above, since both roots are in the domain of (2.1), it is not immediately clear why only k_1^- , and not k_0 , should satisfy (2.61) as a removable singularity of (2.9). Next, we will show that this is indeed the case by taking advantage of the powerful solution representation provided by the Fokas method.

In particular, let us consider the linear BBM equation (2.64) in the context of the wavemaker problem associated with the data (2.36). In this case, observe that the scenario of two distinct real roots of (2.66) corresponds to the range $0 < |2\omega_0| < 1$, since $u(0, t) = -\sum_{n=\pm 1} \frac{\text{sgn}(n)}{2i} e^{in\omega_0 t}$ and, regardless of which root ends up satisfying (2.61), the resulting D-N relation will imply that the Fourier series coefficient b_n of the Neumann value $u_x(0, t)$ vanishes whenever the coefficient a_n of $u(0, t)$ does. Hence, we work with $0 < |2\omega_0| < 1$ and two distinct real roots as shown in Figure 2.2. The solution formula is given by

[42]

$$u(x, t) = \frac{1}{2i\pi} \sum_{n=\pm 1} a_n \int_{\mathcal{C}} e^{ikx} \omega' \frac{e^{in\omega_0 t} - e^{-i\omega t}}{\omega + n\omega_0} dk - e^{-x} \sin(\omega_0 t), \quad a_{\pm 1} = \mp \frac{1}{2i}, \quad (2.68)$$

where the contour \mathcal{C} is a positively oriented, closed contour in the upper half of the complex plane and enclosing $k = i$, as shown in Figure 2.2 and

$$\omega = \omega(k) := \frac{k}{1+k^2} \quad (2.69)$$

with ω' denoting the derivative of ω . Note that the integrand in (2.68) has essential singularities at $k = \pm i$ due to the exponential $e^{-i\omega t}$. In addition, for $k \neq \pm i$ we have $\operatorname{Re}\left(\frac{i\Omega}{1+k^2}\right) = \operatorname{Re}(i\omega)$ and so inside the regions D^- and D^+ of (2.65) we have $\operatorname{Re}(i\omega) < 0$, while outside those regions we have $\operatorname{Re}(i\omega) > 0$.

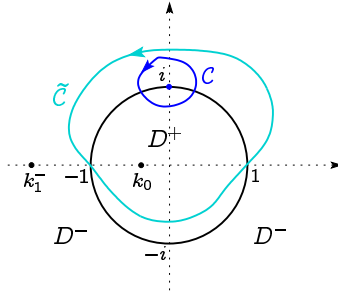


FIGURE 2.2. The regions D^+ and D^- for the linear BBM equation as given by (2.65). In the case of the wavemaker data (2.36), for $0 < |2\omega_0| < 1$ the two roots of $\omega + n\omega_0$ are real and distinct with $k_1^- \in \partial D^-$, $k_0 \in \partial D^+$ as shown. Then, in order to compute the long-time asymptotics of the solution, we deform the contour of integration in the Fokas formula (2.68) from \mathcal{C} to the contour $\tilde{\mathcal{C}}$ along which $\operatorname{Re}(i\omega) > 0$ (except for $k = \pm 1$ where $\operatorname{Re}(i\omega) = 0$). This deformation yields a residue contribution from $k_0 \in \partial D^+$ (as opposed to $k_1^- \in \partial D^-$), justifying the assumption that only k_1^- (and not k_0) should satisfy (2.61).

Thanks to analyticity and Cauchy's theorem, the contour of integration \mathcal{C} in (2.68) can be deformed to the contour $\tilde{\mathcal{C}}$ depicted in Figure 2.2. Thus, differentiating in x , we have

$$u_x(x, t) = \frac{1}{2\pi} \sum_{n=\pm 1} a_n \int_{\tilde{\mathcal{C}}} e^{ikx} k\omega' \frac{e^{in\omega_0 t} - e^{-i\omega t}}{\omega + n\omega_0} dk + e^{-x} \sin(\omega_0 t). \quad (2.70)$$

Since $\tilde{\mathcal{C}}$ does not cross any singularities, we can split the integral with respect to k in two parts:

$$u_x(x, t) = \frac{1}{2\pi} \sum_{n=\pm 1} a_n \left(e^{in\omega_0 t} \int_{\tilde{\mathcal{C}}} e^{ikx} \frac{k\omega'}{\omega + n\omega_0} dk - \int_{\tilde{\mathcal{C}}} e^{ikx} \frac{k\omega' e^{-i\omega t}}{\omega + n\omega_0} dk \right) + e^{-x} \sin(\omega_0 t). \quad (2.71)$$

The contour $\tilde{\mathcal{C}}$ encloses the points $k = i$ and $k = k_0$, which are simple poles of the integrand of the first of the above integrals. Hence, by Cauchy's residue theorem and the fact that k_0 satisfies (2.67),

$$\int_{\tilde{\mathcal{C}}} e^{ikx} \frac{k\omega'}{\omega + n\omega_0} dk = 2\pi \left(e^{-x} + ik_0 e^{ik_0 x} \right). \quad (2.72)$$

Moreover, note that along $\tilde{\mathcal{C}}$ we have $\operatorname{Re}(i\omega) > 0$ except for $k = \pm 1$ where $\operatorname{Re}(i\omega) = 0$. Thus, we expect that the second integral in (2.71) admits a similar bound to (2.46) for the integral on the right-hand side of (2.45). Below, we establish this rigorously. Thanks to analyticity, without loss of generality

we work with $\tilde{C} = \{k \in \mathbb{C} : k = i + \sqrt{2}e^{i\theta}, -\frac{\pi}{2} \leq \theta \leq \frac{3\pi}{2}\}$. Then, $\operatorname{Re}(k) = \sqrt{2} \cos \theta$, $\operatorname{Im}(k) = 1 + \sqrt{2} \sin \theta$ and $|1 + k^2|^2 = 4(3 + 2\sqrt{2} \sin \theta)$, implying

$$\phi(\theta) := \operatorname{Re}(i\omega) = \frac{(1 + \sqrt{2} \sin \theta)^2}{2(3 + 2\sqrt{2} \sin \theta)}.$$

Furthermore, $|k\omega'| \leq 1 + 1/\sqrt{2}$, and $|\omega + n\omega_0| \geq |1 - 2n\omega_0|/2 > 0$ since $|n\omega_0| < 1/2$. Hence,

$$\left| \int_{\tilde{C}} e^{ikx} \frac{k\omega' e^{-i\omega t}}{\omega + n\omega_0} dk \right| \leq \int_{-\frac{\pi}{2}}^{\frac{3\pi}{2}} e^{-(1+\sqrt{2} \sin \theta)x} \frac{|k\omega'| e^{-\operatorname{Re}(i\omega)t}}{|\omega + n\omega_0|} \sqrt{2} d\theta \leq \frac{4(\sqrt{2} + 1)e^{(\sqrt{2}-1)x}}{|1 - 2n\omega_0|} \int_{-\pi/2}^{\pi/2} e^{-t\phi(\theta)} d\theta.$$

For $\theta \in [-\frac{\pi}{2}, \frac{\pi}{2}]$, $\phi(\theta) \geq 0$ with the minimum attained only at $-\frac{\pi}{4}$. This integral can be estimated using Laplace's method (e.g. see Lemma 6.2.3 in [2]), we obtain $\int_{-\pi/2}^{\pi/2} e^{-t\phi(\theta)} d\theta \sim \sqrt{\frac{2\pi}{t}} + O\left(\frac{1}{t\sqrt{t}}\right)$ as $t \rightarrow \infty$. Therefore, for any $x \geq 0$ and $|n\omega_0| < 1/2$, we conclude that

$$\left| \int_{\tilde{C}} e^{ikx} \frac{k\omega' e^{-i\omega t}}{\omega + n\omega_0} dk \right| = O\left(\frac{e^{(\sqrt{2}-1)x}}{\sqrt{t}}\right), \quad t \rightarrow \infty. \quad (2.73)$$

In view of (2.72) and (2.73), the expression (2.71) yields

$$\left| u_x(x, t) - \sum_{n=\pm 1} ik_0 a_n e^{ik_0 x + in\omega_0 t} \right| \lesssim O\left(\frac{e^{(\sqrt{2}-1)x}}{\sqrt{t}}\right), \quad t \rightarrow \infty. \quad (2.74)$$

In particular, first taking the limit $x \rightarrow 0^+$ and then performing the above asymptotic analysis as $t \rightarrow \infty$, we obtain $\lim_{x \rightarrow 0^+} u_x(x, t) \sim \sum_{n=\pm 1} ik_0 a_n e^{ik_0 x + in\omega_0 t}$ as $t \rightarrow \infty$, in agreement with the D-N map (2.15).

A similar analysis of the solution formula (2.68) implies the asymptotic solution for fixed $x \geq 0$

$$u(x, t) \sim \sum_{n=\pm 1} a_n e^{ik_0 x + in\omega_0 t}, \quad t \rightarrow \infty, \quad x = \mathcal{O}(1). \quad (2.75)$$

By linearity, this result extends to the more general boundary data $g_0(t) \sim \sum_{n \in \mathbb{Z}} a_n e^{in\omega_0 t}$. We have proven the asymptotic time periodicity of the solution to the linear BBM wavemaker problem so that Theorem 1 and the radiation condition (1.4) (Corollary 1.1) hold for any frequency $\omega_0 \in \mathbb{R}$ without the need to assume asymptotic time periodicity of the solution.

The asymptotic solution (2.75) is only valid for fixed x as $t \rightarrow \infty$. In Sec. 4, we extend the analysis of the linear BBM wavemaker problem to obtain an asymptotic expansion of the solution for large t that is uniform in $x \geq 0$. We then observe that this analysis quantitatively agrees with viscous core-annular experiments in Sec. 5.

Remark 2.7. In order to establish estimate (2.73), it is crucial for \tilde{C} to lie in regions where $\operatorname{Re}(i\omega) \geq 0$. This requirement implies that only k_0 (and not k_1^-) can be enclosed by \tilde{C} , since attempting to also enclose k_1^- would push \tilde{C} into regions where $\operatorname{Re}(i\omega) < 0$. Consequently, only k_0 (and not k_1^-) contributes in the asymptotics (2.74) (via the residue calculation (2.72)).

3. UNIFORM IN x LONG-TIME ASYMPTOTICS FOR THE LINEAR KdV EQUATION WITH A SINUSOIDAL BOUNDARY CONDITION

Section 2.2 derives the D-N map and the asymptotic solution to the linear KdV wavemaker problem (2.33)–(2.36) for $t \rightarrow \infty$ and a fixed $x > 0$. Herein, we study the KdV wavemaker problem in a different asymptotic limit where $t \rightarrow \infty$ while $\xi = x/t = \mathcal{O}(1)$ is fixed, i.e., we consider the solution along rays in the x - t plane. This limit provides information about how waves propagate away from the origin in the wavemaker problem.

Recall the wavemaker initial-boundary value problem (2.36) in which $u(x, 0) = 0$, $x \geq 0$ and $u(0, t) = -\sin(\omega_0 t)$, $t \geq 0$ where $\omega_0 > 0$ is the input frequency. To obtain the long-time asymptotics, we use the solution formula for the linear KdV wavemaker problem (2.33)–(2.36) given by (2.37), where the contour of integration ∂D^+ is shown in Figure 2.1. Note that the integrand in (2.37) has removable singularities at the six simple zeros k_1, \dots, k_6 of the two cubic equations $\Omega + n\omega_0 = 0$, $n = \pm 1$ where Ω is defined in (2.8). For $0 < \omega_0 < \frac{2}{3\sqrt{3}}$, we have

$$\begin{aligned} k_1 &= \frac{2}{\sqrt{3}} \cos\left(\frac{\alpha}{3}\right) \in \left(\frac{1}{\sqrt{3}}, 1\right), & k_2 &= -\frac{1}{\sqrt{3}} \cos\left(\frac{\alpha}{3}\right) - \sin\left(\frac{\alpha}{3}\right) \in \left(-\frac{2}{\sqrt{3}}, -1\right), \\ k_3 &= -\frac{1}{\sqrt{3}} \cos\left(\frac{\alpha}{3}\right) + \sin\left(\frac{\alpha}{3}\right) \in \left(0, \frac{1}{\sqrt{3}}\right), & k_4 &= \frac{2}{\sqrt{3}} \cos\left(\frac{\theta}{3}\right) \in \left(1, \frac{2}{\sqrt{3}}\right), \\ k_5 &= -\frac{1}{\sqrt{3}} \cos\left(\frac{\theta}{3}\right) - \sin\left(\frac{\theta}{3}\right) \in \left(-1, -\frac{1}{\sqrt{3}}\right), & k_6 &= -\frac{1}{\sqrt{3}} \cos\left(\frac{\theta}{3}\right) + \sin\left(\frac{\theta}{3}\right) \in \left(-\frac{1}{\sqrt{3}}, 0\right), \end{aligned} \quad (3.1)$$

where $\alpha = \pi - \tan^{-1}\left(\frac{\sqrt{12-81\omega_0^2}}{9\omega_0}\right) \in \left(\frac{\pi}{2}, \pi\right)$ and $\theta = \tan^{-1}\left(\frac{\sqrt{12-81\omega_0^2}}{9\omega_0}\right) = \pi - \alpha \in \left(0, \frac{\pi}{2}\right)$. Because all the zeros are real as shown in Figure 3.1(a), we call this the subcritical regime. On the other hand, in the supercritical regime $\omega_0 > \frac{2}{3\sqrt{3}}$ we have

$$\begin{aligned} k_1 &= \frac{1}{2^{2/3}3^{1/3}r_1^{1/3}} + \frac{r_1^{1/3}}{2^{4/3}3^{2/3}} + i\left(-\frac{3^{1/6}}{2^{2/3}r_1^{1/3}} + \frac{r_1^{1/3}}{2^{4/3}3^{1/6}}\right), & k_2 &= -\frac{2^{1/3}}{3^{1/3}r_1^{1/3}} - \frac{r_1^{1/3}}{2^{1/3}3^{2/3}}, \\ k_3 &= \frac{1}{2^{2/3}3^{1/3}r_1^{1/3}} + \frac{r_1^{1/3}}{2^{4/3}3^{2/3}} + i\left(\frac{3^{1/6}}{2^{2/3}r_1^{1/3}} - \frac{r_1^{1/3}}{2^{4/3}3^{1/6}}\right), & k_4 &= \frac{2^{1/3}}{3^{1/3}r_2^{1/3}} + \frac{r_2^{1/3}}{2^{1/3}3^{2/3}}, \\ k_5 &= -\frac{1}{2^{2/3}3^{1/3}r_2^{1/3}} - \frac{r_2^{1/3}}{2^{4/3}3^{2/3}} + i\left(-\frac{3^{1/6}}{2^{2/3}r_2^{1/3}} + \frac{r_2^{1/3}}{2^{4/3}3^{1/6}}\right), \\ k_6 &= -\frac{1}{2^{2/3}3^{1/3}r_2^{1/3}} - \frac{r_2^{1/3}}{2^{4/3}3^{2/3}} + i\left(\frac{3^{1/6}}{2^{2/3}r_2^{1/3}} - \frac{r_2^{1/3}}{2^{4/3}3^{1/6}}\right), \end{aligned} \quad (3.2)$$

where $r_1 = 9\omega_0 - \sqrt{81\omega_0^2 - 12}$ and $r_2 = 9\omega_0 + \sqrt{81\omega_0^2 - 12}$ are real numbers. In this case, the location of the zeros is shown in Figure 3.1(b) and described as follows: k_1 is complex and on the boundary of D_2^- , $k_2 \in (-\infty, -2/\sqrt{3})$ is real, k_3 is complex and on the right boundary of D^+ , $k_4 \in (2/\sqrt{3}, \infty)$ is real, k_5 is complex and on the left boundary of D^+ , and k_6 is also complex and on the boundary of D_1^- . The poles are symmetric with respect to the imaginary and real axes and lie on the ellipse $\frac{\operatorname{Re}(k)^2}{a^2} + \frac{3}{4}\frac{\operatorname{Im}(k)^2}{b^2} = 1$, where $a = |k_2| = |k_4|$ and $b = |\operatorname{Im}(k_1)| = |\operatorname{Im}(k_3)| = |\operatorname{Im}(k_5)| = |\operatorname{Im}(k_6)|$. In addition, $k_{1,3,5,6}$ are also on the hyperbola $3\operatorname{Re}(k)^2 - \operatorname{Im}(k)^2 = 1$, $j = 1, 3, 5, 6$, given as ∂D^+ . We define the critical frequency to be

$$\omega_0 = \omega_{cr} = \frac{2}{3\sqrt{3}}. \quad (3.3)$$

Importantly, once the two t -exponentials in the solution formula (2.37) are separated, the removable singularities k_1, \dots, k_6 turn into simple poles for the respective integrands. Therefore, in order to avoid crossing these poles, prior to splitting (2.37) we first indent ∂D^+ so that the poles are excluded from the interior of ∂D^+ , as shown in Figure 3.1. In what follows, ∂D^+ denotes the indented contour shown in Figure 3.1. Then, by substituting the linear dispersion relation $\Omega = k - k^3$ and expressing the complex exponentials as trigonometric functions, we are able to rewrite the solution (2.37) as

$$u(x, t) = u_1(x, t) + u_2(x, t), \quad (3.4a)$$

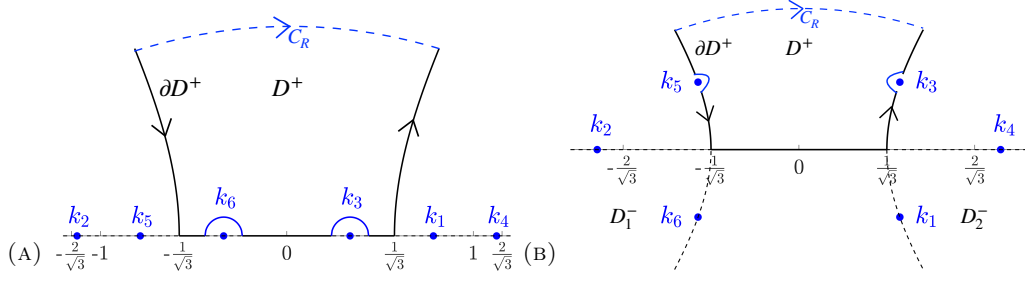


FIGURE 3.1. The positions of the simple poles $k_{1,\dots,6}$ in (3.4) given by $\omega = \pm\omega_0$ for (a) the subcritical regime $0 < \omega_0 < 2/(3\sqrt{3})$ and (b) the supercritical regime $\omega_0 > 2/(3\sqrt{3})$, relative to the contour ∂D^+ for the linear KdV equation. The contour is indented by small semi-circles to avoid the poles and closed from the top with the semicircular arc C_R .

$$u_1(x, t) = \frac{1}{2\pi} \int_{k \in \partial D^+} f(k) e^{ikx} dk, \quad f(k) := \frac{1 - 3k^2}{(k - k^3)^2 - \omega_0^2} [-\omega_0 \cos(\omega_0 t) + i(k - k^3) \sin(\omega_0 t)] \quad (3.4b)$$

$$u_2(x, t) = \frac{\omega_0}{2\pi} \int_{k \in \partial D^+} g(k) e^{ikx - i(k - k^3)t} dk, \quad g(k) := \frac{1 - 3k^2}{(k - k^3)^2 - \omega_0^2}. \quad (3.4c)$$

Note that the dependence of f on t has been suppressed.

We begin by observing that, since all of the poles k_1, \dots, k_6 lie outside the contour ∂D^+ , by Cauchy's theorem inside the region enclosed by ∂D^+ and C_R (the semicircular arcs of radius R in Fig. 3.1), we have $u_1(x, t) = \frac{1}{2\pi} \int_{k \in C_0} f(k) e^{ikx} dk$. To evaluate along the contour C_R , we first notice that the integrand $f(k)$ in (3.4b) is uniformly bounded in $|k|$ ($f(k) = \mathcal{O}(k^{-1})$, $k \rightarrow \infty$). Since $x \geq 0$, we apply Jordan's lemma in the upper half plane by sending $R \rightarrow \infty$ and conclude that

$$u_1(x, t) \equiv 0 \quad \Rightarrow \quad u(x, t) = u_2(x, t). \quad (3.5)$$

The remaining term $u_2(x, t)$ defined by (3.4c) will be asymptotically evaluated in the large-time limit by the method of steepest descent. The difference is that e^{ikx} in $u_1(x, t)$ decays in D^+ so that one can apply Jordan's lemma along C_R , whereas $u_2(x, t)$ involves $e^{ikx - i(k - k^3)t}$ which does not necessarily decay in D^+ .

We now asymptotically approximate $u_2(x, t)$ in (3.4c) using the method of steepest descent. Define $\xi = x/t$ and the phase $\phi(k) = ik\xi - i(k - k^3)$, then $u_2 = \frac{\omega_0}{2\pi} \int_{\partial D^+} g(k) e^{\phi(k)t} dk$. The saddle points are found by requiring $\phi'(\rho_j) = 0$ so that

$$\rho_1 = \sqrt{\frac{1 - \xi}{3}}, \quad \rho_2 = -\sqrt{\frac{1 - \xi}{3}}. \quad (3.6)$$

The saddle points $k_{1,2}$ are real for $0 \leq \xi \leq 1$ and imaginary for $\xi > 1$. Let $k = p + iq$, $p, q \in \mathbb{R}$, so that $\phi(k) = q - 3p^2q + q^3 - q\xi + i(-p + p^3 - 3pq^2 + p\xi)$. We now deform the original contour ∂D^+ onto the steepest descent paths that are defined by $\text{Im}\{\phi(k)\} = \text{Im}\{\phi(\rho_j)\}$ and $\text{Re}\{\phi(k) - \phi(\rho_j)\} < 0$, $j = 1, 2$.

(a) Regime $0 < \xi < 1$.

For the saddles $0 < \rho_1 < \frac{1}{\sqrt{3}}$ and $-\frac{1}{\sqrt{3}} < \rho_2 < 0$, we have the steepest descent contour shown in Figure 3.2a in red with local steepest descent directions $\frac{\pi}{4}, \frac{5\pi}{4}$ from the saddle ρ_1 and $\frac{3\pi}{4}, \frac{7\pi}{4}$ from the saddle ρ_2 . With $\phi(\rho_1) = i\frac{2}{9}\sqrt{3 - 3\xi}(-1 + \xi)$ and $\phi(\rho_2) = -i\frac{2}{9}\sqrt{3 - 3\xi}(-1 + \xi)$, the two curves are

$$\text{Im}\{\phi(k)\} = \text{Im}\{\phi(\rho_1)\} \quad \Rightarrow \quad -p + p^3 - 3pq^2 + p\xi = \frac{2}{9}\sqrt{3 - 3\xi}(-1 + \xi), \quad (3.7a)$$

$$\text{Im}\{\phi(k)\} = \text{Im}\{\phi(\rho_2)\} \quad \Rightarrow \quad -p + p^3 - 3pq^2 + p\xi = -\frac{2}{9}\sqrt{3 - 3\xi}(-1 + \xi), \quad (3.7b)$$

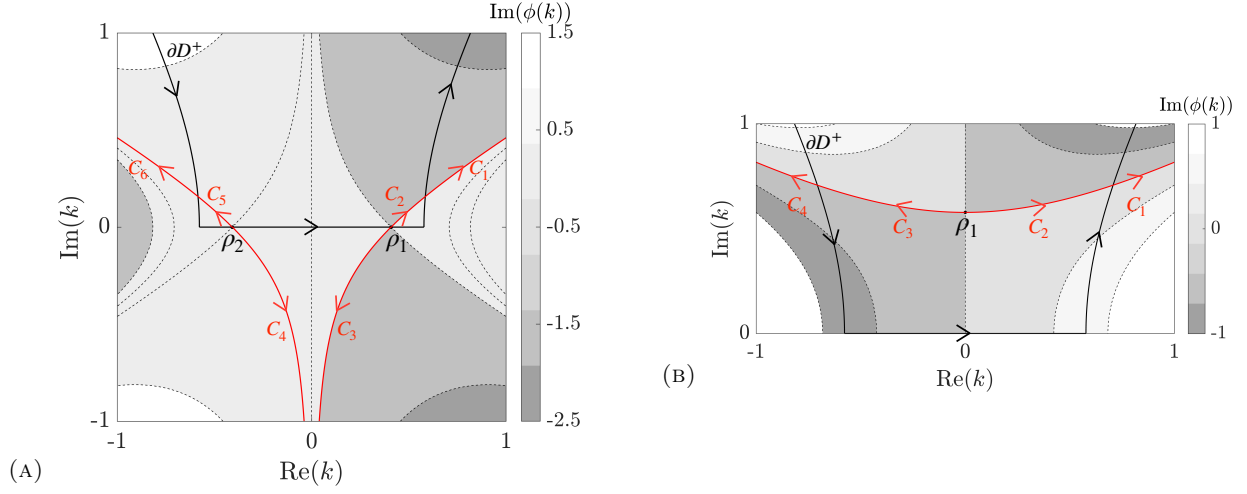


FIGURE 3.2. Illustration of the saddles ρ_j from (3.6) and the steepest descent contour (red) for the solution (3.4c) of the linear KdV wavemaker problem in the case of (a) $0 < \xi < 1$ and (b) $\xi > 1$, against the original contour ∂D^+ (black). The contours $C_1 \cup C_2 \cup C_3$ and $C_4 \cup C_5 \cup C_6$ in (a) are given by Equations (3.7a) and (3.7b) respectively, and the contours $C_1 \cup C_2 \cup C_3 \cup C_4$ in (b) are described by (3.16). The color map indicates levels of $\text{Im}(\phi(k))$ with $\text{Im}(\phi(k))$ constant along the steepest descent path. Recall that the contour ∂D^+ avoids the poles k_1, \dots, k_6 as shown in Figure 3.1.

respectively. Note that the exponential term satisfies $|e^{\phi(k)t}| = 1$ on the steepest descent contour for $0 < \xi < 1$ so it is purely oscillatory. On the right steepest descent path $C_1 \cup C_2 \cup C_3$ in Figure 3.2a, the dominant contribution comes from the neighborhood of ρ_1 . Parameterizing this neighborhood by $k = \rho_1 + (1+i)s$ with small $s \in (-\epsilon, \epsilon)$, we obtain

$$\begin{aligned} \int_{C_1 \cup C_2 \cup C_3} g(k) e^{\phi(k)t} dk &\sim \int_{-\epsilon}^{\epsilon} g(\rho_1 + (1+i)s) e^{t(\phi(\rho_1) + \frac{1}{2}(1+i)^2 s^2 \phi''(\rho_1))} ds \\ &\sim e^{t\phi(\rho_1)} g(\rho_1) \int_{-\infty}^{\infty} e^{is^2 \phi''(\rho_1)} ds, \quad \phi''(\rho_1) = 2i\sqrt{3(1-\xi)}, \\ &= \frac{e^{-i\frac{2}{9}\sqrt{3(1-\xi)}(1-\xi)t}}{\sqrt{t}} \frac{27\xi}{4 - (\xi+3)\xi^2 - 27\omega_0^2} \sqrt{\frac{\pi}{2\sqrt{3(1-\xi)}}}, \quad t \rightarrow \infty. \end{aligned} \quad (3.8)$$

Similarly, on the left steepest descent path $C_4 \cup C_5 \cup C_6$ in Figure 3.2a, we parameterize $k = \rho_2 + (1-i)s$, $s \in (-\epsilon, \epsilon)$. The dominant contribution is the complex conjugate of (3.8)

$$\int_{C_4 \cup C_5 \cup C_6} g(k) e^{\phi(k)t} dk \sim \frac{1}{\sqrt{t}} e^{\frac{2}{9}i\sqrt{3(1-\xi)}(1-\xi)t} \frac{27\xi}{-(\xi+3)\xi^2 - 27\omega_0^2 + 4} \sqrt{\frac{\pi}{2\sqrt{3(1-\xi)}}}, \quad t \rightarrow \infty. \quad (3.9)$$

We now bring in the contribution from the poles $k_{1,\dots,6}$ by considering different cases for the input frequency ω_0 .

(a.1) Subcritical regime: $0 < \omega_0 < \frac{2}{3\sqrt{3}}$.

The two possible scenarios in this case correspond to Regions I and II.a in Figure 3.3. In particular, with both $\rho_1, k_3 \in [0, \frac{1}{\sqrt{3}}]$ and $\rho_2, k_6 \in [-\frac{1}{\sqrt{3}}, 0]$, their relative ordering is important. The boundary between Regions I and II.a is defined by the coalescence $k_3 = \rho_1$ and $k_6 = \rho_2$ so that

$$\xi = 1 - 3k_3^2 = \omega'(k_3), \quad 0 < \omega_0 < 2/(3\sqrt{3}) \text{ and } 0 < \xi < 1. \quad (3.10)$$

We are now in a position to deform the original contour ∂D^+ onto the steepest descent paths. There are two cases to consider. First, the region $0 < \xi < \omega'(k_3)$, which corresponds to the poles lying between the saddle points as shown in Region I of Figure 3.3. Notice that the integrand $g(k)e^{\phi(k)t}$ of (3.4c) decays for $k \rightarrow \infty$ in the region between D_1 and C_1 (also D_5 and C_6) with $|e^{\phi(k)t}| = e^{-\text{Im}(k)\xi t + \text{Im}(k-k^3)t}$, $\xi > 0, t > 0$, where $\text{Im}(k) > 0$ and $\text{Im}(k-k^3) < 0$ in this region. Thus, one can simply deform D_1 onto C_1 and D_5 onto C_6 by Cauchy's theorem and Jordan's lemma so that $\int_{D_1} g(k)e^{\phi(k)t} dk = \int_{C_1} g(k)e^{\phi(k)t} dk$ and $\int_{D_5} g(k)e^{\phi(k)t} dk = -\int_{C_6} g(k)e^{\phi(k)t} dk$. The absence of poles between D_2 and C_2 (D_4 and C_5) and Cauchy's theorem imply $\int_{D_2} g(k)e^{\phi(k)t} dk = \int_{C_2} g(k)e^{\phi(k)t} dk$ and $\int_{D_4} g(k)e^{\phi(k)t} dk = -\int_{C_5} g(k)e^{\phi(k)t} dk$. Finally, since the poles k_3 and k_6 lie inside the region enclosed by D_3, C_3 and C_4 , using Cauchy's residue theorem we compute

$$\int_{D_3+C_3-C_4} g(k)e^{\phi(k)t} dk = -2\pi i (\text{Res}(k_3) + \text{Res}(k_6)),$$

$$\text{Res}(k_3) = \frac{1}{2\omega_0} e^{i(k_3\xi t - \omega_0 t)}, \quad \text{Res}(k_6) = -\text{Res}(k_3)^*,$$

where $k_3 = -k_6 > 0$ satisfies the linear dispersion relation $k_3 - k_3^3 = \omega_0$. Combining these results, we obtain $u_2(\xi; t) = \sin[(k_3\xi - \omega_0)t] + \frac{\omega_0}{2\pi} \int_{C_1+C_2-C_3+C_4-C_5-C_6} g(k)e^{\phi(k)t} dk$. The remaining integral on the right-hand side corresponds to the saddle point contributions (3.8) and (3.9), which are dominated by the pole contributions. Therefore, the large t solution to the wavemaker problem is

$$u(\xi t, t) = \sin[(k_0\xi - \omega_0)t] + \mathcal{O}(t^{-1/2}), \quad t \rightarrow \infty, \quad (3.11)$$

where $k_0 \equiv k_3$ in this case, which satisfies the radiation condition (1.4).

In contrast, the case $\omega'(k_0) < \xi < 1$ occurs when the saddles are in between the poles depicted in Region II.a of Figure 3.3. Using Cauchy's theorem, we can deform ∂D^+ to the steepest descent contour $\cup_{j=1}^6 C_j$ with no pole contributions. Hence, we obtain $u_2(x, t) = \frac{\omega_0}{2\pi} \int_{C_1+C_2-C_3+C_4-C_5-C_6} g(k)e^{\phi(k)t} dk$ so the saddle point contributions (3.8) and (3.9) are asymptotically dominant

$$u(\xi t, t) \sim \frac{\cos\left(\frac{2}{9}t\sqrt{3(1-\xi)(1-\xi)}\right)}{\sqrt{t}} \frac{27\xi\omega_0}{4 - (\xi+3)\xi^2 - 27\omega_0^2} \sqrt{\frac{1}{2\pi\sqrt{3(1-\xi)}}}, \quad t \rightarrow \infty. \quad (3.12)$$

In summary, when $0 < \omega_0 < 2/(3\sqrt{3})$, the leading order solution (3.11) is a traveling wave with real wavenumber k_3 and frequency ω_0 satisfying the dispersion relation $\omega_0 = k_3 - k_3^3$ as $t \rightarrow \infty$ when $0 < \xi = x/t < \omega'(k_3)$. This regime is dominated by the pole contributions from contour deformation. When $x/t > \omega'(k_3)$, i.e., ahead of the boundary-generated, invading wavefront, the leading order solution (3.12) exhibits algebraic decay in time with $u(x, t) = \mathcal{O}(t^{-1/2})$, $\xi = x/t = \mathcal{O}(1)$, $t \rightarrow \infty$. Here, the solution is dominated by saddle point contributions. In contrast to the previous case (3.11) when $0 < \xi < \omega'(k_0)$, the asymptotic solution (3.12) is not time periodic.

Note that the obtained asymptotic approximations are not uniform in ξ . For example, eq. (3.12) is singular when $\xi = \omega'(k_3)$. The cause of nonuniformity is the collisions of the poles $k_{3,6}$ with the saddle points $\rho_{1,2}$. Uniform asymptotic approximations involving the error function with complex argument can be obtained [8, 41, 11].

(a.2) Supercritical regime: $\omega_0 > 2/(3\sqrt{3})$.

In this case, some poles are complex, including $k_{3,5}$, which are avoided by semicircle indentations of the contour ∂D^+ (c.f. Fig. 3.1a). In order to determine the pole locations relative to the steepest descent contours C_j , $j = 1, \dots, 6$ depicted in red in Figure 3.2a (case $0 < \xi < 1$), notice that $C_{1,2}$ and

$C_{5,6}$ intersect with ∂D^+ at

$$(p_1, q_1) = \left(\sqrt{\frac{2+\xi}{6}} \cos \frac{\varphi}{3}, \sqrt{-1 + \frac{2+\xi}{2} \cos^2 \frac{\varphi}{3}} \right), \quad (p_2, q_2) = \left(-\sqrt{\frac{2+\xi}{6}} \cos \frac{\varphi}{3}, \sqrt{-1 + \frac{2+\xi}{2} \cos^2 \frac{\varphi}{3}} \right),$$

where $\varphi = \arctan \left[\frac{3\sqrt{\xi(4-2\xi+\xi^2)}}{2\sqrt{2}(\xi-1)\sqrt{1-\xi}} \right]$. Here, (p_1, q_1) is associated with $C_{1,2} \cap \partial D^+$ and (p_2, q_2) is associated with $C_{5,6} \cap \partial D^+$. We now determine for what value of ξ the poles $k_{3,5}$ coincide with $(p_{1,2}, q_{1,2})$. Letting $\text{Re}(k_3) = p_1, \text{Re}(k_5) = p_2$ and simplifying, results in

$$l_1(\xi, \omega_0) := \frac{1}{2^{2/3} 3^{1/3} r_1^{1/3}} + \frac{r_1^{1/3}}{2^{4/3} 3^{2/3}} - \sqrt{\frac{2+\xi}{6}} \cos \frac{\varphi}{3} = 0, \quad \omega_0 > 2/(3\sqrt{3}) \text{ and } 0 < \xi < 1, \quad (3.13)$$

where r_1 is defined below (3.2). Equation (3.13) determines the curve in the ω_0 - ξ plane that splits Regions II.b and III in Figure 3.3.

When $l_1(\xi, \omega_0) < 0$, the poles $k_{3,5}$ are avoided by the corner contours $D_{2,4}$ with $\text{Im}(k_{3,5}) > 0$ (Region II.b in Figure 3.3). Using Cauchy's theorem and Jordan's lemma where appropriate, we deform each sector of ∂D^+ onto the steepest descent path with no pole contributions. This gives $u_2(\xi; t) = \frac{\omega_0}{2\pi} \int_{C_1+C_2-C_3+C_4-C_5-C_6} g(k) e^{\phi(k)t} dk$ so that the leading-order behavior of $u(\xi t, t)$ is determined by the saddle contributions as in (3.12), with algebraic decay $\mathcal{O}(t^{-1/2})$.

When $l_1(\xi, \omega_0) > 0$ (see Region III in Figure 3.3), the poles k_3 and k_5 lie between the contours D_1, C_1 and D_5, C_6 respectively. Thus, when invoking Cauchy's theorem, the residue contributions from these poles must be taken into account. Computing

$$\text{Res}(k_3) = \frac{1}{2\omega_0} e^{i(k_3 \xi t - \omega_0 t)}, \quad \text{Res}(k_5) = -\text{Res}(k_3)^* \quad (3.14)$$

because $k_3 = -k_5^*$. The pole k_3 corresponds to the singularity on ∂D^+ that determines the D-N map $k_0 := k_3$ and satisfies the dispersion relation $k_3 - k_3^3 = \omega_0$. We find $u_2(\xi t, t) = e^{-\text{Im}(k_0)\xi t} \sin[(\text{Re}(k_0)\xi - \omega_0 t)] + \frac{\omega_0}{2\pi} \int_{C_1+C_2-C_3+C_4-C_5-C_6} g(k) e^{\phi(k)t} dk$. In light of (3.8) and (3.9), we deduce

$$u(\xi t, t) \sim e^{-\text{Im}(k_0)\xi t} \sin[(\text{Re}(k_0)\xi - \omega_0 t)] + \frac{1}{\sqrt{t}} \frac{27\xi\omega_0 \cos\left(\frac{2}{9}t\sqrt{3(1-\xi)}(1-\xi)\right)}{-(\xi+3)\xi^2 - 27\omega_0^2 + 4} \sqrt{\frac{1}{2\pi\sqrt{3(1-\xi)}}}, \quad t \rightarrow \infty. \quad (3.15)$$

The second term in (3.15) is the dominant contribution, with $\mathcal{O}(t^{-1/2})$ for $\xi = \mathcal{O}(1)$. The first term is beyond all orders. In other words, the asymptotic behavior of the solution in Region III is the same as the asymptotic behavior (3.12) in Regions II.a and II.b. However, as we now analyze, both terms in (3.15) are required for obtaining a uniform asymptotic expansion that is also valid as $\xi \rightarrow 0^+$, i.e., x fixed and $t \rightarrow \infty$.

Rewriting (3.15) in terms of $x = \xi t$ and t , we obtain

$$u(x, t) \sim e^{-\text{Im}(k_0)x} \sin(\text{Re}(k_0)x - \omega_0 t) + \frac{1}{t^{3/2}} \frac{27\omega_0 x}{-(x/t+3)(x/t)^2 - 27\omega_0^2 + 4} \cos\left[\frac{2}{9}t\sqrt{3(1-x/t)}(1-x/t)\right] \sqrt{\frac{1}{2\pi\sqrt{3(1-x/t)}}},$$

for $x \in [0, L]$, some $L > 0$ and $t \rightarrow \infty$. This expression is asymptotically equivalent to

$$u(x, t) = e^{-\text{Im}(k_0)x} \sin(\text{Re}(k_0)x - \omega_0 t) + \mathcal{O}(t^{-3/2}), \quad t \rightarrow \infty.$$

The asymptotics of $u(x, t)$ match our earlier analysis using the D-N map for fixed x and large t given in Equation (2.17). Therefore, keeping both terms in (3.15) gives a uniform in x asymptotic expansion as $t \rightarrow \infty$.

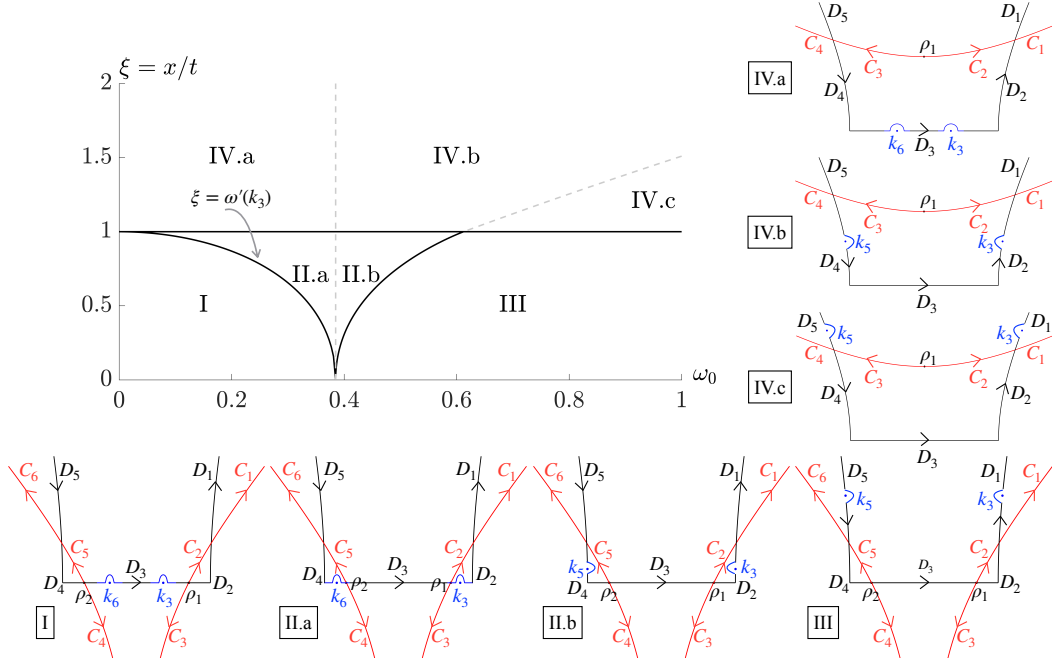


FIGURE 3.3. Phase diagram of the long-time asymptotics for the linear KdV equation (2.33) subject to the sinusoidal boundary condition (2.36). The solution in each region is described in Section 3. The insets show the locations of the saddles and the poles relative to the original contour $\partial D^+ = \cup_{j=1}^5 D_j$ and the steepest descent contours $C_1 \cup C_2 \cup C_3$ and $C_4 \cup C_5 \cup C_6$ that are determined by the values of $\xi = x/t$ and the boundary frequency ω_0 . The solid curves separating various regions in the ω_0 - ξ plane are $\xi = 1$, Equations (3.10) and (3.13). The dashed curves are $\omega_0 = 2/(3\sqrt{3})$ and (3.19).

(b) Regime $\xi > 1$.

Now the saddles are purely imaginary $\rho_1 = i\sqrt{\frac{\xi-1}{3}}$, $\rho_2 = -i\sqrt{\frac{\xi-1}{3}}$ and the local steepest descent directions are $\theta_1 \in \{0, \pi\}$ at ρ_1 and $\theta_2 \in \{\frac{\pi}{2}, \frac{3\pi}{2}\}$ at ρ_2 , because $\phi''(\rho_1) = -2\sqrt{3(\xi-1)} < 0$, $\phi''(\rho_2) = 2\sqrt{3(\xi-1)} > 0$. However, ρ_2 is disregarded since $\phi(\rho_2) = \frac{2}{9}\sqrt{3\xi-3}(\xi-1) > 0$ so $e^{t\phi(\rho_2)}$ is unbounded as $t \rightarrow \infty$. On the other hand, since $\phi(\rho_1) = -\frac{2}{9}\sqrt{3\xi-3}(\xi-1) < 0$, $e^{t\phi(\rho_1)}$ decays as $t \rightarrow \infty$. The deformed contour, which follows the steepest descent directions emanating from the saddle ρ_1 , is shown in red in Figure 3.2b and is described by setting $k = p + iq$, $p, q \in \mathbb{R}$ and

$$\text{Im}(\phi(k)) = \text{Im}(\phi(\rho_1)) \implies p(p^2 - 1 - 3q^2 + \xi) = 0. \quad (3.16)$$

Knowing that the main contribution along the contours C_1, \dots, C_4 in Figure 3.2b comes from the neighborhood of the saddle ρ_1 , we parameterize $k = \rho_1 + s$ with small $s \in (-\epsilon, \epsilon)$ so that, using the Laplace method, we find

$$\begin{aligned} \int_{C_1+C_2-C_3-C_4} g(k)e^{\phi(k)t} dk &\sim \int_{-\epsilon}^{\epsilon} \frac{(1-3(\rho_1+s)^2)\omega_0}{\left((\rho_1+s)-(\rho_1+s)^3\right)^2 - \omega_0^2} e^{t\phi(\rho_1+s)} ds \\ &\sim \frac{(1-3\rho_1^2)\omega_0}{(\rho_1-\rho_1^3)^2 - \omega_0^2} e^{t\phi(\rho_1)} \int_{-\infty}^{\infty} e^{t\frac{s^2}{2}\phi''(\rho_1)} ds \\ &\sim \frac{e^{-\frac{2}{9}\sqrt{3\xi-3}(\xi-1)t}}{\sqrt{t}} \frac{27\xi\omega_0}{4-(\xi+3)\xi^2-27\omega_0^2} \sqrt{\frac{\pi}{\sqrt{3(\xi-1)}}}, \quad t \rightarrow \infty. \end{aligned} \quad (3.17)$$

Now we deform ∂D_+ onto C_1, \dots, C_4 taking the poles into consideration.

(b.1) Subcritical regime: $0 < \omega_0 < 2/(3\sqrt{3})$.

This case corresponds to Region IV.a in Figure 3.3. The poles $k_{3,6}$ are real and lie below ∂D^+ . Consequently, they lie outside the region enclosed by C_2, C_3, D_2, D_3, D_4 , so that Cauchy's theorem implies $u_2(\xi t, t) = \frac{\omega_0}{2\pi} \int_{C_1+C_2-C_3-C_4} g(k)e^{\phi(k)t} dk$. Using (3.17), the leading-order solution in this region decays exponentially

$$u(\xi t, t) \sim \frac{e^{-\frac{2}{9}\sqrt{3\xi-3}(\xi-1)t}}{\sqrt{t}} \frac{27\xi\omega_0}{8-2(\xi+3)\xi^2-54\omega_0^2} \sqrt{\frac{1}{\pi\sqrt{3(\xi-1)}}}, \quad t \rightarrow \infty. \quad (3.18)$$

(b.2) Supercritical regime: $\omega_0 > 2/(3\sqrt{3})$.

This case corresponds to Regions IV.b and IV.c in Figure 3.3. In particular, the poles $\kappa_{3,5}$ are now near the right and left edge of the contour ∂D^+ , respectively, with $\text{Re}(k_3) = -\text{Re}(k_5)$ and $\text{Im}(k_3) = \text{Im}(k_5) > 0$. Thus, we need to distinguish how they are located relative to the deformed contours C_1, \dots, C_4 . Note from Figure 3.2b that these contours intersect with ∂D^+ when $k = p + iq$, $-p + p^3 - 3pq^2 + p\xi \Big|_{q=\sqrt{3p^2-1}} = 0$, i.e., at the points

$$(p_3, q_3) = \left(\frac{\sqrt{2+\xi}}{2\sqrt{2}}, \sqrt{-1 + \frac{3}{8}(2+\xi)} \right), \quad (p_4, q_4) = \left(-\frac{\sqrt{2+\xi}}{2\sqrt{2}}, \sqrt{-1 + \frac{3}{8}(2+\xi)} \right).$$

The poles $k_{3,5}$ coincide with these intersection points when $p_3 = \text{Re}(k_3)$ or, equivalently, $p_4 = \text{Re}(k_5)$, i.e. when

$$l_2 := \frac{1}{2^{2/3}3^{1/3}r_1^{1/3}} + \frac{r_1^{1/3}}{2^{4/3}3^{2/3}} - \frac{\sqrt{2+\xi}}{2\sqrt{2}} = 0, \quad \omega_0 > 2/(3\sqrt{3}) \text{ and } \xi > 1, \quad (3.19)$$

where r_1 is defined below (3.2). Equation (3.19) determines the curve in the ω_0 - ξ plane that splits Regions IV.b and IV.c in Figure 3.3. When $l_2(\xi, \omega_0) < 0$, then the poles $\kappa_{3,5}$ lie outside the region enclosed by C_2, C_3, D_2, D_3, D_4 (see Region IV.b in Figure 3.3), thus $u_2(\xi t, t) = \frac{\omega_0}{2\pi} \int_{C_1+C_2-C_3-C_4} g(k)e^{\phi(k)t} dk$ so that the leading-order behavior of $u(\xi t, t)$ is given by (3.18). On the other hand, when $l_2(\xi, \omega_0) > 0$ then k_3 and k_5 are inside the regions enclosed by C_1, D_1 and C_4, D_5 respectively (Region IV.c in Figure 3.3) so in view of (3.14) we have the additional residue contribution $u_2(\xi t, t) = e^{-\text{Im}(k_3)\xi t} \sin(\text{Re}(k_3)\xi t - \omega_0 t) + \frac{\omega_0}{2\pi} \int_{C_1+C_2-C_3-C_4} g(k)e^{\phi(k)t} dk$. Hence, using once again (3.17), the leading-order asymptotics of the solution in this region is described by

$$u(\xi t, t) \sim e^{-\text{Im}(k_3)\xi t} \sin(\text{Re}(k_3)\xi t - \omega_0 t) + \frac{e^{-\frac{2}{9}\sqrt{3\xi-3}(\xi-1)t}}{\sqrt{t}} \frac{27\xi\omega_0}{8-2(\xi+3)\xi^2-54\omega_0^2} \sqrt{\frac{1}{\pi\sqrt{3(\xi-1)}}}, \quad t \rightarrow \infty. \quad (3.20)$$

Observe that both terms on the right-hand side decay exponentially. In order to figure out which one of them is dominant, we notice that when $l_2 > 0$, i.e. $\text{Re}(k_3) > \sqrt{(2+\xi)/8}$, we have $\text{Im}(k_3)^2 = 3\text{Re}(k_3)^2 - 1 > (3\xi - 2)/8$ so that $\text{Im}(k_3)\xi > \frac{2}{9}\sqrt{3\xi-3}(\xi-1)$. Thus, (3.20) is dominated by the second term. Therefore, in the regime $\xi > 1$, the leading-order behavior of $u(\xi t, t)$ is always given by (3.18) in both the subcritical and the supercritical regime, i.e. regardless of the range of values of ω_0 .

When ξ passes through 1, the asymptotic expansion abruptly changes from oscillatory to exponential, e.g., (3.15) to (3.20). This nonuniformity is due to the collision of the saddle points $\rho_{1,2}$, which can be cast as a uniform asymptotic expansion by use of Airy-type integrals [11].

The large t solution given in eqs. (3.11), (3.12), (3.15), (3.18), and (3.20) proves Theorem 1.2. We now carry out a much simpler calculation of a subset of these results using modulation theory.

Remark 3.1 (Linear modulation theory). Wave modulation theory is one of the primary techniques to describe slow modulations of periodic waves. Herein, we use linear modulation theory to obtain the wave's amplitude, wavenumber and frequency for the linear KdV boundary value problem (2.33)-(2.36) and compare with the long-time asymptotic approximation just obtained. The modulation equations of wave conservation are [43]

$$k(\omega)_t + \omega_x = 0, \quad (3.21a)$$

$$(a^2)_t + (\omega'(k)a^2)_x = 0, \quad (3.21b)$$

where ω is the angular frequency and $k(\omega)$ is one of the roots of the linear dispersion relation $k - k^3 = \omega$. Translating the initial-boundary value problem (2.33)-(2.36) for $u(x, t)$ to the initial-boundary value problem for $k(x, t)$ and $a(x, t)$, we have

$$\begin{aligned} \omega(x, 0) = 0, \quad a(x, 0) = 0, \quad x > 0, \\ \omega(0, t) = \omega_0, \quad a(0, t) = 1, \quad t > 0. \end{aligned} \quad (3.22)$$

Equations (3.21) are a system of quasi-linear equations with the double characteristic speed (eigenvalue) $c_g(\omega_0)$ that has a one-dimensional eigenspace. Equation (3.21a) and the initial-boundary conditions (3.22) are invariant under the hydrodynamic scaling symmetry $x \rightarrow bx$, $t \rightarrow bt$ for any $b > 0$. Consequently, we seek a self-similar solution that preserves this symmetry: $\omega = \omega(\xi)$, where $\xi = x/t$. Since $k(\omega)_t = \omega_t/c_g(\omega)$, either $\omega'(\xi) = 0$ or $c_g(\omega) = \xi$, where $c_g(\omega) = 1/k'(\omega) = 1 - 3k(\omega)^2$ is the group velocity. Combining these in a piecewise fashion, we obtain the solution

$$\omega(\xi) = \begin{cases} \omega_0, & 0 \leq \xi \leq c_g(\omega_0) \\ \frac{1}{9}\sqrt{3-3\xi}(2+\xi), & c_g(\omega_0) < \xi \leq 1 \end{cases}, \quad k(\xi) = \begin{cases} k_0, & 0 \leq \xi \leq c_g(\omega_0) \\ \sqrt{\frac{1-\xi}{3}}, & c_g(\omega_0) < \xi \leq 1 \end{cases}, \quad (3.23)$$

where $k_0 = k(\omega_0)$ satisfies the linear dispersion relation $k_0 - k_0^3 = \omega_0$.

Here we encounter the issue of selecting $k(\omega_0)$ from the three possible wavenumbers that satisfy the cubic polynomial linear dispersion relation. In the context of modulation theory, there are two admissibility conditions for the solution (3.23) to be well-defined: i) $c_g(\omega_0) > 0$ so that $\xi = x/t$ varies across non-negative values and ii) $\text{Im } k(\omega_0) = 0$ so that the solution is real-valued. These are equivalent to the radiation condition (1.4) when $0 < \omega_0 < 2/(3\sqrt{3})$. We proved in Sec. 2.2 the adherence of the linear KdV equation wavemaker problem to the radiation condition (1.4) so a unique $k(\omega_0)$ branch exists with these properties ($k_0 = k_3$ from eq. (3.1)). With an input frequency $\omega_0 \in (0, 2/(3\sqrt{3}))$, the solution consists of a plane wave with constant frequency ω_0 and wavenumber k_0 for $0 < \xi < c_g(\omega_0)$. The group velocity demarcates the invading front of the plane wave into the quiescent region.

By integrating the generalized wavenumber $\theta_x = k(x/t)$ and generalized frequency $\theta_t = -\omega(x/t)$ relations, as well as invoking the boundary data $u(0, t) = -\sin(\omega_0 t)$ (2.36), we can obtain the phase $\theta(x, t)$ up to an integration constant $\theta_0 \in \mathbb{R}$ (more generally, θ_0 can be slowly varying [22])

$$\theta(x, t) = \begin{cases} k_0 x - \omega_0 t, & 0 \leq x \leq c_g(\omega_0)t \\ -\frac{2\sqrt{3}}{9}t(1-x)^{3/2} + \theta_0, & c_g(\omega_0)t < x \leq t. \end{cases} \quad (3.24)$$

In addition, solving (3.21b) yields the amplitude

$$a(\xi, t) = \begin{cases} 1, & 0 \leq \xi \leq c_g(\omega_0) \\ \frac{F(\xi)}{\sqrt{t}}, & c_g(\omega_0) < \xi \leq 1 \end{cases}. \quad (3.25)$$

The self-similar solution (3.25) for a does not preserve the hydrodynamic scaling symmetry when $c_g(\omega_0) < \xi \leq 1$ and $F(\xi)$ can be any smooth function. This is due to the degeneracy of the double characteristic speed $c_g(\omega_0)$.

These results agree with the large t asymptotic solutions in eqs. (3.11) and (3.12). Note that neither the phase θ nor the amplitude a are continuous at $\xi = c_g(\omega_0)$. Here, θ_0 and $F(\xi)$ cannot be determined through leading order modulation theory. However, we can appeal to our long time asymptotic result (3.12) in order to identify

$$\theta_0 = 0, \quad F(\xi) = \frac{27\omega_0\xi}{(4 - 27\omega_0^2 - \xi^2(\xi + 3))\sqrt{2\pi}\sqrt{3(1 - \xi)}}. \quad (3.26)$$

It is interesting to note that, for $c_g(\omega_0)t < x \leq t$, the phase $\theta(x, t)$ is independent of the boundary data. In this region, the phase is determined by a structural property of the linear KdV equation, namely the saddle points $\rho_{1,2}$, which are independent of ω_0 . See the discussion leading up to (3.12).

In summary, modulation theory is a simple method for determining some features of the long-time asymptotic solution. However, its leading order manifestation does not provide information on the integrated phase θ_0 , the amplitude function $F(\xi)$, nor any information on the supercritical regime $\omega_0 > 2/(3\sqrt{3})$ or when $\xi > 1$. Yet, the properties that can be ascertained from modulation theory such as the frequency ω , wavenumber k , and amplitude a agree with the leading order, long-time asymptotic solutions (3.11) and (3.12) of Regions I and II.a, respectively in Fig. 3.3.

4. UNIFORM IN x LONG-TIME ASYMPTOTICS FOR THE LINEAR BBM EQUATION WITH A SINUSOIDAL BOUNDARY CONDITION

This section studies the linear BBM wavemaker problem in the asymptotic limit $t \rightarrow \infty$ and $\xi = x/t = \mathcal{O}(1)$. The analysis is similar to that for the linear KdV wavemaker problem studied in the previous section. Consider the linear BBM initial-boundary value problem (2.64) posed on the semi-infinite line with initial data $u(x, 0) = 0$, $x \geq 0$ and the time-periodic sinusoidal boundary condition $u(0, t) = -\sin(\omega_0 t)$, $t \geq 0$, where $\omega_0 > 0$. The solution of the problem can be derived via the Fokas method given by Equation (2.68), where the contour of integration \mathcal{C} is a small, closed contour around $k = i$ as shown in Figure 2.2. We rewrite the solution (2.68) in terms of trigonometric functions

$$u(x, t) = u_1(x, t) + u_2(x, t) + e^{-x} \sin(-\omega_0 t), \quad (4.1a)$$

$$u_1(x, t) = \frac{1}{2\pi} \int_{\mathcal{C}} \frac{(1 - k^2)e^{ikx}}{k^2 - (1 + k^2)^2\omega_0^2} \left[-\omega_0 \cos(\omega_0 t) + i \frac{k}{1 + k^2} \sin(\omega_0 t) \right] dk, \quad (4.1b)$$

$$u_2(x, t) = \frac{\omega_0}{2\pi} \int_{\mathcal{C}} h(k) e^{ikx - i \frac{k}{1+k^2} t} dk, \quad h(k) := \frac{1 - k^2}{k^2 - (1 + k^2)^2\omega_0^2}. \quad (4.1c)$$

The integrand in equation (4.1b) has the simple pole $k = i$ inside the contour \mathcal{C} so computing the corresponding residue gives $u_1(x, t) = \sin(\omega_0 t)e^{-x}$. Therefore, the solution of the linear BBM wavemaker problem is reduced to evaluating (4.1c) whose integrand possesses an essential singularity at $k = i$. Then, the solution is simply $u(x, t) = u_2(x, t)$.

We appeal to the method of steepest descent for studying the long-time asymptotic behavior of the integral (4.1c). The poles of $h(k)$ occur when $k^2 - (1 + k^2)^2\omega_0^2 = 0$ and are given by $k = k_j$ where

$$k_1 = \frac{1 + \sqrt{1 - 4\omega_0^2}}{2\omega_0}, \quad k_2 = \frac{1 - \sqrt{1 - 4\omega_0^2}}{2\omega_0}, \quad k_3 = \frac{-1 + \sqrt{1 - 4\omega_0^2}}{2\omega_0}, \quad k_4 = \frac{-1 - \sqrt{1 - 4\omega_0^2}}{2\omega_0}. \quad (4.2)$$

When $0 < \omega_0 < 1/2$, all the poles are real and this corresponds to the subcritical regime. When $\omega_0 > 1/2$, the poles are complex and corresponds to the supercritical regime. We therefore define

$$\omega_0 = \omega_{cr} = 1/2 \quad (4.3)$$

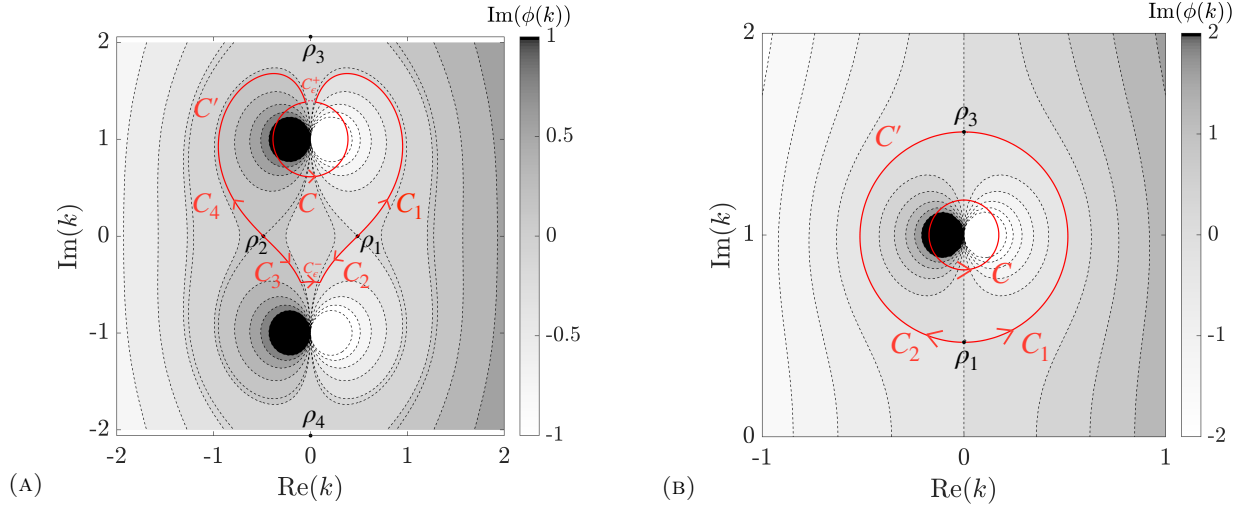


FIGURE 4.1. The deformed, steepest descent contour \mathcal{C}' (red) for the linear BBM wavemaker problem solution (4.1c) in the case of (a) $0 < \xi < 1$ and (b) $\xi > 1$. The positions of the saddles ρ_j are given by (4.4). The closed curve \mathcal{C} is the original small contour around $k = i$. The steepest descent contours $\mathcal{C}_1 \cup \mathcal{C}_2$, $\mathcal{C}_3 \cup \mathcal{C}_4$ in (a) are given by Equations (4.5a),(4.5b), and $\mathcal{C}_1 \cup \mathcal{C}_2$ in (b) is (4.14). The color map indicates levels of $\text{Im}(\phi(k))$.

as the critical frequency. Defining the phase $\phi(k) = ik\xi - i\frac{k}{1+k^2}$, where $\xi = x/t$, then the saddle points satisfy $\phi'(k) = i\xi - i\frac{1-k^2}{(1+k^2)^2} = 0$ and hence are located at

$$\begin{aligned} \rho_1 &= \sqrt{-1 - \frac{1 - \sqrt{1 + 8\xi}}{2\xi}}, & \rho_2 &= -\sqrt{-1 - \frac{1 - \sqrt{1 + 8\xi}}{2\xi}}, \\ \rho_3 &= \sqrt{-1 - \frac{1 + \sqrt{1 + 8\xi}}{2\xi}}, & \rho_4 &= -\sqrt{-1 - \frac{1 + \sqrt{1 + 8\xi}}{2\xi}}. \end{aligned} \quad (4.4)$$

If $0 < \xi < 1$, we have $\rho_1, \rho_2 \in \mathbb{R}$ with $\rho_1 \in (0, 1)$, $\rho_2 \in (-1, 0)$, and ρ_3, ρ_4 are purely imaginary with $\text{Im}(\rho_3) > \sqrt{3}$ and $\text{Im}(\rho_4) < -\sqrt{3}$. If $\xi > 1$, all four saddle points are purely imaginary and symmetrically distributed along the imaginary axis with $\text{Im}(\rho_1) \in (0, 1)$, $\text{Im}(\rho_2) \in (-1, 0)$, $\text{Im}(\rho_3) \in (1, \sqrt{3})$, and $\text{Im}(\rho_4) \in (-\sqrt{3}, -1)$. Let $k = p+iq$ so that $\phi(k) = \left(-\xi q + \frac{-p^2 q - q^3 + q}{4p^2 q^2 + (p^2 - q^2 + 1)^2}\right) + i\left(\xi p + \frac{-p^3 - pq^2 - p}{4p^2 q^2 + (p^2 - q^2 + 1)^2}\right)$. The steepest descent paths occur when $\text{Im}\{\phi(k)\} = \text{Im}\{\phi(\rho_j)\}$ is a constant and $\text{Re}\{\phi(k) - \phi(\rho_j)\} < 0$, $j = 1, 2, 3, 4$.

Now we select the steepest descent contours \mathcal{C}' passing through the saddles that avoid the essential singularities at $k = \pm i$. Then, we deform \mathcal{C} onto \mathcal{C}' and consider the large t behavior. Our general strategy will be to first consider the limit $t \rightarrow \infty$ and then show that the remaining contributions from avoiding the essential singularities are negligible. Depictions of the contours in Figure 4.1 will be discussed after splitting the range of ξ into different intervals.

(a) Regime $0 < \xi < 1$.

The deformed heart-shaped contour (reminiscent of the *Catalpa* tree leaf) is shown in Figure 4.1a, which passes through the saddles ρ_1 and ρ_2 . It is not necessary to deform onto the saddles ρ_3 and ρ_4 . The steepest descent curves passing through the saddles $\rho_{1,2}$ are respectively given by

$$\text{Im}(\phi(k)) = \text{Im}(\phi(\rho_1)) \implies \xi p + \frac{-p^3 - pq^2 - p}{4p^2 q^2 + (p^2 - q^2 + 1)^2} = -\frac{2\sqrt{2\xi}(-2\xi + \sqrt{8\xi + 1} - 1)^{3/2}}{(\sqrt{8\xi + 1} - 1)^2}, \quad (4.5a)$$

$$\operatorname{Im}(\phi(k)) = \operatorname{Im}(\phi(\rho_2)) \implies -\xi p + \frac{-p^3 - pq^2 - p}{4p^2q^2 + (p^2 - q^2 + 1)^2} = \frac{2\sqrt{2\xi}(-2\xi + \sqrt{8\xi + 1} - 1)^{3/2}}{(\sqrt{8\xi + 1} - 1)^2}. \quad (4.5b)$$

The heart-shaped steepest descent paths (4.5) intersect at $k = \pm i$ for all ξ ; however, the contours we use avoid $k = \pm i$ by introducing a small opening \mathcal{C}_ϵ^+ of the circle near $k = i$ and a small arc \mathcal{C}_ϵ^- near $k = -i$ as shown in Fig. 4.1a. By parameterizing k on \mathcal{C}_ϵ^+ as $k = i + \epsilon e^{i\theta}$ for small ϵ , we have the restriction $\theta \in [\pi/2 - \delta(\epsilon), \pi/2 + \delta(\epsilon)]$ and $0 < \delta(\epsilon) < \pi/2$ is defined by the intersection of C and C' (see Fig. 4.1a). Then, we obtain

$$\left| \int_{\mathcal{C}_\epsilon^+} h(k) e^{t\phi(k)} dk \right| \leq \epsilon \int_{\pi/2 - \delta(\epsilon)}^{\pi/2 + \delta(\epsilon)} |h(i + \epsilon e^{i\theta})| e^{t\operatorname{Re}(\phi(i + \epsilon e^{i\theta}))} d\theta.$$

Because $\operatorname{Re}(\phi(i + \epsilon e^{i\theta})) = -\frac{\sin\theta}{2\epsilon} - (\frac{1}{4} + \xi) + \mathcal{O}(\epsilon) < 0$ when $0 < \epsilon \ll 1$ and $|h(i + \epsilon e^{i\theta})| < M$ is bounded, we obtain $\left| \int_{\mathcal{C}_\epsilon^+} h(k) e^{t\phi(k)} dk \right| \leq \epsilon 2M\delta(\epsilon)$. Since this bound is independent of $t \geq 0$, taking $t \rightarrow \infty$ and then $\epsilon \rightarrow 0$ results in a vanishing contribution. A similar argument implies that the contribution to the integral from the small arc \mathcal{C}_ϵ^- above $k = -i$ vanishes $\epsilon \rightarrow 0$. Therefore, we can refine the deformed contour \mathcal{C}' as

$$\begin{aligned} \int_{\mathcal{C}'} h(k) e^{t\phi(k)} dk &= \int_{(C - \mathcal{C}_\epsilon^+) - \mathcal{C}_1 + \mathcal{C}_2 - \mathcal{C}_3 + \mathcal{C}_4 - \mathcal{C}_\epsilon^-} h(k) e^{t\phi(k)} dk \\ &= \int_{C - \mathcal{C}_1 + \mathcal{C}_2 - \mathcal{C}_3 + \mathcal{C}_4} h(k) e^{t\phi(k)} dk + \int_{-\mathcal{C}_\epsilon^+ - \mathcal{C}_\epsilon^-} h(k) e^{t\phi(k)} dk, \end{aligned}$$

so that the solution u in Equation (4.1) can be represented as

$$u(\xi t, t) = \int_C h(k) e^{t\phi(k)} dk = \int_{\mathcal{C}'} h(k) e^{t\phi(k)} dk + \int_{\mathcal{C}_1 - \mathcal{C}_2 + \mathcal{C}_3 - \mathcal{C}_4} h(k) e^{t\phi(k)} dk + \int_{\mathcal{C}_\epsilon^+ + \mathcal{C}_\epsilon^-} h(k) e^{t\phi(k)} dk. \quad (4.6)$$

We have just proven that the third integral on the right hand side vanishes in the limit $\epsilon \rightarrow 0$ for any $t > 0$. We now consider the second integral on the right hand side and prove that its dominant contributions come from the saddles on $\mathcal{C}_1 \cup \mathcal{C}_2$ and $\mathcal{C}_3 \cup \mathcal{C}_4$. The first integral may give pole contributions, which we consider afterward.

Now, we require $0 < \epsilon < 1$. On the contour $\mathcal{C}_1 \cup \mathcal{C}_2$ of Figure 4.1a, the neighborhood of ρ_1 dominates. In a neighborhood of ρ_1 , the path $\mathcal{C}_1 \cup \mathcal{C}_\epsilon$ is approximately parameterized by $k = \rho_1 \pm (1+i)s$, $s \in (-\epsilon, \epsilon)$, so that by the Laplace method, we obtain

$$\int_{\mathcal{C}_1 - \mathcal{C}_2} h(k) e^{t\phi(k)} dk \sim \frac{e^{i\operatorname{Im}(\phi(\rho_1))}}{\sqrt{t}} \frac{1 - \rho_1^2}{\rho_1^2(1 - 2\omega_0^2) - \omega_0^2(1 + \rho_1^4)} \sqrt{\frac{\pi}{|\phi''(\rho_1)|}}, \quad t \rightarrow \infty. \quad (4.7)$$

Similarly, on the contour $\mathcal{C}_3 \cup \mathcal{C}_4$ of Figure 4.1a, we obtain the dominant contribution by integrating over a neighborhood of ρ_2 . Since $\rho_1^2 = \rho_2^2$, $\operatorname{Im}(\phi(\rho_1)) = -\operatorname{Im}(\phi(\rho_2))$ and $|\phi''(\rho_1)| = |\phi''(\rho_2)|$, we sum up the saddle point contributions as

$$\int_{\mathcal{C}_1 - \mathcal{C}_2 + \mathcal{C}_3 - \mathcal{C}_4} h(k) e^{t\phi(k)} dk \sim \frac{\cos[\operatorname{Im}(\phi(\rho_1))t]}{\sqrt{t}} \frac{2(1 - \rho_1^2)}{\rho_1^2(1 - 2\omega_0^2) - \omega_0^2(1 + \rho_1^4)} \sqrt{\frac{\pi}{|\phi''(\rho_1)|}}, \quad t \rightarrow \infty, \quad (4.8)$$

which is $\mathcal{O}(t^{-1/2})$. To determine how the poles k_j , $j = 1, 2, 3, 4$, in Equation (4.2) enter the contour integral, we need to consider different cases for ω_0 .

(a.1) Subcritical regime: $0 < \omega_0 < 1/2$.

In this case, all the poles lie on the real line with $k_1 \in (1, \infty)$, $k_2 \in (0, 1)$, $k_3 \in (-1, 0)$ and $k_4 \in (-\infty, -1)$. While it is easy to see that $k_{1,4}$ are outside of the heart-shaped contour \mathcal{C}' , $k_{2,3}$

are inside \mathcal{C}' when $k_2 < \rho_1$ and $k_3 > \rho_2$. Observe that

$$\omega'(k_2) = \frac{1 - 4\omega_0^2 + \sqrt{1 - 4\omega_0^2}}{2}, \quad 0 < \omega_0 < 1/2 \quad \text{and} \quad 0 < \xi < \omega'(k_2). \quad (4.9)$$

When $\xi < \omega'(k_2)$, $k_{2,3}$ are in \mathcal{C}' (see Region I in Figure 4.2). Applying Cauchy's residue theorem and using

$$\text{Res}_h(k_2) = -\frac{1}{2\omega_0} \exp \left[i \left(-\frac{x}{2\omega_0} + \frac{x\sqrt{1-4\omega_0^2}}{2\omega_0} + \omega_0 t \right) \right], \quad \text{Res}_h(k_4) = \text{Res}_h(k_2)^*,$$

we obtain the asymptotic solution to the linear BBM sinusoidal initial-boundary value problem

$$u(\xi t, t) = \sin \left[\left(\frac{1 - \sqrt{1 - 4\omega_0^2}}{2\omega_0} \xi - \omega_0 \right) t \right] + \mathcal{O}(t^{-1/2}), \quad t \rightarrow \infty, \quad (4.10)$$

where the saddle contribution in Equation (4.8) is the $\mathcal{O}(t^{-1/2})$ correction. We notice that $k_0 := k_2 = \frac{1 - \sqrt{1 - 4\omega_0^2}}{2\omega_0}$ corresponds to the unique root that is given by the D-N map and satisfies the radiation condition (1.4).

When $\xi > \omega'(k_2)$, $k_{2,3}$ are outside \mathcal{C}' (see Region II in Figure 4.2) so that there are no pole contributions and the saddle contributions dominate. Using eq. (4.8), we obtain the leading-order asymptotic solution as $t \rightarrow \infty$

$$\begin{aligned} u(\xi t, t) &\sim \frac{\cos \left[\frac{2\sqrt{2\xi}}{(\Xi-1)^2} (-2\xi + \Xi - 1)^{3/2} t \right]}{\sqrt{t}} \frac{\omega_0 (-4\xi + \Xi - 1) \xi^{1/4} (\Xi - 1)^{3/2}}{2^{5/4} \sqrt{\pi} ((4\xi - \Xi + 1)\omega_0^2 + \xi(2\xi - \Xi + 1)) (\Xi^2 - \Xi)^{1/2} (-2\xi - 1 + \Xi)^{1/2}}, \\ &:= u_{s1}(\xi t, t), \end{aligned} \quad (4.11)$$

where $\Xi := \sqrt{8\xi + 1}$. The solution (4.11) is $\mathcal{O}(t^{-1/2})$, indicating the typical algebraic decay in time of dispersive waves propagating faster than the group velocity.

(a.2) Supercritical regime: $\omega_0 > 1/2$.

The poles k_j , $j = 1, 2, 3, 4$, are all complex and lie on the unit circle $\text{Re}(k_j)^2 + \text{Im}(k_j)^2 = 1$. Furthermore, $k_{2,4}$ are in the lower half plane and are not enclosed by \mathcal{C}' , while $k_{1,3}$ are inside \mathcal{C}' when $\text{Im}\phi(k_1) < \text{Im}\phi(\rho_1)$. Setting $\text{Im}\phi(k_1) = \text{Im}\phi(\rho_1)$ defines the curve

$$l_3(\xi, \omega_0) := \frac{\xi}{2\omega_0} - \omega_0 + \frac{2\sqrt{2\xi}(-2\xi + \Xi(\xi) - 1)^{3/2}}{(\Xi(\xi) - 1)^2} = 0, \quad \omega_0 > 1/2 \quad \text{and} \quad 0 < \xi < 1, \quad \Xi := \sqrt{8\xi + 1}, \quad (4.12)$$

in the ω_0 - ξ plane. When $l_3(\xi, \omega_0) > 0$ (Region III in Figure 4.2), $k_{1,3}$ are inside the heart-shaped contour \mathcal{C}' and give the pole contributions

$$\text{Res}_h(k_1) = \frac{1}{2\omega_0} \exp \left[i \left(\frac{\xi}{2\omega_0} - \omega_0 \right) - \frac{\xi t \sqrt{4\omega_0^2 - 1}}{2\omega_0} \right], \quad \text{Res}_h(k_3) = -\text{Res}_h(k_1)^*.$$

The pole k_1 is consistent with the singularity k_0 that lies on ∂D^+ in the D-N map and satisfies the radiation condition (1.4). Combining the pole and saddle contributions, we obtain the asymptotic solution

$$u(\xi t, t) \sim \exp \left[-\frac{t\xi \sqrt{4\omega_0^2 - 1}}{2\omega_0} \right] \sin \left[\left(\frac{\xi}{2\omega_0} - \omega_0 \right) t \right] + u_{s1}(\xi t, t), \quad t \rightarrow \infty, \quad (4.13)$$

where u_{s1} is the contribution from the saddles given in (4.11). Similar to the long-time asymptotic solution of the linear KdV wavemaker problem (3.15), both terms in (4.13) are required for a uniform asymptotic expansion in $x = \xi t$.

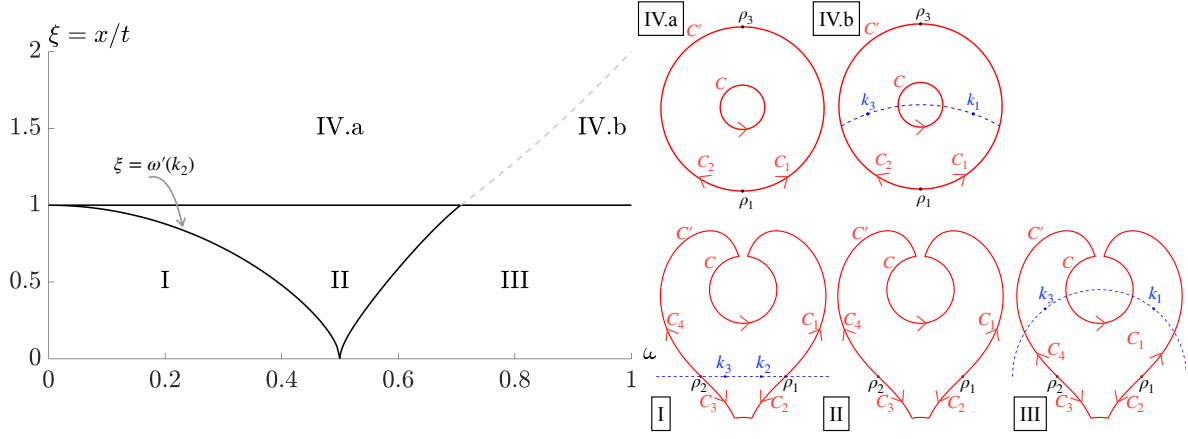


FIGURE 4.2. Phase diagram of the long-time asymptotic solutions to the linear BBM equation (2.64) time-periodic sinusoidal boundary value problem. The leading-order solutions of each region are given in Section 4. The insets present the contour deformation and the positions of the poles for different values of ξ and ω_0 .

On the other hand, when $l_3(\xi, \omega_0) < 0$ (Region II in Figure 4.2), i.e. no poles are inside the deformed contour \mathcal{C}' , the neighborhoods of the saddles $\rho_{1,2}$ dominate and the leading-order solution is given by (4.11). The transition from regions I or III to region II in ξ corresponds to the collision of the poles $k_{2,3}$ with saddle points $\rho_{1,2}$ and can be made uniform in ξ [11].

(b) Regime $\xi > 1$.

Under the condition $\xi > 1$, all the saddle points ρ_j are imaginary and the second derivative $\phi''(\rho_j)$ at each saddle ρ_j , $j = 1, 2, 3, 4$, is real. Shown in Figure 4.1b, the curve $\mathcal{C}' = \mathcal{C}_1 \cup \mathcal{C}_2$ passing through ρ_1 and ρ_3 has constant $\text{Im}(\phi(k))$ defined by

$$\text{Im}(\phi(k)) = \text{Im}(\phi(\rho_1)) = 0 \implies \xi p + \frac{-p^3 - pq^2 - p}{4p^2q^2 + (p^2 - q^2 + 1)^2} = 0, \quad (4.14)$$

where $k = p + iq$. The steepest descent direction follows the circular contour $\mathcal{C}_1 \cup \mathcal{C}_\epsilon$, and therefore, the neighborhood of the saddle point ρ_1 gives the dominant contribution for the integral. With $\phi(\rho_1), \phi''(\rho_1) \in \mathbb{R}$ and $\phi(\rho_1) < 0, \phi''(\rho_1) < 0$, we apply the Laplace method and obtain

$$\int_{\mathcal{C}_1 - \mathcal{C}_2} h(k) e^{t\phi(k)} dk \sim \frac{\exp[t\phi(\rho_1)]}{\sqrt{t}} \frac{(1 - \rho_1^2)}{\rho_1^2(1 - 2\omega_0^2) - \omega_0^2(1 + \rho_1^4)} \sqrt{\frac{2\pi}{-\phi''(\rho_1)}}, \quad t \rightarrow \infty. \quad (4.15)$$

Now we deform the original small closed contour \mathcal{C} onto the steepest descent curve \mathcal{C}' ; in doing so, we incorporate the pole contributions from k_j in (4.2) when necessary.

(b.1) Subcritical regime: $0 < \omega_0 < 1/2$.

All the poles (4.2) are on the real line and so are not enclosed in \mathcal{C}' (see Region IV.a in Figure 4.2). This indicates that $\int_{\mathcal{C}} h(k) e^{t\phi(k)} dk = \int_{\mathcal{C}'} h(k) e^{t\phi(k)} dk$. We use the saddle contribution from (4.15) to obtain the leading-order solution

$$u(\xi t, t) \sim -\frac{e^{-\alpha(\xi)t} \omega_0 \left(\frac{\xi^{1/2}(\Xi-1)^3}{\sqrt{2\xi-\Xi+1}(\Xi^2-\Xi)} \right)^{1/2} (4\xi + \Xi + 8\omega_0^2 - 1)}{\sqrt{t} \cdot 4 \cdot 2^{3/4} \sqrt{\pi} ((4\xi - 1)\omega_0^2 + (\xi - 1)\xi + 4\omega_0^4)}, \quad t \rightarrow \infty, \quad (4.16)$$

$$:= u_{s2}(\xi t, t)$$

where

$$\alpha(\xi) = \frac{\sqrt{2\xi^2 - \xi\Xi + \xi(\Xi - 3)}}{\sqrt{2}(\Xi - 1)}, \quad \Xi := \sqrt{8\xi + 1}. \quad (4.17)$$

The solution in this region has rapid decay in time of order $\mathcal{O}(t^{-1/2}e^{-\alpha(\xi)t})$.

(b.2) Supercritical regime: $\omega_0 > 1/2$.

The poles $k_{1,3}$ are in the first and second quadrants on a unit circle centered at the origin, so are enclosed in \mathcal{C}' when $\text{Im}(\phi(k_1)) < \text{Im}(\phi(\rho_1)) = 0$ and, equivalently, $\text{Im}(\phi(k_3)) > \text{Im}(\phi(\rho_1)) = 0$. This implies, $k_{1,3}$ are inside \mathcal{C}' when $\omega_0 > \frac{1}{\sqrt{2}}$, $1 < \xi < 2\omega_0^2$ (see Region IV.b in Figure 4.2) and outside \mathcal{C}' when $\frac{1}{2} < \omega_0 \leq \frac{1}{\sqrt{2}}$, $\xi > 1$ or $\omega_0 > \frac{1}{\sqrt{2}}$, $\xi > 2\omega_0^2$ (Region IV.a in Figure 4.2). The poles $k_{2,4}$ are in the third and fourth quadrants so are outside of the deformed contour \mathcal{C}' .

For $k_{1,3}$ outside the contour in Region IV.a, the asymptotic solution is given by (4.16). In Region IV.b, the contour integral over \mathcal{C} can be expressed as

$$\int_{\mathcal{C}} h(k)e^{t\phi(k)} dk = \int_{\mathcal{C}'} h(k)e^{t\phi(k)} dk - 2\pi i(\text{Res}_h(k_1) + \text{Res}_h(k_3)), \quad (4.18)$$

as shown by the deformation of \mathcal{C} to \mathcal{C}' in Figure 4.2. Evaluating the residues, we obtain

$$\text{Res}_h(k_1) = \frac{1}{2\omega_0} \exp \left[i \left(\frac{\xi}{2\omega_0} - \omega_0 \right) t - \xi t \frac{\sqrt{4\omega_0^2 - 1}}{2\omega_0} \right], \quad \text{Res}_h(k_3) = -\text{Res}_h(k_1)^*.$$

Then, the large t asymptotics are

$$u(\xi t, t) \sim \exp \left[-\frac{\xi t \sqrt{4\omega_0^2 - 1}}{2\omega_0} \right] \sin \left[\left(\frac{\xi}{2\omega_0} - \omega_0 \right) t \right] + u_{s2}, \quad t \rightarrow \infty, \quad (4.19)$$

where u_{s2} is the saddle contribution given in (4.16). Because the exponential decay rate $|\phi(\rho_1)|$ of u_{s2} is monotone increasing, in Region IV.b where $1 < \xi < 2\omega_0^2$, we have $|\phi(\rho_1)| < |\phi(\rho_1)|_{\xi=2\omega_0^2} < \xi \sqrt{4\omega_0^2 - 1} / (2\omega_0)$. Then, the solution (4.19) is dominated by the saddle contribution u_{s2} . Therefore, for large t , the leading order contribution for all ω_0 and $\xi > 1$ is the same and is given by u_{s2} .

The large t solution given in eqs. (4.10), (4.11), (4.13), (4.16), and (4.19) proves Theorem 1.3.

Remark 4.1. At a qualitative level, the large t solutions of the linear BBM and KdV wavemaker problems exhibit similar bifurcation diagrams in Figures 3.3 and 4.2. Consequently, the solution behavior is qualitatively similar, with traveling periodic waves in Region I, algebraically decaying waves in Region II, and exponential decay in Regions III and IV of the ω_0 - ξ plane.

Remark 4.2 (Linear modulation theory). The modulation equations (3.21) are applicable for general linear dispersive PDEs. Following a path similar to that of the previous section, we now solve (3.21) with the associated boundary values (3.22) where, in this case, $\omega = k/(1+k^2)$. For $\xi = x/t$, the self-similar solution is

$$\omega(\xi) = \begin{cases} \omega_0, & 0 \leq \xi \leq c_g(\omega_0) \\ \frac{\sqrt{1-4\xi+\sqrt{1+8\xi}}}{2\sqrt{2}}, & c_g(\omega_0) < \xi \leq 1 \end{cases}, \quad k(\xi) = \begin{cases} k_0, & 0 \leq \xi \leq c_g(\omega_0) \\ \sqrt{\frac{-1-2\xi+\sqrt{1+8\xi}}{2\xi}}, & c_g(\omega_0) < \xi \leq 1 \end{cases}, \quad (4.20)$$

where $k_0 = k(\omega_0) > 0$ satisfies the linear dispersion relation $\omega_0 = k_0/(1+k_0^2)$. There are two choices for k_0 . Admissibility of the simple wave solution in the subcritical regime $0 < \omega_0 < 1/2$ implies the radiation condition $c_g(\omega_0) > 0$. Then, $k(\omega_0)$ is uniquely determined ($k_0 = k_2$ in eq. (4.2)) and

$$c_g(\omega_0) = \frac{1}{2} \left(1 - 4\omega_0^2 + \sqrt{1 - 4\omega_0^2} \right). \quad (4.21)$$

Suitable integration of $\theta_x = k(x/t)$, $\theta_t = -\omega(x/t)$ determines the phase

$$\theta(x, t) = \begin{cases} k_0 x - \omega_0 t, & 0 \leq x \leq c_g(\omega_0)t, \\ \frac{2\sqrt{2}x(\sqrt{t(t+8x)}-t-2x)^{3/2}}{t(\sqrt{1+8x/t}-1)^2} + \theta_0, & c_g(\omega_0)t < x < t, \end{cases} \quad (4.22)$$

where $\theta_0 \in \mathbb{R}$. The amplitude a has the solution (3.25) with $c_g(\omega_0)$ given in (4.21) and $F(\xi)$ an arbitrary, smooth function. As before, these results agree with the asymptotic solutions (4.10) and (4.11) if we take

$$\theta_0 = 0, \quad F(\xi) = \frac{\omega_0(-4\xi + \Xi - 1)\xi^{1/4}(\Xi - 1)^{3/2}}{2^{5/4}\sqrt{\pi}((4\xi - \Xi + 1)\omega_0^2 + \xi(2\xi - \Xi + 1))(\Xi^2 - \Xi)^{1/2}(-2\xi - 1 + \Xi)^{1/2}}, \quad (4.23)$$

where $\Xi = \sqrt{8\xi + 1}$.

5. COMPARISON WITH CONDUIT EXPERIMENTS

In the long-wavelength, small amplitude regime, the linear BBM equation (equivalent to the linearized conduit equation [32]) describes the interfacial wave dynamics of a particular type of viscous two-fluid core-annular flow [34, 27] that models magma migration through the upper mantle [5] and channelized water flow through glaciers [38]. This flow system comprises a pressure-driven, buoyant, Stokes core fluid within an annulus of another, miscible, heavier Stokes fluid, with a small core-to-annular fluid viscosity ratio. At the injection site, a piston pump acts as a wavemaker by injecting a steady stream of core fluid with an added, small amplitude, time-periodic injection to generate interfacial waves (see [32]). The system can be realized in a simple laboratory setting and provides a quantitative experimental platform for the study of linear and nonlinear wave propagation [34, 35, 23, 26, 30, 28, 4, 29, 32, 31]. The linear BBM equation was found to more accurately capture the dispersive wave properties of this viscous core-annular flow across a wider range of frequencies than the asymptotically equivalent long wave, linear KdV equation [32]. In this section, we investigate the linear time-periodic wavemaker problem in this viscous core-annular system and compare our experimental observations with the long-time asymptotic solutions of the linear BBM equation, derived in section 4.

Consider the linearized BBM equation initial-boundary value problem

$$u_t + u_x - u_{xxt} = 0, \quad x > 0, \quad t > 0, \quad (5.1a)$$

$$u(x, 0) = 0, \quad x > 0, \quad (5.1b)$$

$$u(0, t) = \sin(-\omega_0 t), \quad t > 0. \quad (5.1c)$$

The dependent variable u represents small amplitude fluctuations of the two-fluid interfacial cross-sectional area scaled by the steady, constant cross-sectional area of the established, vertical, straight conduit; x is proportional to the vertical distance from the boundary, and t is proportional to time. See [32] for the non-dimensionalization. Here, we will use the dimensional length L and time T scalings as fitting parameters, which amounts to fitting the fluid viscosities and density difference, in order to compare with experiment. Past work has demonstrated quantitative agreement between the nonlinear extension of the linearized BBM equation (the conduit equation) and experiment with no fitting parameters [26, 28, 29]. A linear time-periodic sinusoidal time-series of unit amplitude and frequency ω_0 is generated at the boundary and propagates into the constant background.

The experimental configuration is identical to that employed in [32]. The experiments are conducted within a vertical square acrylic column that has the cross-section 5 cm \times 5 cm and a height of 180 cm. The core fluid is composed of dyed, diluted glycerin which exhibits lower density and significantly less viscosity than the reservoir fluid into which it is injected. The core fluid rises buoyantly in an external pure glycerin reservoir to establish a circularly symmetric free interface between the two fluids.

A computer-programmed flow rate pump is used to regulate the flow rate \tilde{Q} (cm³/s) of the core fluid, with the cross-sectional area \tilde{A} (cm²) at the injection site satisfying the Hagen-Poiseuille pipe flow law

$$\tilde{Q} \propto \tilde{A}^2, \quad (5.2)$$

with a constant of proportionality involving the ratio of the fluid density difference to the interior viscosity. The imposition of the time-periodic boundary data in (5.1c) is realized by the injection flow rate

$$\tilde{Q}(\tilde{t}) = \tilde{Q}_0(1 + 2a \sin(-\tilde{\omega}_0 \tilde{t})), \quad a \ll 1, \quad \tilde{t} \geq 0, \quad (5.3)$$

where \tilde{Q}_0 (cm³/s) is the background flow rate, a is the (nondimensional) amplitude, $\tilde{\omega}_0$ (rad/s) denotes the dimensional angular input frequency and \tilde{t} (s) is time. A high-resolution camera with a 3 Hz sampling rate is used for data acquisition above the injection boundary to capture the evolving wavetrains. The conduit edges are extracted from camera images using edge detection and smoothing algorithms. At each vertical image pixel, the conduit diameter is calculated as the number of horizontal pixels between the two conduit edges. The diameter is then converted to the dimensionless conduit cross-sectional area A by dividing by the number of horizontal pixels in the undisturbed conduit prior to commencing time-periodic injection and squaring the result.

For experimental comparison with theoretical predictions, we appeal to the nondimensionalization parameters L (cm) as the vertical length scale, U (cm/s) as the vertical velocity scale and $T = L/U$ (s) as the time scale. For each experiment presented below, approximately 15 sets of linear periodic traveling waves were first generated for calibration, and the dimensional angular frequency and wavenumber ($\tilde{\omega}, \tilde{k}$) were measured. The scales L and U were determined by fitting the dimensional quantities ($\tilde{\omega}, \tilde{k}$) to the BBM linear dispersion relation

$$f(\tilde{k}) = \frac{U\tilde{k}}{1 + L^2\tilde{k}^2}. \quad (5.4)$$

The scales associated with each displayed data set are reported. We scale the dimensional space and time as $x = \tilde{x}/L$, $t = \tilde{t}/T$, respectively. Upon linearization of the cross-sectional area A on the uniform background

$$A(x, t) = 1 + au(x, t), \quad a \ll 1, \quad (5.5)$$

and using the boundary condition (5.3) and the Hagen-Poiseuille law (5.2) as

$$\begin{aligned} A(0, t) &= 1 + au(0, t) \\ &= \sqrt{\frac{\tilde{Q}(Tt)}{\tilde{Q}_0}} = \sqrt{1 + 2a \sin(-\tilde{\omega}_0 Tt)} \\ &\sim 1 + a \sin(-\omega_0 t), \quad a \rightarrow 0, \end{aligned} \quad (5.6)$$

where the dimensionless input frequency is $\omega_0 = \tilde{\omega}_0 T$, we obtain the initial, boundary value problem (5.1a), which we compare with experiment.

Previous viscous core-annular flow experiments examined the accuracy of the linear dispersion relation (5.4), the existence of the critical frequency ω_{cr} separating sub and supercritical regimes, and the sinusoidal spatial profiles of linear waves, in addition to their nonlinear counterparts [32]. The BBM dispersion relation (5.4) was shown to be an accurate model of observed linear waves, with discrepancies due to a weak recirculating flow in the outer, annular fluid. In what follows, we compare new experiments with asymptotic predictions of i) the spatial structure of waves along rays $x/t = \text{constant}$ in the sub and supercritical regimes and ii) the subcritical group velocity transition between Regions I and II in Fig. 4.2.

The space-time contour plot in Figure 5.1a depicts the dimensionless cross-sectional area A for the wavemaker problem in the subcritical regime $0 < \omega_0 < \omega_{cr} = 1/2$. The color scale denotes

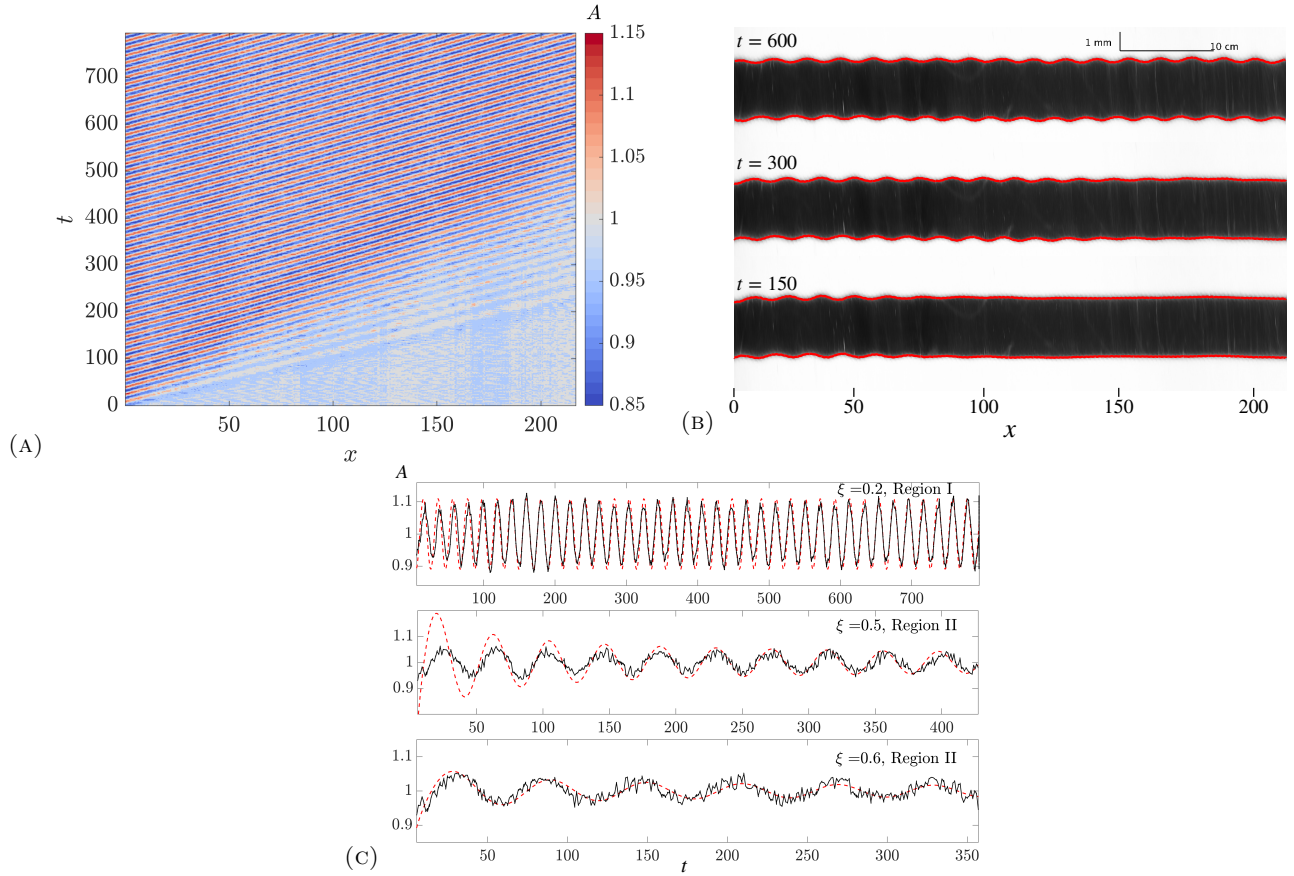


FIGURE 5.1. Viscous core-annular flow experiment in the subcritical regime. (a) Space-time contour of normalized cross-sectional area A for time-periodic injection of core fluid into a uniform background. The measured periodic wave amplitude and angular frequency are $(a, \omega) = (0.11 \pm 0.02, 0.41 \pm 0.02)$, with the nondimensionalization scales $(L, U) = (0.28 \pm 0.01 \text{ cm}, 0.96 \pm 0.02 \text{ cm/s})$. (b) 90° clockwise rotated, rescaled experimental time-lapse. The red curves are obtained from edge detection. (c) Comparison of the experimental data from (a) (black solid) with the long-time asymptotic solutions in Regions I (4.10) and II (4.11) (red dashed) at different, fixed ξ .

wave amplitude with the red-blue region representing waves of substantial amplitude, whereas the lighter-colored, blue region corresponds to the small amplitude, noisy background. The method for measuring the parameters of the periodic traveling wave is described in [32]. Measurement of this experimental dataset yields the periodic wave amplitude, angular frequency and wavenumber $(a, \omega, k) = (0.11 \pm 0.02, 0.41 \pm 0.02, 0.52 \pm 0.02)$, respectively. Figure 5.1b displays example time-lapse images captured by a high-resolution camera during the experiment. At $t = 150$ and $t = 300$, the interfacial wave is observed as it enters the uniform conduit, resulting in decay at the leading edge. Subsequently, as the wave propagates, for example at $t = 600$, it attains local periodicity with small amplitude relative to the average cross-sectional diameter or area. In Figure 5.1c, we compare the experimentally extracted traveling wave data from Fig. 5.1a along rays $x/t = \text{constant}$ with the long-time asymptotic solutions of the linear BBM wavemaker problem. The comparison utilizes the transformation (5.5) and the solutions (4.10, 4.11) in Regions I and II of Figure 4.2, with $a = 0.11$, $\omega_0 = 0.41$, and the previously fitted scaling parameters L and T . However, the experiment identifies $x = 0$ with the starting point of the cropped image and $t = 0$ with the initiation of imaging, which

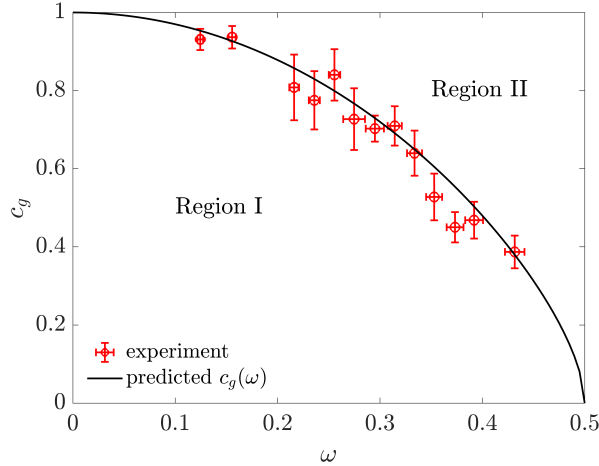


FIGURE 5.2. Comparison of the experimentally measured threshold between Regions I (periodic traveling waves) and II (algebraically decaying waves) at varied angular frequencies ω (red dots) in the subcritical regime with the group velocity (4.21) (black curve), predicted by the long-time asymptotic analysis of the linear BBM wavemaker problem. The nondimensionalization scales for all thirteen measurements are $(L, U) = (0.31 \pm 0.01 \text{ cm}, 1.14 \pm 0.02 \text{ cm/s})$.

differ slightly from the location of the injection site and the initiation of the periodic time-series for the injection rate. Consequently, a shift is applied to x and t everywhere they appear in the solution formulas. For example,

$$\xi = \frac{x - x_0}{t - t_0}. \quad (5.7)$$

The experiment in Figure 5.1c is subject to the shifts $x_0 = 6$ ($\approx 2 \text{ cm}$) and $t_0 = 6$ ($\approx 2 \text{ s}$), which are selected by comparing the experimental data with the theoretical solutions at various ξ . The shift in x is consistent with the experimental setup, in which case the injection site is, while not shown, on the left of the experimental images in Figure 5.1b. The shift t_0 is the best fit time shift. In Figure 5.1c, good agreement is achieved for the comparison between the experiment and the long-time asymptotic solutions in Regions I ($0 < \xi < c_g$) and II ($c_g < \xi < 1$). Region I contains the solutions asymptoting to periodic traveling waves, and the solutions in Region II asymptote to algebraically time-decaying waves. According to the linear BBM theoretical prediction, the corresponding threshold between Regions I and II, i.e. the group velocity, at $\omega_0 = 0.41$ is predicted to be $c_g = \omega'(k_2) = 0.45$ (cf. Equation (4.9)). For small t , the asymptotic solution deviates somewhat from experiment. However, this is expected since the formula represents the large t asymptotics of the solution. In particular, the observed oscillation amplitude, period and phase for sufficiently large t are very close to experiment. Note that the small, noisy oscillations correspond to the resolution of our imaging system. In particular, we observe diameter fluctuations on the order of four pixels, which, for a 30 pixel diameter established conduit corresponds to $(4/30)^2 \approx 0.02$ fluctuations in the nondimensional cross-sectional area A . The reason for this resolution is the 200:1 vertical to horizontal aspect ratio of the imaging system used to capture the data in Figure 5.1a.

As shown in Figure 5.1, wave propagation is periodic when ξ is less than a threshold ξ_g and decays when $\xi > \xi_g$. To obtain a value for this threshold from experiment, we employ the following method. Time slices are extracted from the dataset for $t \in [30, 150]$. In each time slice, the rightmost location $x_g(t)$ is defined to be the last spatial peak with a value greater than 80% of the averaged periodic wave amplitude at the leading edge where the wave starts to decay. The fitted slope of $x_g(t)$, ξ_g , is a

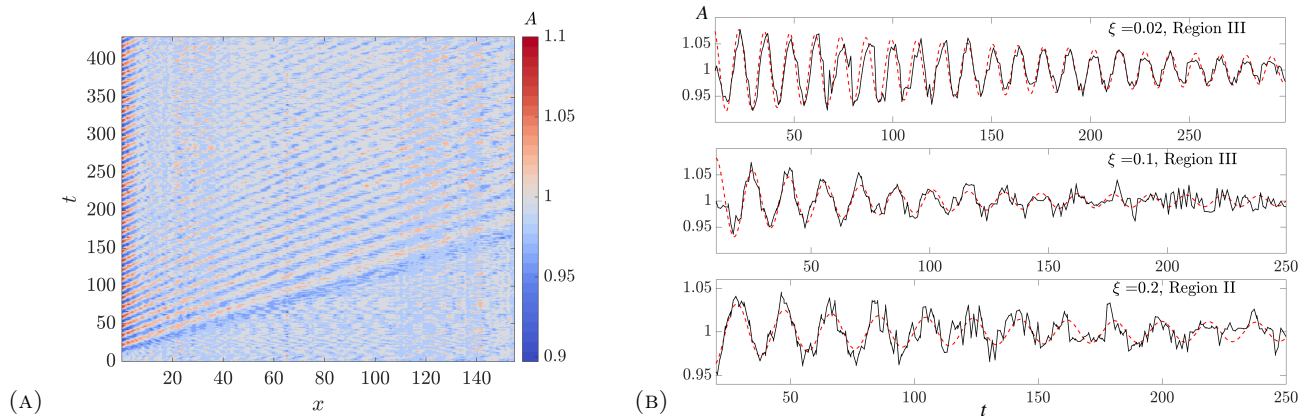


FIGURE 5.3. Viscous core-annular flow experiment in the supercritical regime. (a) Space-time contour of normalized cross-sectional area A for time-periodic injection of core fluid into a uniform background. The measured angular frequency near the boundary is $\omega = 0.51 \pm 0.02$, and the nondimensionalization scales are $(L, U) = (0.32 \pm 0.01 \text{ cm}, 1.04 \pm 0.02 \text{ cm/s})$. (b) Comparison of the experimental data in (a) (black solid) with the long-time asymptotic solutions in Regions II (4.11) and III (4.13) (red dashed) at different, fixed ξ .

reliable approximation of the threshold between Regions I and II. This measurement method is applied to thirteen distinct datasets of linear waves generated from varied input frequencies in the subcritical regime. Figure 5.2 compares the measurement of ξ_g with the group velocity $c_g(\omega)$ (4.21) at different input angular frequencies ω . The angular frequencies are measured and averaged over the periodic wave region. The error bars presented in Figure 5.2 represent the uncertainties resulting from the linear fit of $x_g(t)$ and the variation in the measured wave frequency. Figure 5.2 verifies the threshold ξ_g as the linear BBM group velocity prediction experimentally.

Figure 5.3 depicts an experiment in the supercritical regime with an input frequency greater than the critical value, i.e., $\omega_0 > 1/2$ (see [32] for an experimental study of the critical value). The wave appears to be time-periodic near the boundary and rapidly decays as it propagates. Near the boundary, the measured angular frequency is $\omega = 0.51 \pm 0.02$, very close to the critical value. The space-time data in Fig. 5.3a is compared with the long-time asymptotic solutions of the linearized BBM wavemaker problem for fixed ξ in Fig. 5.3b. Applying the transformation (5.5) and fixing ξ as defined in (5.7), where the shift parameters are $x_0 = 0.3$ ($\approx 0.1 \text{ cm}$) and $t_0 = -1$ (imaging started $\approx 0.3 \text{ s}$ ahead), the experiment is compared to the linear BBM long-time asymptotic solutions (4.11) in Region II and (4.13) in Region III of Figure 4.2 using the mean wave parameters ($a = 0.08, \omega_0 = 0.51$). The predicted threshold between Regions II and III at $\omega_0 = 0.51$ is $\xi = 0.12$ (cf. Equation (4.12)). Figure 5.3b shows that the wave amplitude, frequency, and phase of the experimental result agree with the theoretical predictions.

6. CONCLUSIONS

This work presents the long-time, asymptotic analysis of initial-boundary value problems for linear, scalar evolution equations on the half-line with time-periodic boundary conditions. We obtain the Dirichlet-to-Neumann (D-N) map for a general third-order model with Dirichlet boundary data that is sufficiently smooth and asymptotically periodic in time. The uniqueness of the D-N map is established (Theorem 1.1) if and only if the well-known radiation condition in physics (Corollary 1.1) holds. By

employing the D-N map, we obtain the leading-order asymptotic solution for fixed x and $t \rightarrow \infty$. These results hinge upon the assumption of asymptotic time-periodicity of the solution.

This assumption is proven in the specific case of the wavemaker problems for the linear KdV and linear BBM equations with zero initial condition and sinusoidal boundary condition with frequency ω_0 (Theorems 1.2 and 1.3). Using the Fokas method and steepest descent analysis, we obtain the leading-order, asymptotic solution as $t \rightarrow \infty$ that is uniform in $x \geq 0$. Crossing the interval of frequencies $(-\omega_{cr}, \omega_{cr})$ identifies a bifurcation in solution behavior. When $|\omega_0| < \omega_{cr}$, the solution is asymptotically the propagating wave $u(x, t) \sim \sin(k_0x - \omega_0t)$, $t \rightarrow \infty$ for $x \in [0, c_g(\omega_0)t)$ where $c_g(\omega_0) = \omega'(k_0)$ is the group velocity and $k_0 = k_0(\omega_0)$ is the unique branch of the dispersion relation $\omega_0 = \omega(k_0)$ such that $c_g(\omega_0) > 0$ and $\text{Im} k_0 = 0$. This choice of k_0 corresponds to the radiation condition. When $|\omega_0| > \omega_{cr}$, the asymptotic solution is the time-periodic, spatially decaying, causal solution $u(x, t) \sim \exp(-\text{Im}(k_0)x) \sin(\text{Re}(k_0)x - \omega_0t)$ for $x = \mathcal{O}(1)$, $t \rightarrow \infty$ where $k_0 = k_0(\omega_0)$ is the unique branch of $\omega_0 = \omega(k_0)$ such that $\text{Im} k_0 > 0$ that again satisfies the radiation condition.

We observe quantitative agreement between viscous core-annular fluid wavemaker experiments and the linearized BBM predictions. In particular, we observe the bifurcation in solution behavior at the group velocity and the convergence of spatial profiles to propagating waves, waves that temporally decay $\mathcal{O}(t^{-1/2})$, and waves that exponentially decay in space $\mathcal{O}(\exp(-\text{Im}(k_0)x))$.

We conclude this section by noting that the Fokas method has also found application in the rigorous study of initial-boundary value problems for nonlinear evolution equations that are not necessarily completely integrable. In those non-integrable but still physically relevant cases, the linear solutions obtained via the Fokas method provide the starting point for developing the corresponding well-posedness theory. This is done by treating the nonlinear problem as a perturbation of its forced linear counterpart and invoking the contraction mapping theorem, e.g. see the works [21, 16, 24] and the references therein. Additionally, there are open questions regarding the long-time analysis of the nonlinear wavemaker problem. Whitham modulation theory is a promising analysis tool for integrable and non-integrable equations although it presently lacks a rigorous foundation. As the analogue of the inverse scattering transform for boundary value problems, the Fokas method could also be used for the rigorous analysis of the nonlinear wavemaker problem in integrable systems [12, 6, 13, 9].

REFERENCES

1. *Astronomy Picture of the Day: 2017 January 21 - Daphnis the Wavemaker*, <https://apod.nasa.gov/apod/ap170121.html>, 2017, Cassini Imaging Team, SSI, JPL, ESA, NASA.
2. Mark J Ablowitz and Athanassios S Fokas, *Complex variables: introduction and applications*, Cambridge University Press, 2003.
3. K. Aki and P. G. Richards, *Quantitative Seismology*, 2 ed., University Science Books, Sausalito, CA, 2002.
4. Dalton V Anderson, Michelle D Maiden, and Mark A Hoefer, *Controlling dispersive hydrodynamic wavebreaking in a viscous fluid conduit*, *Physical Review Fluids* **4** (2019), no. 7, 074804.
5. Victor Barcilon and Frank M. Richter, *Nonlinear Waves in Compacting Media*, *J. Fluid Mech. Digit. Arch.* **164** (1986), no. -1, 429–448.
6. A. Boutet De Monvel, A. S. Fokas, and D. Shepelsky, *The mKdV equation on the half-line*, *J. Inst. Math. Jussieu* **3** (2004), no. 2, 139–164. MR 2055707
7. Oliver Bühler, *Waves and mean flows*, second ed., Cambridge Monographs on Mechanics, Cambridge University Press, New York, NY, 2014.
8. P. C. Clemmow, *Some extensions to the method of integration by steepest descents*, *Quart. J. Mech. Appl. Math.* **3** (1950), no. 2, 241–256.
9. B. Deconinck, A. S. Fokas, and J. Lenells, *The implementation of the unified transform to the nonlinear Schrödinger equation with periodic initial conditions*, *Lett. Math. Phys.* **111** (2021), no. 1, Paper No. 17, 18. MR 4215332
10. Bernard Deconinck, Thomas Trogdon, and Vishal Vasan, *The method of Fokas for solving linear partial differential equations*, *SIAM Rev.* **56** (2014), no. 1, 159–186. MR 3246302

11. L. B. Felsen and N. Marcuvitz, *Asymptotic Evaluation of Integrals*, Radiation and Scattering of Waves, 1994, pp. 370–441.
12. A. S. Fokas and A. R. Its, *The linearization of the initial-boundary value problem of the nonlinear Schrödinger equation*, SIAM J. Math. Anal. **27** (1996), no. 3, 738–764. MR 1382831
13. A. S. Fokas and J. Lenells, *Explicit soliton asymptotics for the Korteweg-de Vries equation on the half-line*, Nonlinearity **23** (2010), no. 4, 937–976. MR 2608593
14. A. S. Fokas, B. Pelloni, and D. A. Smith, *Time-periodic linear boundary value problems on a finite interval*, Quart. Appl. Math. **80** (2022), no. 3, 481–506. MR 4453778
15. A. S. Fokas and E. A. Spence, *Synthesis, as opposed to separation, of variables*, SIAM Rev. **54** (2012), no. 2, 291–324. MR 2916309
16. Athanassios Fokas, A Himonas, and Dionyssios Mantzavinos, *The nonlinear Schrödinger equation on the half-line*, Transactions of the American Mathematical Society **369** (2017), no. 1, 681–709.
17. Athanassios Fokas and Maria Christina van der Weele, *The unified transform for evolution equations on the half-line with time-periodic boundary conditions*, Studies in Applied Mathematics **147** (2021), 1339–1368.
18. Athanassios S Fokas, , and Beatrice Pelloni, *Unified transform for boundary value problems: applications and advances*, SIAM, 2015.
19. Athanassios S Fokas, *A unified transform method for solving linear and certain nonlinear pdes*, Proceedings of the Royal Society of London. Series A: Mathematical, Physical and Engineering Sciences **453** (1997), no. 1962, 1411–1443.
20. ———, *A unified approach to boundary value problems*, SIAM, 2008.
21. Athanassios S Fokas, A Alexandrou Himonas, and Dionyssios Mantzavinos, *The Korteweg-de Vries equation on the half-line*, Nonlinearity **29** (2016), no. 2, 489.
22. Richard Haberman, *The Modulated Phase Shift for Weakly Dissipated Nonlinear Oscillatory Waves of the Korteweg-de Vries Type*, Stud. Appl. Math. **78** (1988), no. 1, 73–90.
23. Karl R Helfrich and John A Whitehead, *Solitary waves on conduits of buoyant fluid in a more viscous fluid*, Geophysical & Astrophysical Fluid Dynamics **51** (1990), no. 1-4, 35–52.
24. A Alexandrou Himonas and Dionyssios Mantzavinos, *Well-posedness of the nonlinear Schrödinger equation on the half-plane*, Nonlinearity **33** (2020), no. 10, 5567.
25. A Alexandrou Himonas, Dionyssios Mantzavinos, and Fangchi Yan, *The Korteweg-de Vries equation on an interval*, Journal of Mathematical Physics **60** (2019), no. 5, 051507.
26. Nicholas K. Lowman, M. A. Hoefer, and G. A. El, *Interactions of large amplitude solitary waves in viscous fluid conduits*, J. Fluid Mech. **750** (2014), 372–384.
27. Nicholas K Lowman and Mark A Hoefer, *Dispersive hydrodynamics in viscous fluid conduits*, Physical Review E **88** (2013), no. 2, 023016.
28. Michelle D. Maiden, Dalton V. Anderson, Nevil A. Franco, Gennady A. El, and Mark A. Hoefer, *Solitonic Dispersive Hydrodynamics: Theory and Observation*, Phys. Rev. Lett. **120** (2018), no. 14, 144101.
29. Michelle D Maiden, Nevil A Franco, EG Webb, GA El, and MA Hoefer, *Solitary wave fission of a large disturbance in a viscous fluid conduit*, Journal of Fluid Mechanics **883** (2020), A10.
30. Michelle D Maiden, Nicholas K Lowman, Dalton V Anderson, Marika E Schubert, and Mark A Hoefer, *Observation of dispersive shock waves, solitons, and their interactions in viscous fluid conduits*, Physical review letters **116** (2016), no. 17, 174501.
31. Yifeng Mao, Sathyanarayanan Chandramouli, Wenqian Xu, and Mark A Hoefer, *Creation and interaction of dark and bright topological breathers from soliton-cnoidal wave collisions*, arXiv preprint arXiv:2302.11161 (2023).
32. Yifeng Mao and Mark A Hoefer, *Experimental investigations of linear and nonlinear periodic travelling waves in a viscous fluid conduit*, Journal of Fluid Mechanics **954** (2023), A14.
33. Cathleen S. Morawetz, *The limiting amplitude principle*, Commun. Pure Appl. Math. **15** (1962), no. 3, 349–361.
34. Peter Olson and Ulrich Christensen, *Solitary wave propagation in a fluid conduit within a viscous matrix*, Journal of Geophysical Research: Solid Earth **91** (1986), no. B6, 6367–6374.
35. David R Scott, David J Stevenson, and John A Whitehead Jr, *Observations of solitary waves in a viscously deformable pipe*, Nature **319** (1986), no. 6056, 759–761.
36. A. Sommerfeld, *Partial Differential Equations in Physics*, Academic Press, 1949.
37. Robert Strichartz, *A guide to distribution theory and Fourier transforms*, CRC, 1994.
38. Aaron G. Stubblefield, Marc Spiegelman, and Timothy T. Creyts, *Solitary waves in power-law deformable conduits with laminar or turbulent fluid flow*, J. Fluid Mech. **886** (2020), A10.
39. A. G. Sveshnikov, *Radiation principle*, Dokl. Akad. Nauk SSSR **5** (1950), 917–920.
40. A. N. Tikhonov and A. A. Samarskii, *On the radiation principle*, Zh. Eksp. Teor. Fiz. **18** (1948), no. 2, 243–248.

41. B. L. van der Waerden, *On the method of saddle points*, Appl. sci. Res. **2** (1952), no. 1, 33–45.
42. Vishal Vasan and Bernard Deconinck, *Well-posedness of boundary-value problems for the linear Benjamin-Bona-Mahony equation*, Discrete & Continuous Dynamical Systems-A **33** (2013), no. 7, 3171.
43. Gerald Beresford Whitham, *Linear and nonlinear waves*, John Wiley & Sons, 2011.
44. Mingzhong Wu, *Nonlinear Spin Waves in Magnetic Film Feedback Rings*, Solid State Physics (Robert E. Camley and Robert L. Stamps, eds.), vol. 62, Academic Press, San Diego, CA, 2010, pp. 163–224.